ANL-80-44

ANL-80-44

FAILURE ANALYSIS OF MARK IA LITHIUM/IRON SULFIDE BATTERY

by

V. M. Kolba, J. E. Battles,
J. D. Geller, and K. Gentry

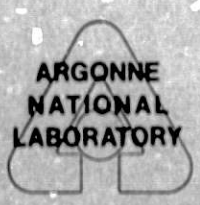

ARGONNE NATIONAL LABORATORY, ARGONNE, ILLINOIS

Prepared for the U. S. DEPARTMENT OF ENERGY
under Contract W-31-109-Eng-38

Distribution Category:
Energy Storage—Electrochemical-
Advanced Batteries (UC-94cb)

ANL-80-44

ARGONNE NATIONAL LABORATORY
9700 South Cass Avenue
Argonne, Illinois 60439

FAILURE ANALYSIS OF MARK IA LITHIUM/IRON SULFIDE BATTERY

by

V. M. Kolba, J. E. Battles,
J. D. Geller,* and K. Gentry**

Chemical Engineering Division

October 1980

*Quality Assurance Division, ANL
**Eagle-Picher Industries, Inc., Joplin, Mo.

TABLE OF CONTENTS

TABLE OF CONTENTS (contd)

LIST OF FIGURES

LIST OF FIGURES (contd)

LIST OF FIGURES (contd)

LIST OF FIGURES (contd)

LIST OF TABLES

FAILURE ANALYSIS OF MARK IA LITHIUM/IRON SULFIDE BATTERY

by

V. M. Kolba, J. E. Battles, J. D. Geller, K. Gentry

ABSTRACT

The Mark IA lithium/iron sulfide electric-vehicle battery, which consisted of two 20 kW-hr modules containing 60 cells each, was fabricated by Eagle-Picher Industries, Inc. and delivered to ANL for testing in May 1979. During startup heating prior to electrical testing, a short circuit developed in one of the modules, which resulted in a progressive failure of the cells. The other module, which was alongside and connected in series, was unaffected by the failure. The initial indication of difficulty was a small drop in the voltage of several cells, followed by short circuits in the balance of the cells and localized temperatures above 1000°C. A team consisting of ANL and Eagle-Picher personnel conducted a detailed failure analysis as the failed module was disassembled. The other module was also examined for purposes of comparison. The general conclusion was that the short circuit was initiated by (1) electrolyte leakage and resulting corrosion in the nearby region which formed metallic bridges between cells and the cell tray, or (2) arcing between cells and the cell tray through the butt joints in the electrical insulation. The above two mechanisms were also believed to be responsible for the failure propagation.

I. INTRODUCTION

A. The Lithium/Metal Sulfide System

The objective of the lithium/metal sulfide battery program at Argonne National Laboratory (ANL) is to develop high-performance, rechargeable batteries for electric-vehicle propulsion and stationary energy storage. At present, the emphasis is on the electric-vehicle application. The battery cells that are currently under development for this application consist of Li-Al alloy negative electrodes, FeS positive electrodes, a BN cloth or felt separator to provide electric insulation between the electrodes, and molten LiCl-KCl electrolyte. The melting point of the electrolyte at the eutectic composition (58.2 mol % LiCl) is 352°C, and the battery is operated at temperatures of 400 to 500°C.

The overall electrochemical reaction for the Li-Al/FeS cell can be written as follows:

$$2LiAl + FeS \underset{\text{(charge)}}{\overset{\text{(discharge)}}{\overset{2e^-}{\rightleftharpoons}}} Li_2S + Fe + 2Al$$

The theoretical specific energy for this reaction is about 460 W-hr/kg, and the open-circuit voltage vs. capacity curve has a voltage plateau at about 1.3 V. The average discharge voltage of the cells under load is about 1.2 V.

All of the cells currently under development for the electric-vehicle application have a rectangular, prismatic configuration with two or more positive electrodes and facing negative electrodes. The cells can be fabricated in a charged, uncharged, or partially charged state by using various combinations of reactants and products in the electrodes. Both the negative and the positive electrodes are normally fabricated by cold- or hot-pressing methods.

B. Electric-Vehicle Battery Program

The major requirements for an electric-vehicle battery are a high specific energy (W-hr/kg), high volumetric energy density (W-hr/L), and high specific power (W/kg). Economic considerations require a minimum battery lifetime of about 3 yr (about 500 deep discharge cycles or equivalent) and a maximum cost of about $50-60/kW-hr (1979 dollars).

The long-range program on the electric-vehicle battery involves the development, design, and fabrication of a series of full-scale lithium/metal sulfide batteries, which have been designated as Mark IA*, Mark II, and Mark III. The main purpose of the Mark IA program was to investigate the overall technical feasibility of the lithium/metal sulfide battery for the electric-vehicle application and to identify potential problem areas. The Mark II battery has somewhat higher performance goals than Mark IA, but the major objective is to develop designs and materials that will have a potential for low-cost manufacture in mass production. The Mark II battery is expected to have commercial potential for certain limited applications. The Mark III battery is planned as a high-performance prototype suitable for evaluation and demonstration in a passenger automobile. The performance and lifetime goals for the Mark IA, II, and III batteries are presented in Table I-1.

*The original plan was to develop a series of Mark I batteries (IA, IB, and IC); however, a decision was made to proceed directly from Mark IA to Mark II in the development program.

Table I-1. Program Goals for the Lithium/Metal Sulfide Electric-Vehicle Battery

Goal	Mark IA	Mark II	Mark III
Battery Capacity, kW-hr	40	50-60	35-50
Specific Energy[a], W-hr/kg			
Cell (Average)	80	125	160
Battery	60	100	130
Energy Density, W-hr/liter			
Cell (Average)	240	400	525
Battery	100	200	300
Peak Power[b], W/kg			
Cell (Average)	80	125	200
Battery	60	100	160
Battery Heat Loss[c], W	400	150[d]	125
Lifetime			
Deep Discharges	200	500	1,000
Equivalent Kilometers	32,000	95,000	240,000
Equivalent Miles	20,000	60,000	150,000
Year	1979	1983	1986

[a]Calculated at the 4-hr discharge rate.

[b]Peak power sustainable for 15 sec at 0 to 50% state of discharge; at 80% discharge, the peak power is 70% of the values shown.

[c]The values shown represent the heat loss of the battery through the insulated case; under some operating conditions, additional heat removal may be required.

[d]The 150-W goal is for an automobile application. Van batteries developed in the Mark II program could have a heat loss rate as high as 500 W.

II. MARK IA BATTERY

A. Introduction

In August 1977, a decision was made to proceed with the development, design, and fabrication of the Mark IA battery. A request for proposals was issued in November, and a contract was awarded to Eagle-Picher Industries, Inc. in Joplin, Missouri. The contract, which went into effect in February 1978, called for a 40 kW-hr battery package consisting of two 20 kW-hr modules containing 60 cells in each module, to be delivered to ANL in 12 months. The programmatic goals for the Mark IA battery were to (1) evaluate the feasibility of powering a vehicle with a lithium/metal sulfide battery, (2) evaluate the reliability of the battery, (3) operate the first high-temperature battery having a low heat loss and high efficiency, and (4) determine unforeseen problems in the design, fabrication, and operation of the battery. In the statement of work for the Mark IA contract, the performance goals for the battery were listed in the following order of preference: (1) operability, (2) energy output, (3) power output, (4) specific energy, (5) specific power, and (6) lifetime. The specific technical goals for the Mark IA battery are presented in Table II-1. When the Mark IA battery was delivered to ANL, it was to be tested first in the laboratory and then in an electric van.

Table II-1. Technical Goals for the Mark IA Battery

Battery Characteristics	Goals
Energy Output[a], kW-hr	40
Power Output[b], kW	30
Maximum Weight, kg	680
Maximum Volume, liters	400
Specific Energy[c], W-hr/kg	60
Energy Density[c], W-hr/liter	100
Operating Temperature, °C	400-500
Maximum Heat Loss, W	400
Battery Voltage, V	144
Cycle Life	200

[a]Discharge to 1.00 V/cell at the 4-hr rate.

[b]Sustained through a 15-sec pulse at 50% state of charge.

[c]To 20% loss of the design capacity.

B. Cell Development and Fabrication

In the cell development phase of the Mark IA program, approximately 120 cells were fabricated by Eagle-Picher. The purpose of these developmental cells was to evaluate the effects of various cell design parameters and materials on the performance and lifetime characteristics of the cells. During this phase of the program, much emphasis was placed on reaching the performance goals indicated in Table II-1. To accomplish these goals, Eagle-Picher fabricated and tested a series of cell matrices, designated A, B, C, and D, prior

to the final fabrication of cells for the Mark IA battery. Each cell matrix consisted of 19 to 45 cells with design variables both in the cell electrochemistry and the hardware. Many of the problems encountered during the cell development phase were of a minor nature and involved only assembly techniques; others, however, were more complex and affected the cell performance as demonstrated by cell tests. These problems, which included cell gassing during activation and cycling, high internal resistance, and cell dimensions outside the tolerance limits, were all investigated and solutions were found to minimize the effects.

Based upon the results of the cell development phase, the final design for the Mark IA cell was chosen. Fig. II-1 is a cutaway view of the Mark IA cell, Fig. II-2 is a photograph of a cross-section of a cell (from the 'B' matrix), and Fig. II-3 shows the cell exterior. The design details of the Mark IA cell are listed in Table II-2. The optimum cell design was found to be a vertical, prismatic, multiplate configuration with three positive and four negative electrodes separated by BN cloth; the two outermost negative electrodes are half-thickness and are in contact with the cell can. The cell has outside dimensions of 19.8 x 18.9 x 3.9 cm (not including the positive terminal feedthrough), and it weighs about 4.0 kg. The theoretical capacity is 410 A-hr.

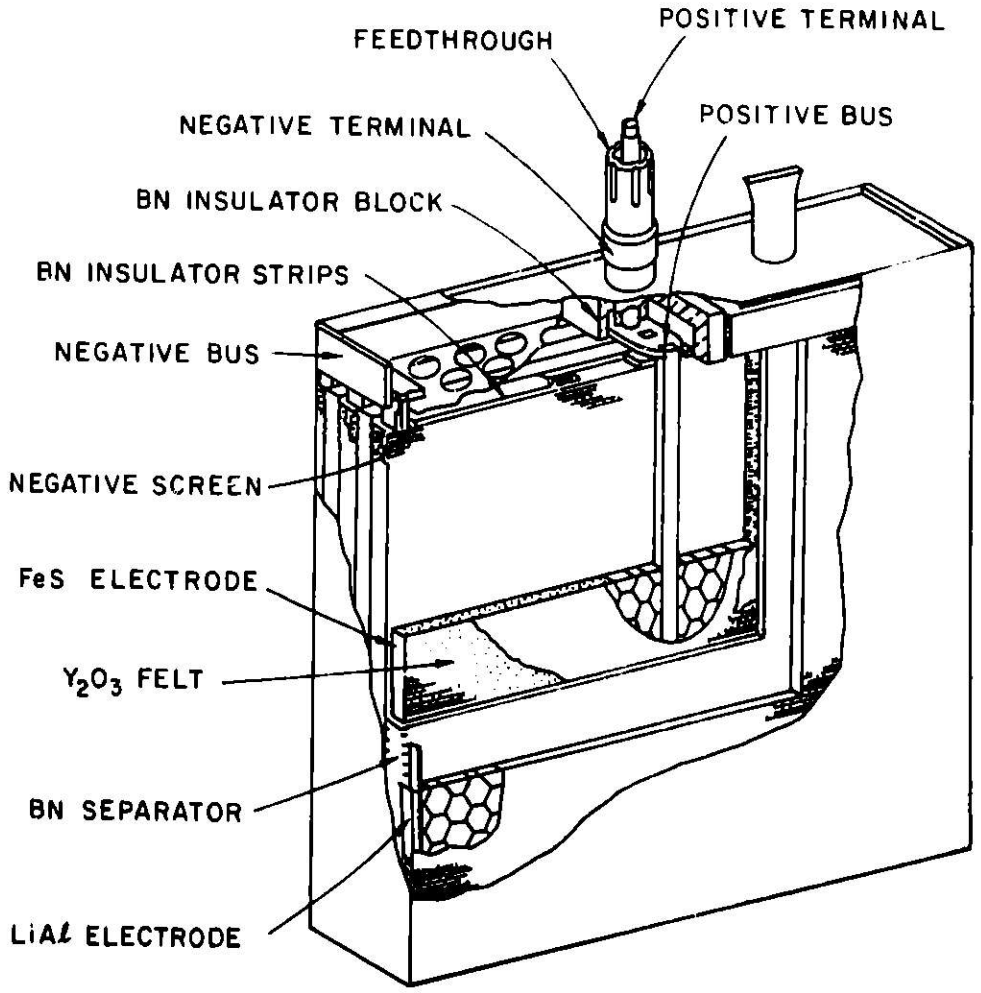

Fig. II-1. Mark IA Lithium/Iron Sulfide Cell

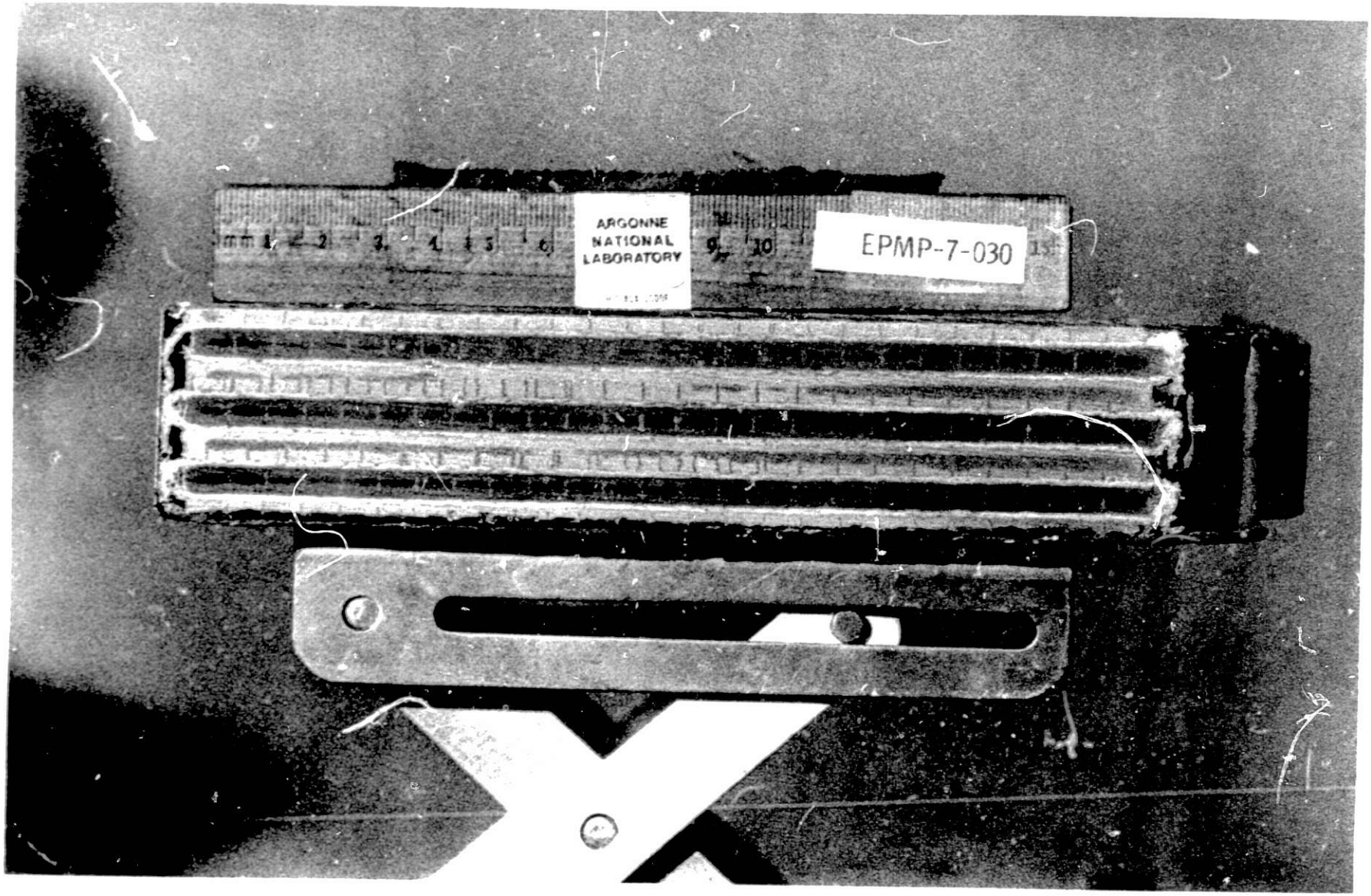

Fig. II-2. Cross-Section of Mark IA Cell

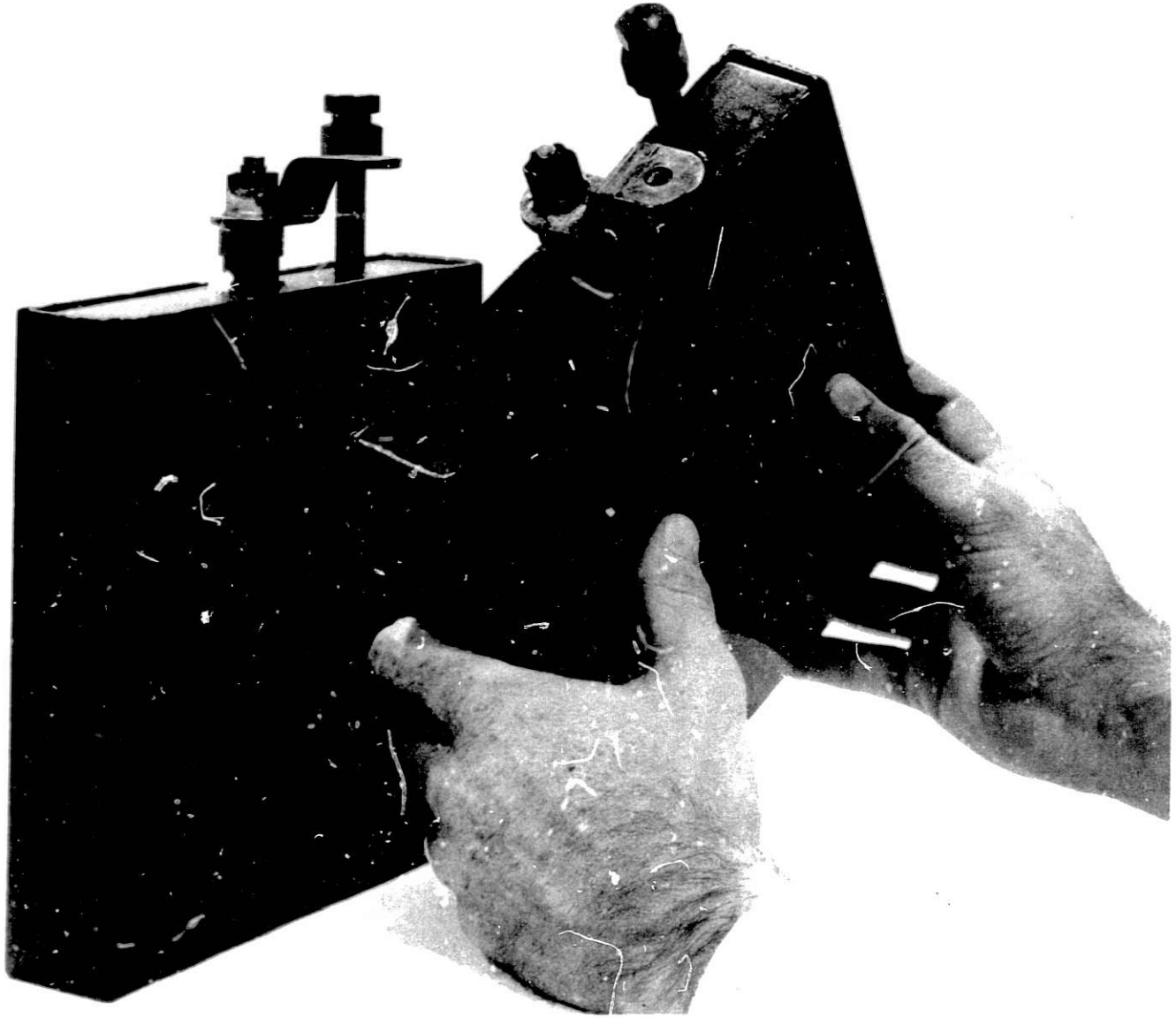

Fig. II-3. Exterior View of Mark IA Cell

Table II-2. Mark IA Cell Design

External Cell Dimensions	
Height (to top of cell can)	19.8 cm
Height (including positive terminal)	24.1 cm
Width	18.9 cm
Thickness	3.9 cm
Weight	3.9-4.0 kg
Theoretical Capacity	410 A-hr
Outer Cell Container (Cell Can)	
Material	AISI 1008 or 1010 low-carbon steel
Thickness	0.61 mm
Positive Electrode	
Height	16.9 cm
Width	17.8 cm
Thickness	3.3 mm
Composition	
FeS	204 g/plate
Cu_2S	36 g/plate
LiCl-KCl (eutectic)	30 g/plate
Theoretical capacity	410 A-hr
Current collector material	AISI 1010 low-carbon steel honeycomb
Particle retainer material	Y_2O_3 felt sheet inside 200-mesh Type 304SS screen.
Terminal	Crimped-type feedthrough with preformed BN powder seal, Al_2O_3 upper insulator, and BeO lower insulator; 7.9-mm dia iron terminal rod with 6.4-mm dia copper core.
Negative Electrodes	
Height	16.9 cm
Width	17.8 cm
Thickness	5.8 mm[a]
Composition	
Li-Al (46 at. % Li)	206 g/plate[a]
LiCl-KCl (eutectic)	20 g/plate[a]
Theoretical capacity	440 A-hr
Current collector material	AISI 1010 low-carbon steel honeycomb
Particle retainer material	200-mesh Type 304 SS screen
Terminal	Copper tube brazed to outside of feedthrough housing and to copper strip brazed on top of cell can
Separator	Woven BN fabric formed into cups enclosing the positive electrode; thickness, 1.8 mm.

[a]These values pertain to the inner negative electrodes only; the values for the two outer negative electrodes are one-half of those indicated.

For the Mark IA battery, Eagle-Picher fabricated 120 "production" cells and 12 spares that met selected acceptance criteria. After it was fabricated, each cell to be used in the battery assembly was checked for quality criteria such as weight, dimensions, and leak tightness. In addition, each cell was subjected to at least five deep discharge-charge cycles to determine whether its electrical performance was acceptable. The qualification criteria in these tests included capacity (>320 A-hr), coulombic efficiency (>99%), resistance at operating temperature (<1.5 mΩ), and general performance. At the end of these qualification cycles, the resistance was measured at room temperature to assure that no short circuits were present (resistance >90Ω). During these qualification tests, the cell was heated to about 500°C for the electrolyte-filling procedure, cooled to room temperature, reheated to the operating temperature (465°C) for the cycling tests, and then cooled again to room temperature for final inspections and assembly of the battery.

C. Cell Performance Tests

Electrical performance tests were conducted on development cells from the A, B, C, and D matrices and on the Mark IA production cells. The results from those cells attaining a cycle life >100 hr are summarized in Table II-3. The specific energy of these cells was about 100 W-hr/kg at a four-hour discharge rate, with an average capacity decline of 0.2-0.3% per cycle. Most of the cells were operated through more than 100 cycles. As shown in this table, the Mark IA production cell attained the specific energy but not cycle life goals listed in Table II-1.

Table II-3. Performance Summary for Mark IA Development and Production Cells[a]

	Development Series					
	A	B	C	D	Mark IA Production	Total
Number of Cells	7	18	13	24	21	83
Ave. Specific Energy[b], W-hr/kg	95.4	100.5	102.4	97.2	100.7	99.2
Ave. Discharge Rate, hr	5	4	4	4	4	4
Ave. Number of Cycles	97	100	111	119	122	110
Ave. % Decline in Specific Energy	20	23	36	28	26	27
Ave. % Decline in Specific Energy per Cycle	0.21	0.23	0.32	0.24	0.24	0.25

[a] Sixty-five cells tested at Eagle-Picher; 18 at ANL.

[b] Measured after less than 24 cycles.

D. Six Volt Battery

During the development phase of the program, Eagle-Picher fabricated a 6-V (1.8 kW-hr) battery to aid in the development of the final design for the 40-kW-hr Mark IA battery. This battery consisted of five development cells in a tray that was inserted into a small insulating case; this case had a design similar to that used for the 20-kW-hr Mark IA battery modules (basically one corrugated Inconel 718* box inside another and layers of aluminum foil in the evacuated annulus between the boxes). The cells in the 6-V battery were oriented sideways in this case (at 90° relative to the cell orientation in the Mark IA battery.)

Prior to shipment to ANL, the 6-V battery was operated for 10 deep discharge cycles at Eagle-Picher. During one of these discharges, it was subjected to vibration testing; vibration had no observable effect either on the electrical performance or the thermal efficiency of the case. The battery was then allowed to cool to room temperature, and shipped to ANL where it was reheated to operating temperature and then tested. After 60 additional deep discharge cycles, the battery developed short circuits in the electrical feedthroughs of two of the cells. At a four-hour discharge rate, the capacity of the battery ranged from about 260 to 280 A-hr when charged with cell equalization† and 208 to 260 A-hr when charged without equalization.

Although the heat loss from the insulating case was initially greater than the design value of 150 W due to a poor vacuum in the annulus, it was subsequently reduced to about 150 W. The spread in cell temperatures was about 10-20°C. Most of the gas that was pumped from the vacuum annulus proved to be hydrogen. This was attributed primarily to water vapor produced by the thermal decomposition of asbestos electrical insulation between the cells, followed by reaction of the water with hot, metallic cell and battery components to form hydrogen, which diffused rapidly through the inner wall of the insulating case at operating temperature (about 450°C). A small amount of hydrogen may also have escaped from the cells themselves due to impurities in the cell materials. As a result of this experience, Vitrabond‡ (an inorganically bonded mica paper) rather than the Raybestos** insulation used in the 6-V battery was selected for the major electrical insulation in the Mark IA battery. In addition, room-temperature SAES getter pumps†† were added to the vacuum system to remove hydrogen.

---

*Huntington Alloys, Inc. Huntington, W. Va.

†In the cell equalization charging procedure, the battery is charged as a whole at a constant current until one of the cells reaches a predetermined cutoff voltage. The individual cells are then charged simultaneously at a constant voltage (about 1.6 V maximum); the current tapers from a maximum of about 10 A to a selected lower limit of about 1 A or for a prescribed period of time (e.g., 4 hr).

‡Midwest Mica and Insulation Co., Cleveland, Ohio.

**Raybestos-Manhattan Inc, Trumbull, Conn.

††SAES Getters/USA, Colorado Springs, Colo.

In a mobile test, the 6-V battery was connected in series with the existing 144-V lead-acid battery pack in an electric Volkswagen Transporter. The general conclusions from this test were as follows: (1) there was no observable inductive interaction between the 6-V battery and the chopper, (2) the temperature of the 6-V battery decreased from 475 to 470°C during one hour of driving, and (3) road vibration and high peak currents had no measurable effects on the performance of the 6-V battery. Except for its relatively short cycle life, the 6-V battery performed as predicted from the design.

E. Mark IA Battery Design

During the cell development phase of the Mark IA program, a parallel effort was directed toward the development and design of the battery hardware and the insulating containers for the two battery modules. The primary objective of the battery development effort was to meet all of the technical goals listed in Table II-1. These goals necessitated a very compact design, which resulted in a number of design problems.

The overall design philosophy for the Mark IA battery was based on the following major requirements: (1) to limit the heat loss to a maximum of 400 W, (2) to contain and restrain swelling of the individual cells, (3) to electrically insulate all the cell cans from one another and the other battery hardware, and (4) to provide the intercell connections, thermocouples, and other electrical circuits within the module. These requirements accounted for most of the design effort in the battery development program.

The battery, based on the above philosophy, consisted of two 20-kW-hr modules, D-001 and D-002, each of which contained 60 cells in series; the two modules were also connected in series to give a nominal operating voltage of 144 V. Each module consisted of two rows of 30 cells in a tray, which provided mechanical support to prevent cell swelling. Force was provided to the faces of the cells by a clamping plate at the rear of the tray, and to the edges of the cells by the sides of the tray and crossover straps. The cells were electrically insulated from one another and from the tray by sheets of Vitrabond insulation.

The cells in each module were connected in series by nickel-clad copper intercell connectors that were brazed to the positive terminal of one cell and to the exterior of the feedthrough assembly on the adjacent cell. Each cell was provided with nickel-clad copper leads* for equalization charging and voltage measurements. Thirteen thermocouples were provided in each module, one for temperature control, one for a safety circuit, and the remainder for temperature monitoring.

A sketch of the cell and tray assembly and the electrical insulation is shown in Fig. II-4. Figure II-5 is a photograph of the various components used in the modules. The cell tray and resistance heaters are shown in the right of the photograph. In the center foreground is the header (cover plate) for the insulating containment vessel, which is to the left. The header has insulated electrical feedthroughs for the main power, heater, thermocouple, and cell voltage sensing and equalization leads. Openings are also provided for purge gas to the cell chamber and air to the cooling tubes.

*Briscoe Mfg., Columbus, Ohio.

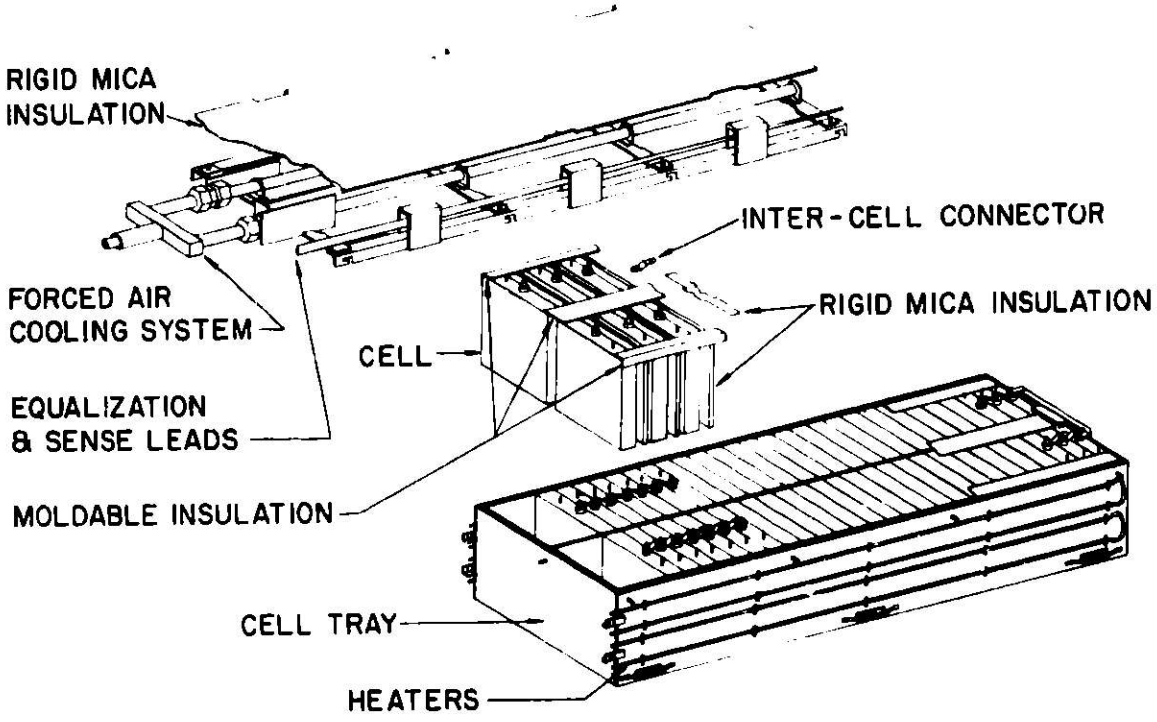

Fig. II-4. Drawing of Cell Tray and Other Battery Hardware

The hardware behind the header in the photograph was used to hold the cells in place in the cell tray. During final assembly of the module, the tray containing the cells was inserted into the insulating containment vessel.

To attain optimum performance of the battery, all of the cells must be maintained at the proper operating temperature. This requires a thermal management system with efficient thermal insulation to minimize heat losses. The thermal management system for each of the Mark IA modules consisted of the insulating containment vessel, the front plug, heaters, tubular heat exchangers with an air blower, and the instrumentation and control devices.

The front of each module was thermally insulated by a 22.9-cm-thick plug assembled from sections of Min-K* insulation. The plug, which was located between the header plate and the front of the cell tray, was designed to accommodate the electrical lead and gas lines and to minimize heat loss by direct radiation from the cell tray.

The insulating containment vessel for each module consisted of one Inconel 718 corrugated box within another and 100 layers of aluminum-foil insulation in the evacuated annulus between the boxes. These vessels were supplied by Thermo Electron Corp., Waltham, Mass. The corrugated design was used to provide the strength required to withstand the atmospheric pressure on the vessel walls. The Inconel 718 was selected for its high-temperature strength, which permitted a lightweight design. The vacuum in the annulus

*A product of Johns Manville Corp., Denver, Colo.

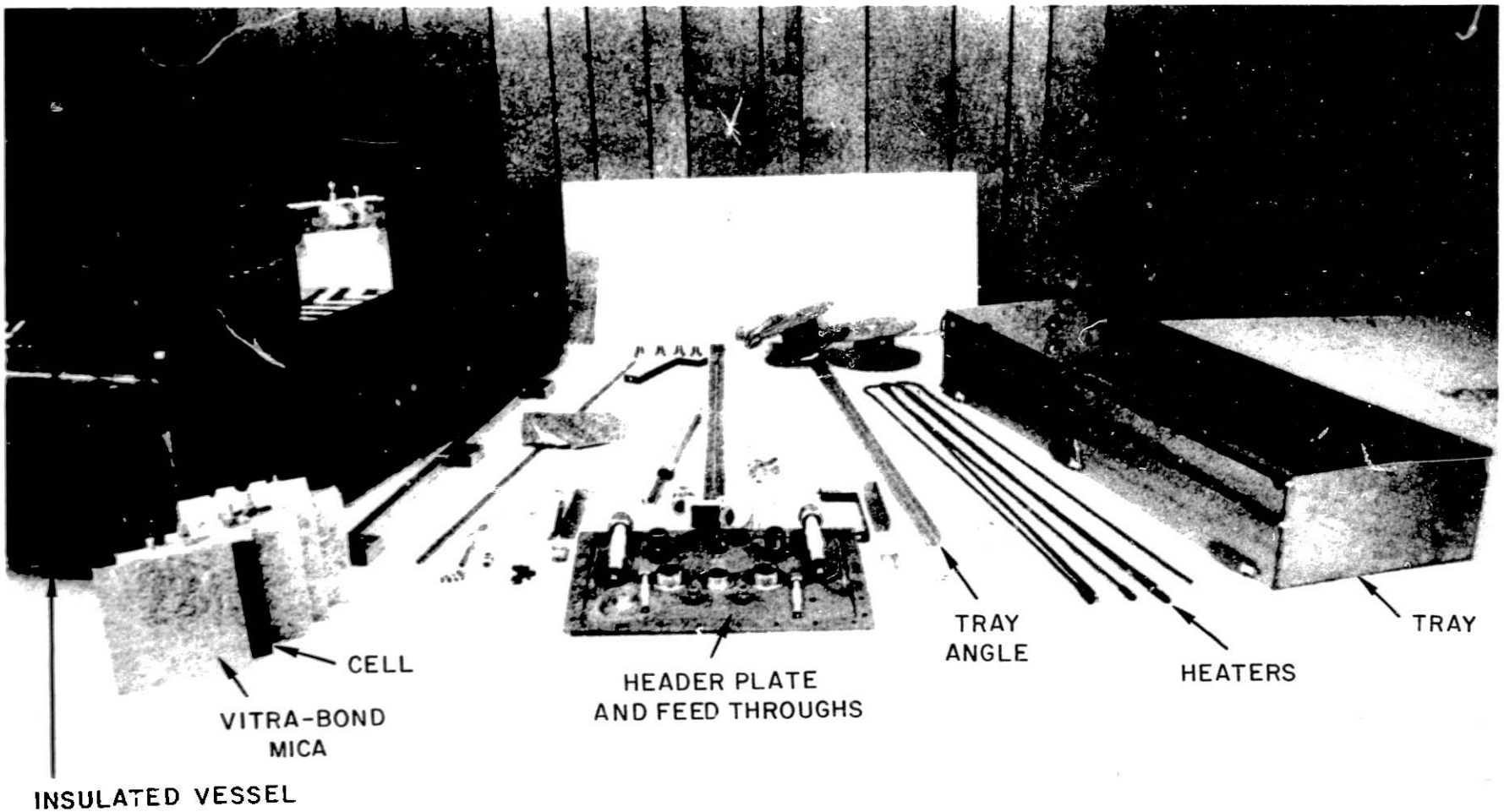

Fig. II-5. Components of Module

was generated by an ion pump and maintained by SAES gettering pumps. The outside dimensions of each containment vessel were 1.56 x 0.46 x 0.33 m.

The modules were heated by WATROD tubular resistance heaters* attached to the outside of the cell tray; the heater capacity for each module was 5 kW. Cooling was provided by forced air through a concentric-tube, double-pass heat exchanger placed above the cells in the tray. The cooling capacity for each module was 1.1 kW at operating temperature. The forced air was provided by a 90-W blower at a rate of $0.37 m^3/min$ (13 cfm) and an inlet temperature of 25°C.

The thermal management console contained two temperature controllers, one to maintain the module at the desired temperature and the other to serve as a "fail-safe" unit. The console also provided for an automatic heating or cooling mode, depending on the temperature of the module. Two modes were provided for heating the module: (1) use of an external AC source for initial heat-up, and (2) when an AC power source is not available, operational heating by power from the module itself.

The major design and fabrication problems with the Mark IA battery were encountered with the insulating containment vessels. Leak-free welding of these vessels was particularly difficult to attain because of the corrugated configuration and the type of material used (Inconel 718). The heat-loss goals were met, however, and satisfactory performance of the containment vessels was verified.

Other problems included providing electrical isolation of the cells within the battery and developing compatible intercell connectors. Many types of electrical insulating materials were rejected owing to poor fabrication characteristics or inadequate high-temperature performance. As mentioned earlier, Vitrabond mica was chosen just prior to final assembly of the battery because the Raybestos used earlier had proved to be thermally unstable at the operating temperature. This change required modification of the insulation design because of the different fabrication characteristics of the two materials. The intercell connector design that was selected proved to be adequate for the operating conditions, but the design required the development of suitable assembly procedures.

Specific tests and calculations pertinent to the battery design included the following: (1) measurements of the expansion forces of a cell during charge-discharge cycling, (2) determinations of the differential thermal expansion due to dissimilar materials of construction, and (3) various materials compatibility tests. In addition to these empirical data, analytical data were used in the system design. Figure II-6 is a plot of the cell expansion force as a function of state of charge for a Mark IA cell. These data were a major input factor to the cell tray design.

Where possible, the individual battery components were tested prior to final battery assembly; qualification testing of the overall system was to be done during initial heat-up and electrical cycling at ANL. Figure II-7 is a photograph of an assembled module as shipped to ANL for start-up and testing. Appendix A gives a list of the materials used for the battery; the melting points of some of these materials are given in Appendix B.

*Watlow Electric Mfg. Co., St. Louis, Mo.

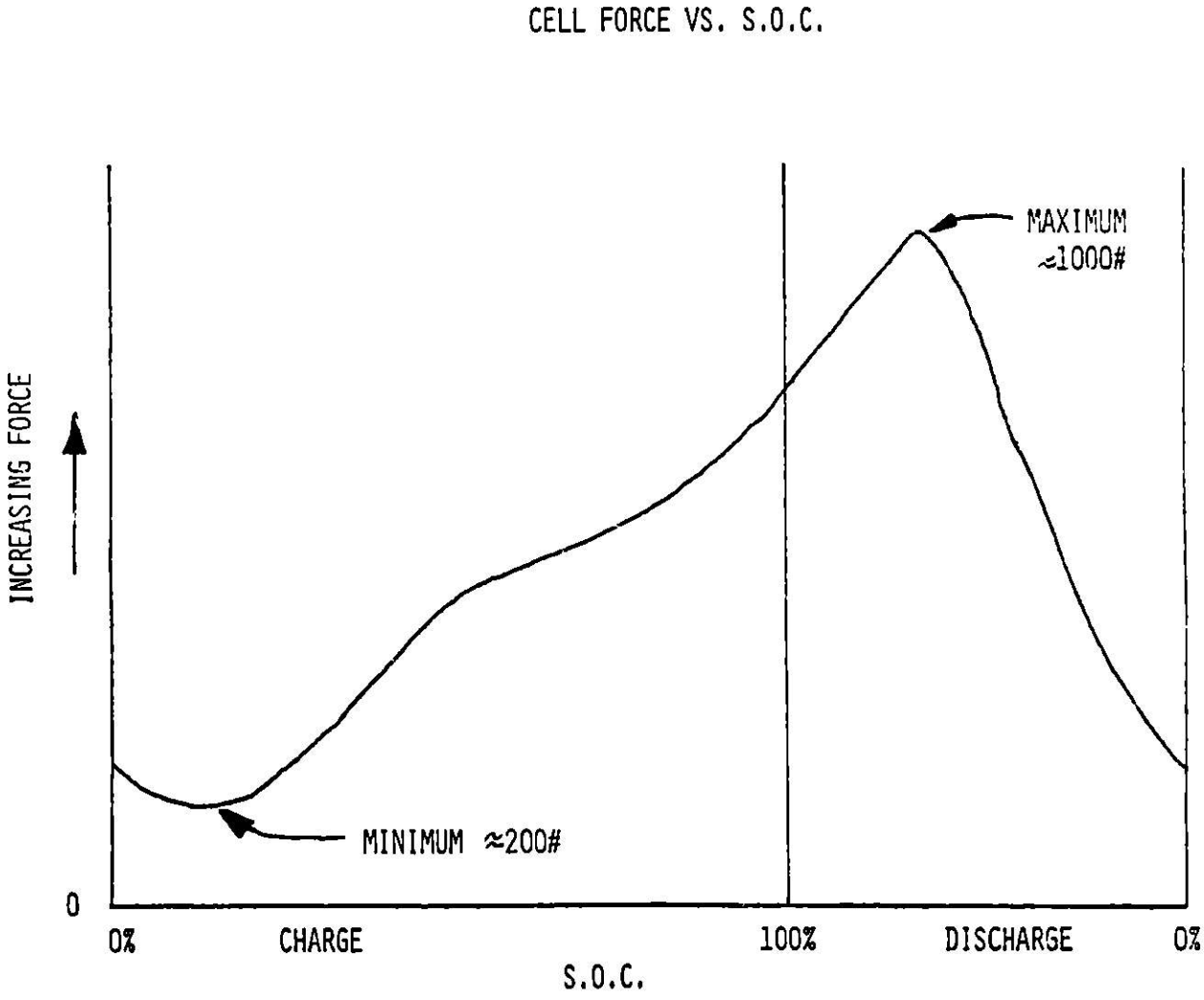

Fig. II-6. Plot of Expansion Force vs. State of Charge for Mark IA Cell

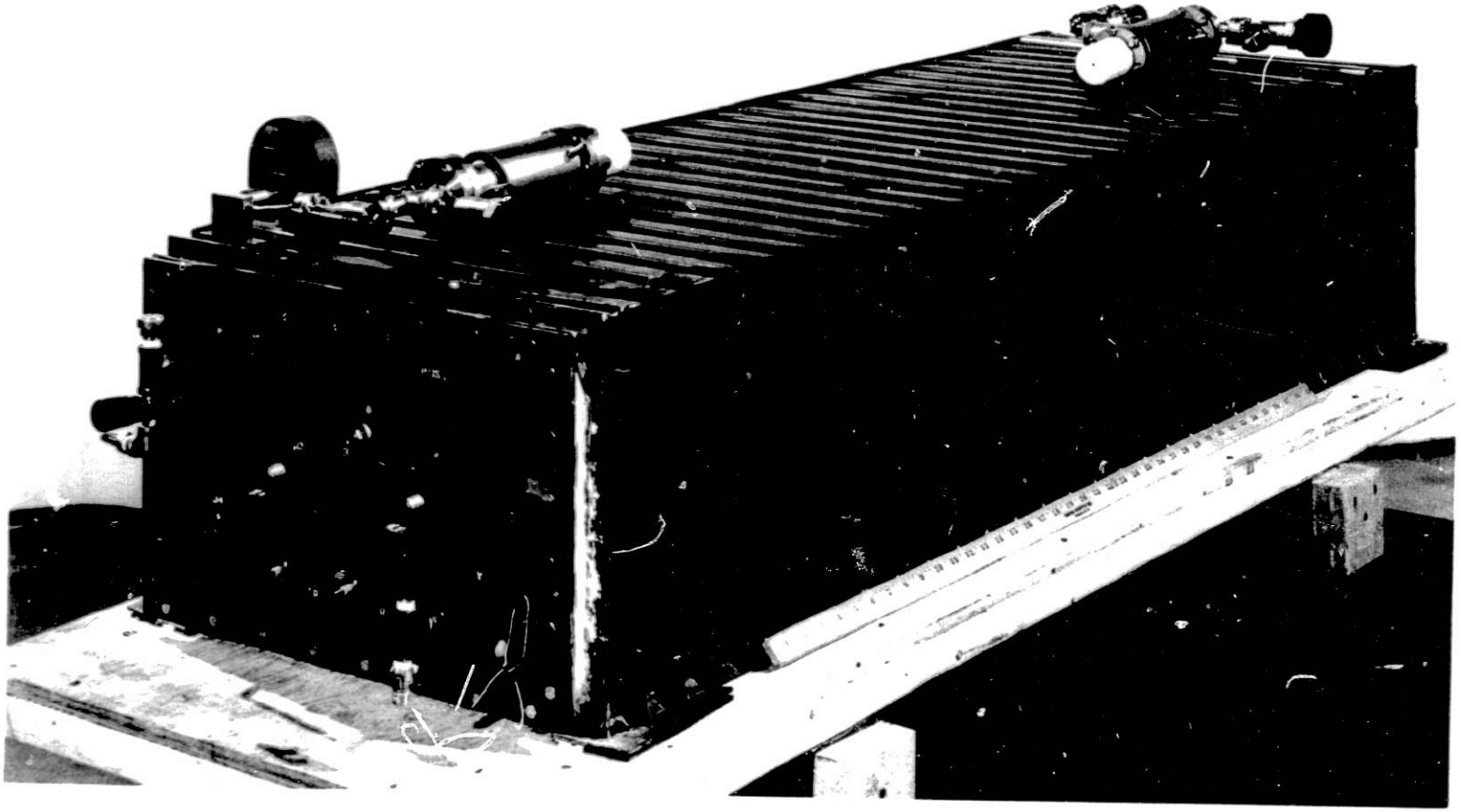

Fig. II-7. Assembled Mark IA Module

III. BATTERY FAILURE

A. Status at Time of Failure

Module D-002 of the Mark IA battery was shipped from Eagle-Picher to ANL on May 8, 1979. Upon the receipt of D-002 at ANL, room-temperature resistance measurements were made on the module and the individual cells and no abnormal results were obtained. The vacuum annulus in the insulating containment vessel was being maintained at a satisfactorily low pressure of 8×10^{-3} Pa (6×10^{-5} torr) by a 1 L/sec ion pump. The vacuum system for the containment vessel was attached to the module, which was then installed in a Volkswagen Transporter electric van on May 14. No other significant work was performed on D-002 until the arrival of Module D-001 on May 22. Upon the arrival of D-001, room-temperature resistance measurements were made on the module and the individual cells, with no abnormal findings, and the unit was installed in the van on May 25. Figure III-1 shows the two modules in the van. The modules were connected in series, but left on open circuit. Final installation of the auxiliary equipment was completed on May 27.

Figure III-2 is a schematic diagram of the electrical/electronic systems and their connections to the battery. The cell and thermocouple locations, which are referred to later in this report, are shown in Fig. III-3 for both modules. Temperature data taken by a computerized data acquisition system were limited by the equipment capability to eight locations in each module. The remaining temperatures were taken manually, using a thermocouple switch and digital readout. The data acquisition system channels and the switch positions for the manual readout corresponding to the thermocouple locations are listed in Table III-1. Thermocouple #3 was used to operate the temperature controller, and thermocouple #4 was used to activate the fail-safe system to prevent overheating of the battery by the resistance heaters.

An auxiliary lead-acid battery, which was used to supply power for a blower to provide air to the cooling tubes, was not connected, since it was not anticipated that cooling would be required during the initial thermal testing. The system, however, had been checked out earlier and found to operate properly, i.e., the thermocouple signal activated the relay which turned on the blower.

During the initital setup, the instrumentation on the battery included a computer data acquisition system (DAS) that recorded the battery voltage, individual voltages of the 120 cells, and 16 (8 from each module) thermocouple readings (up to 1040°C) every minute. The individual cell voltages were also displayed (to 10 mV) on a cathode ray tube (CRT) terminal. Fourteen thermocouple readings (7 from each module) could also be taken manually by a selector switch and digital meter (up to 1000°C). A flowmeter was used to monitor the argon flow rate (70 L/hr) through the cell chambers in each of the modules. Pressure in the ion-pump system, which was attached to the vacuum annulus, was indicated by a strip chart recorder; and a mass spectrometer was attached to the system for periodic gas analysis. The system for equalization charging was initially connected to the battery, but it was disconnected during the final stage of the battery heat-up. After heat-up, thermal testing of the modules at 450°C was planned prior to the initiation of charge-discharge cycling. A brief summary of the status of the battery prior to the failure is presented in Table III-2.

Fig. III-1. Modules D-001 and D-002 in Electric Van

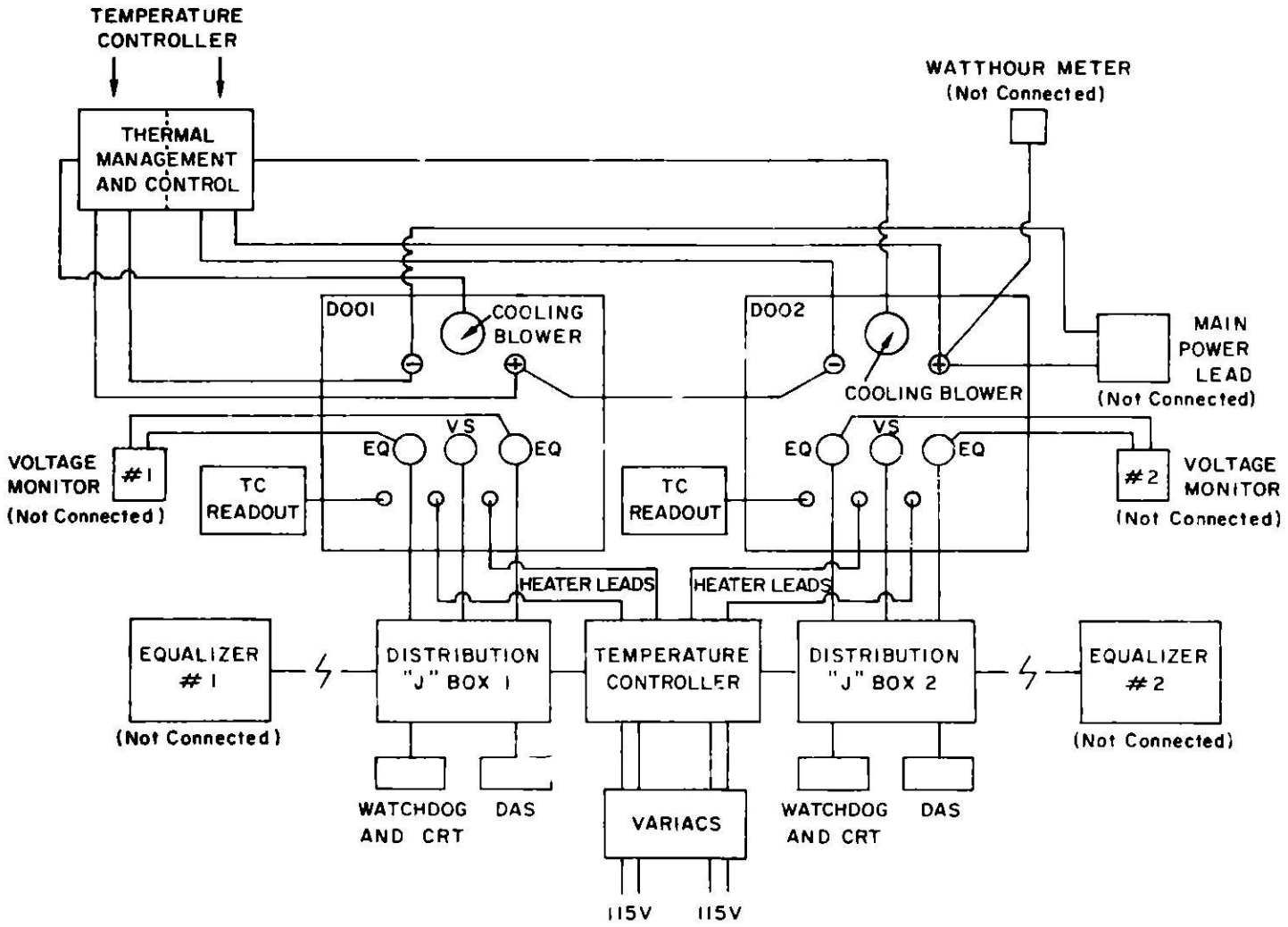

Fig. III-2. Schematic Diagram of Electrical/Electronic System for Mark IA Battery

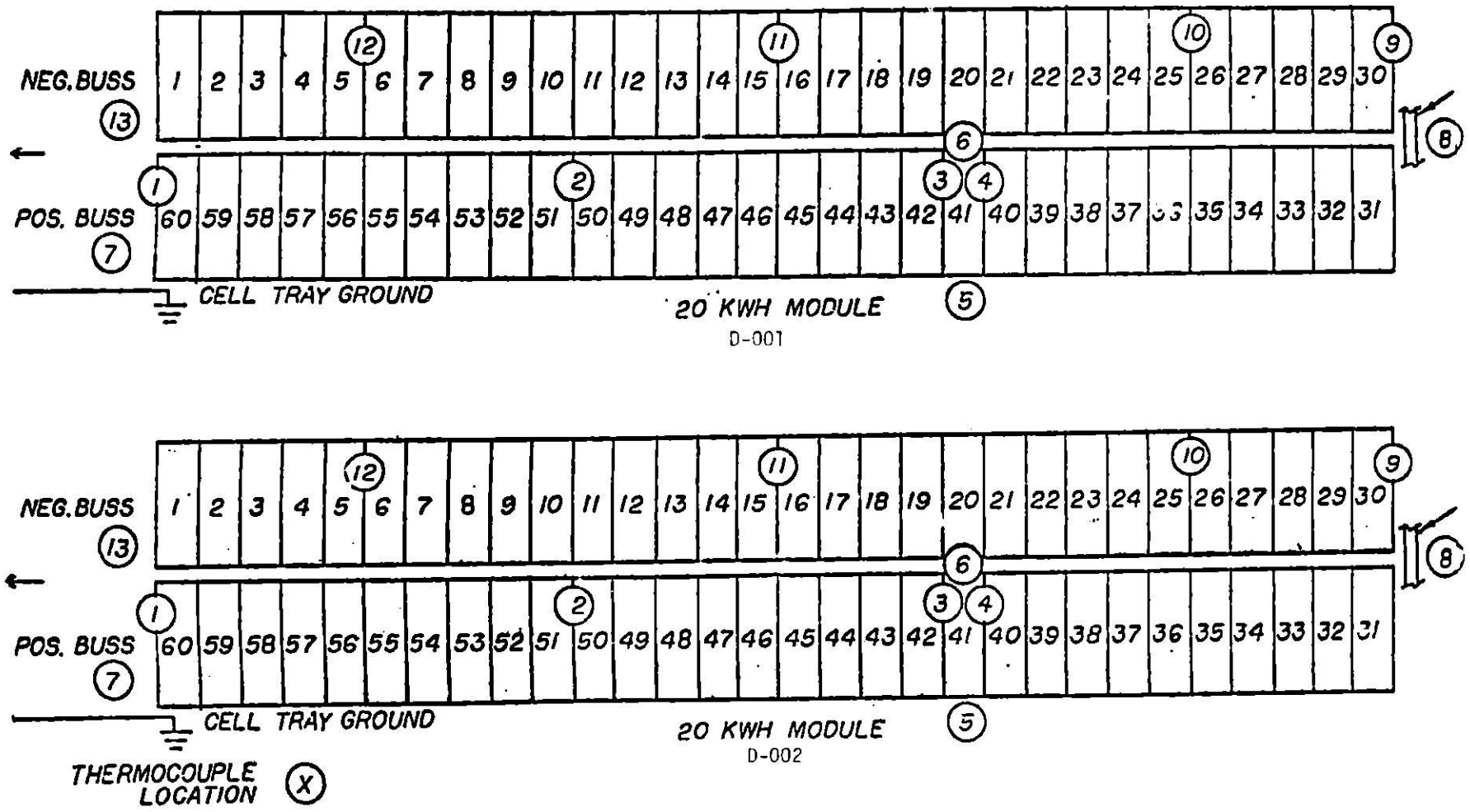

Fig. III-3. Mark IA Cell and Thermocouple Arrangement

Table III-1. Relationship of Thermocouple Locations to Data Acquisition System Channels and Manual Readout Switch Positions

	Thermocouple Location[a]	DAS Channel	Manual Switch Position
Module D-001	1	1	
	2	2	
	3		3
	4	3	
	5		5
	6		6
	7		7
	8	4	
	9	5	
	10	6	
	11	7	
	12	8	
	13		4
	Outer Case		2
	Room Temperature		1
Module D-002	1	9	14
	2	10	
	3		9
	4	11	
	5		11
	6		12
	7		13
	8	12	
	9	13	
	10	14	
	11	15	
	12	16	
	13		10
	Outer Case		8

[a]See Fig. III-3.

The positive terminal of Module D-001 was connected to the negative terminal of D-002, and the positive terminal of D-002 and the negative terminal of D-001 were attached to a main power-lead connector, which was not coupled to the vehicle electrical system. The on-board instrumentation (e.g., voltage monitors and the watt-hour meter) was installed but not connected to the modules. The thermal management system was connected to the AC power and the system switches were set to provide heater power from a Variac-controlled AC supply. The equalizers were not connected.

Heat-up of the battery to operating temperature was initiated at 1300, May 27. At this time, around-the-clock surveillance of the test was provided by two technical staff personnel from the battery program on each eight-hour

shift. Written instructions were provided and reviewed with the shift personnel. These instructions included possible problems and the actions to be taken.

Table III-2. Mark IA Battery Status at Time of Failure

HEAT-UP PERIOD	
Heating initiated	1300, May 27
Electrolyte melted	1500, May 28
Reached operating temperature (450°C)	1800, May 29
PREPARATIONS FOR THERMAL TESTING	
Systems Connected to Modules	
Data acquisition system (CAMAC and LSI-11)	
Thermocouples	
Cell voltage sense leads	
Voltage display (CRT)	
Temperature controllers	
Heaters	
Argon purge system	
Vacuum system (1 L/sec and 11 L/sec ion pumps)	
Systems Not Connected to Modules	
Power supply (Robicon) for charge-discharge cycling	
Cell equalization charger	
Power for module cooling	

During the heat-up period, the data acquisition system was unavailable for about four hours (about 1230-1700, May 28) for software modifications that were needed to transfer data from a disc to a new magnetic tape unit. Memory limitations prevented the software modifications and acquisition of data at the same time.

Both modules were heated at a rate of 10-15°C/hr; this heat-up was accomplished with internal resistance heaters limited by Variac transformers and controlled by the thermal management system, which included control thermocouples inside the modules. The leads from the cell equalization charger were disconnected from both modules at 1230, May 28. The two modules reached the melting point of the electrolyte (352°C) at about 1500, May 28, and portions of the battery began to reach the operating temperature (425°C) at about 1200, May 29.

At about 1235, May 29, the voltage of Cell No. 93 in Module D-002 (location #33 in Fig. III-3) began a slow decline, dropping to 1.4 V in about 1.5 hr. The voltage then continued to decrease gradually to 0.1 V over a two-hour period. No thermal effects were evident. At 1800, May 29, the voltage of Cell No. 105 in Module D-002 (location #45 in Fig. III-3) began to decrease, and on May 30 it dropped from 1.3 V to zero in about three hours. Although no temperature rise was observed during this voltage drop, the

heaters in Module D-002 stopped cycling and remained off for about four hours (0800-1200, May 30). The cell equalization system was re-connected to Module D-002, and an attempt was made to recharge Cells 93 and 105. Neither cell, however, would accept a charge, and charging efforts were discontinued after about seven hours, at 1625, May 30. The equalization leads were then disconnected from D-002. With a portion of the battery at or near operating temperature, the heating rate was adjusted in preparation for thermal loss tests. It was anticipated that the thermal gradients noted at 1100 May 30 would decrease with time while the battery stood at operating temperature.

B. Failure Description

A detailed series of log entries, made during the failure of Module D-001, is given in Appendix C and summarized in Table III-3.

Table III-3. Description of Event (May 30-31, 1979)

Time	Remarks
1800	All readings normal; reduced voltage on heaters.
2047	Voltage increased on heaters.
2300	All readings normal.
2316	Slight voltage drop observed on CRT in Cells 24-27 in Module D-001 and by Data Acquisition System.
2340	Heaters turned off to D-001; vacuum loss in D-001; thermocouple reading off scale (999.9°C).
2350	Blower for air cooling started. Fire department arrived.
0020	All cell voltage (D-001) except #60 at "0" volts (CRT).
0045	Added fans to cool case exterior (T 113°C), exhaust cooling air 266°C.
0250	Annulus pressure at 1 atm. Put on mechanical pump.
0800	Electrolyte below melting point in D-001.
1132	Started cooling of D-002.

Until 2316, May 30, the temperatures, cell voltages, annulus vacuum pressure, argon flow rate to the cell chamber, and other readings for both modules were normal. At that time, however, a small decrease (0.1-0.2 V) was noticed in the voltages of Cells 24 through 27 on the CRT terminal.

At this time, an argon flowmeter on the exit line from the cell chamber was off-scale on the maximum, 85 L/hr (3 cfh); however, the flow was readily decreased to the desired value of 68 L/hr (2.4 cfh). This high reading could have resulted from a change in gas volume due to a temperature increase or a minor pressure surge in the cell chamber. At the same time, the pressure in the vacuum annulus rose from 1.2×10^{-2} to 1.5×10^{-2} Pa (9.0×10^{-5} to 1.1×10^{-4} torr), as shown in Fig. III-4. The vacuum annulus of D-001 was connected via a manifold to an 11 L/sec ion pump. The annulus of D-002 was connected to the same manifold, but it was valved off from the manifold. The

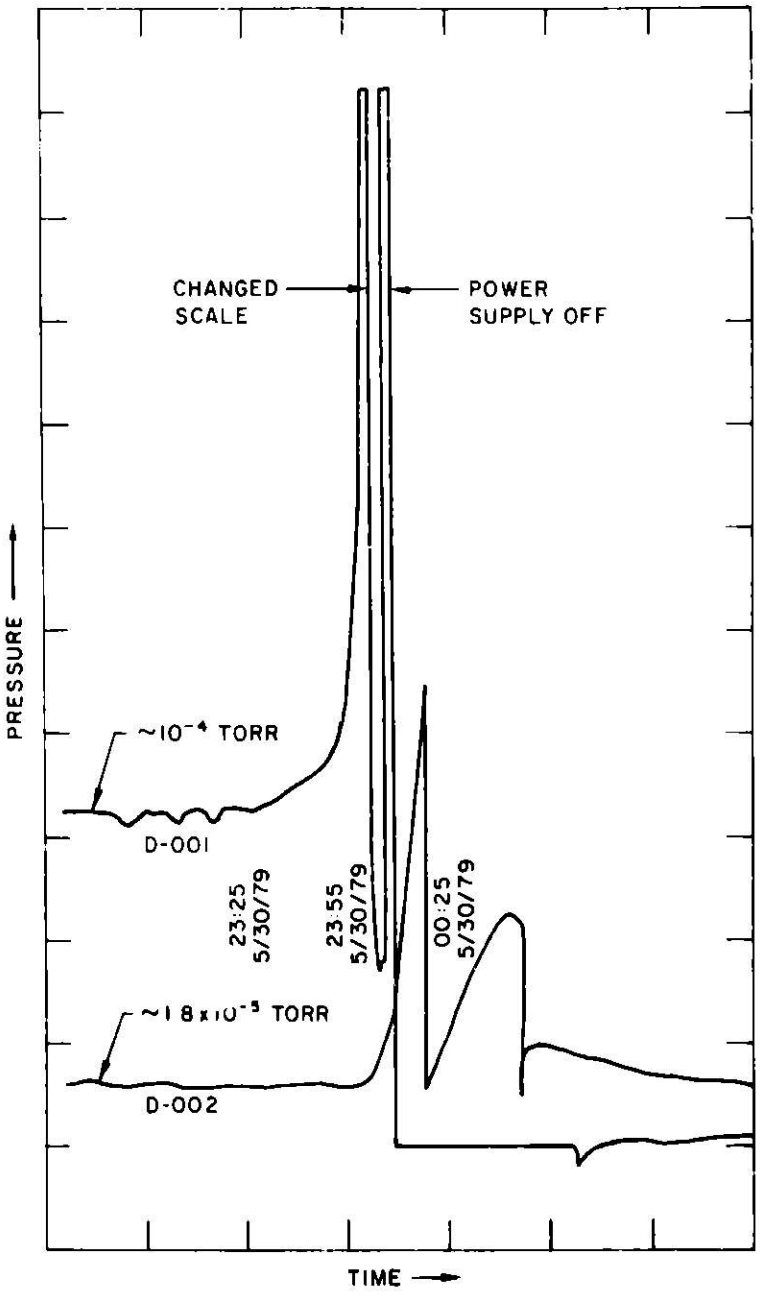

Fig. III-4. Pressure in Vacuum Annulus of Insulating Containment Vessels

annulus pressure in D-002, however, showed a slight increase, which was attributed to a slight leak in the isolation valve. The voltage declines for Cells 22 through 31 are shown as a group in Fig. III-5, and those for Cells 24 through 27, which were the first cells to exhibit voltage decline, are shown individually in Fig. III-6. At about 2327, the voltages of Cells 24 through 37 began to drop significantly, and this effect progressed to the other cells. Between 2316 and 2333, the battery voltage had dropped from 173 to 90 V. The progression of cell-voltage decline (in 0.25-V increments) and temperature changes is shown in Fig. III-7. The decline in voltage of the entire Mark IA battery during the failure is given in Fig. III-8. There appear to be at least three major sections in this curve between 28 and 32 minutes. The slopes of the curve at approximatley 28 and 32 minutes appear to be the same while the slope at 30 minutes is about one-half of the other two.

The data in Fig. III-7 indicates that the temperature rise lagged behind the voltage decay of the cells in the vicinity of the thermocouples at locations #2, 4, 8, 9, 10, 11, and 12 (Table III-1). Temperature versus time curves for four thermocouples near the region where the first declines in cell voltage occurred are shown in Fig. III-9. The cause of the abrupt temperature rise at thermocouple locations #4, 9, and 10 and the generally erratic behavior of these thermocouples is not fully understood, but it may have been due to pickup of spurious voltages or intermittent contacts with molten materials.

The cell heaters on Module D-001 were turned off automatically by the thermal management and control system at about 2330, and the Variac transformers were turned of manually at about 2340.

At 2340 the gas from the vacuum annulus was checked on the mass spectrometer, which showed a peak at Mass No. 40 (argon), thereby indicating a leak from the cell chamber into the vacuum annulus. The ion pump on the annulus stopped operating as a result of the rising pressure, and the sorption pump on the system was activated. At this same time, the thermocouple at location #3 had exceeded the temperature scale (maximum 999.9°C) on the digital meter. The air blower on the concentric cooling tube was activated, and air fans were directed on the outside of the battery.

By 0020, May 31, all of the cells except No. 60 in Module D-001 had reached zero voltage, and by 0045 the temperatures at the various interior thermocouple locations had leveled out in the general range of 750-850°C. The thermocouple on the outside of the insulating containment vessel indicated 113°C; other locations on the surface may have been at lower or higher temperatures. A small amount of condensate (a yellow liquid) had collected in the argon exit line. A subsequent analysis of this material showed the presence of iron and cadmium.

By 0800, May 31, Module D-001 had cooled below the melting point of the electrolyte (352°C), and it was allowed to continue to cool to room temperature. At 1132, the heaters in Module D-002 were turned off, and this module was subsequently cooled at a rate of about 10°C/hr.

Figure III-10 is a view of the modules after the short circuit. In this figure, the insulation caps for the power leads, which are above Module D-001 (left side of photograph), show some charring of the low-temperature tape used

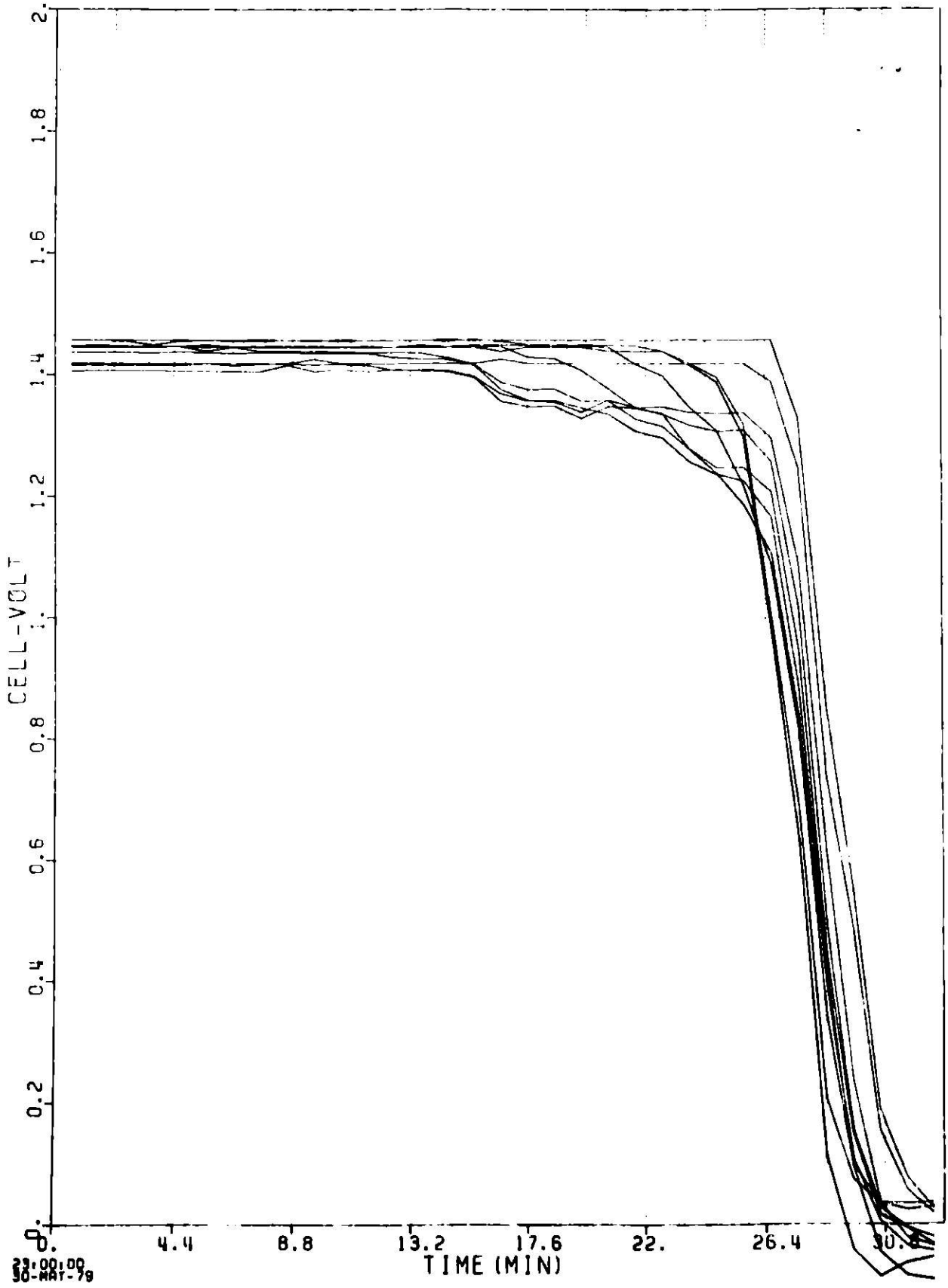

Fig. III-5. Voltage Decrease with Time for Cells 22-31 in Module D-001

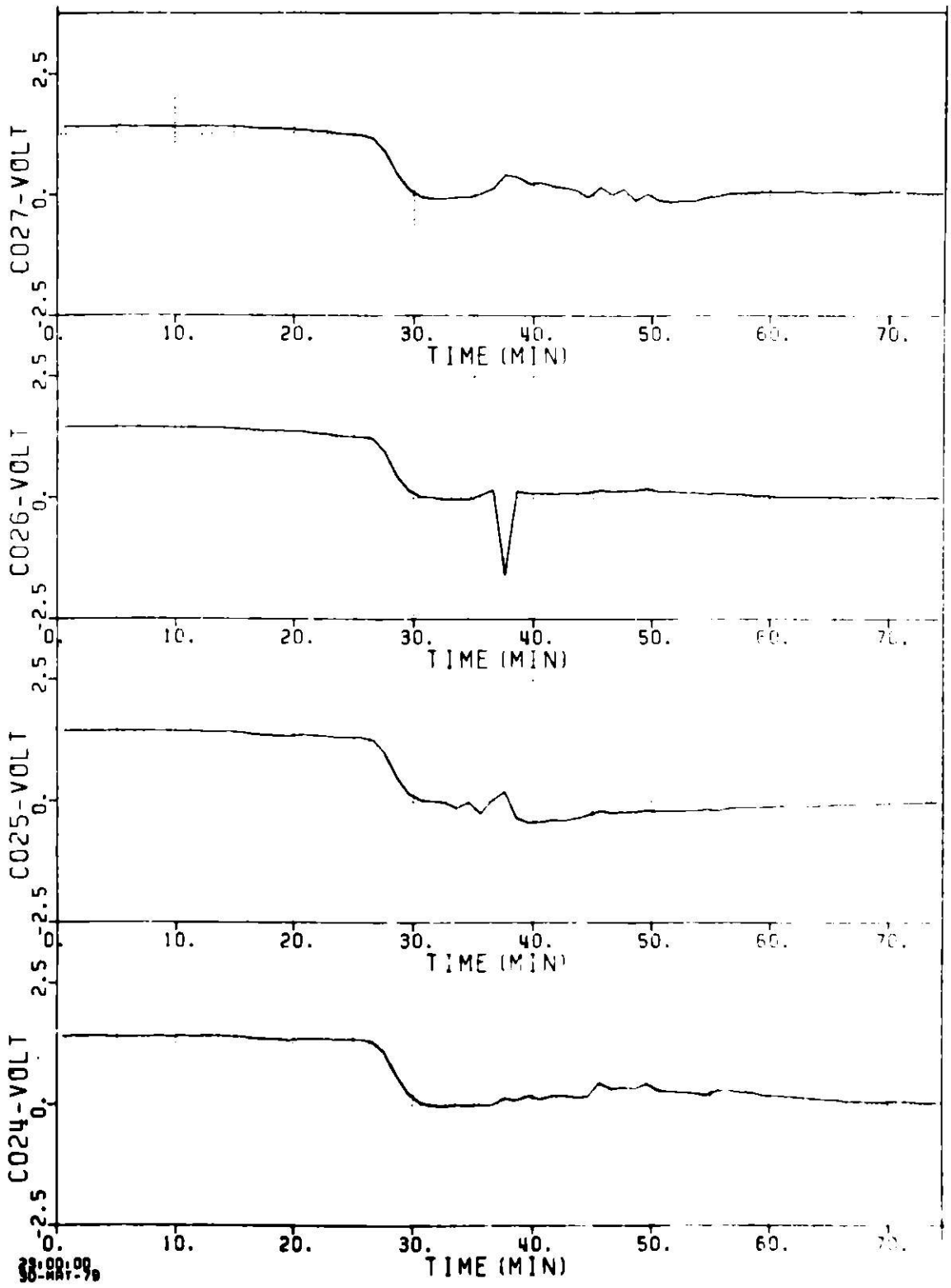

Fig. III-6. Voltage Decrease with Time for Cells 24-27 in Module D-001

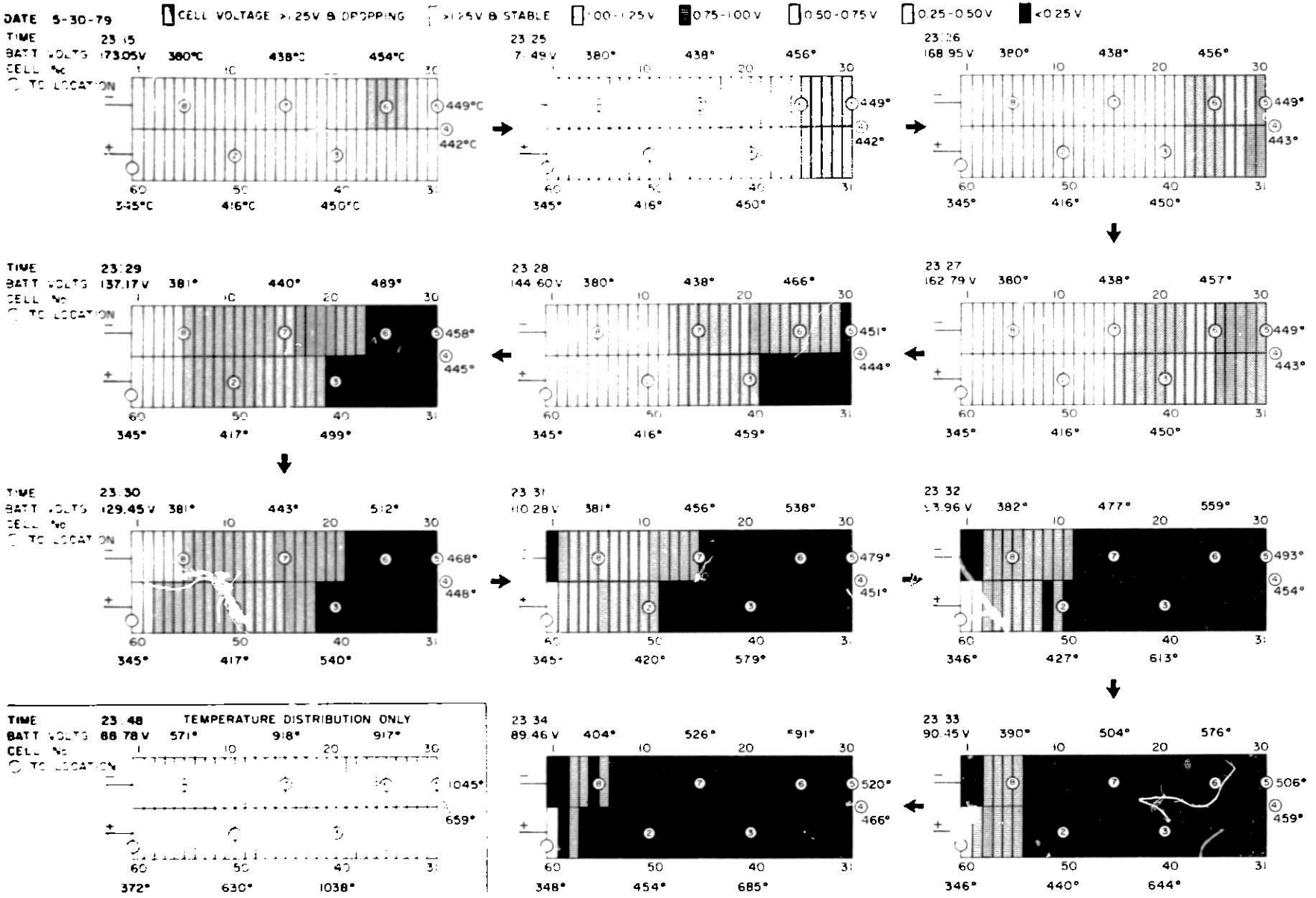

Fig. III-7. Change of Cell Voltages and Temperature with Time in Module D-001

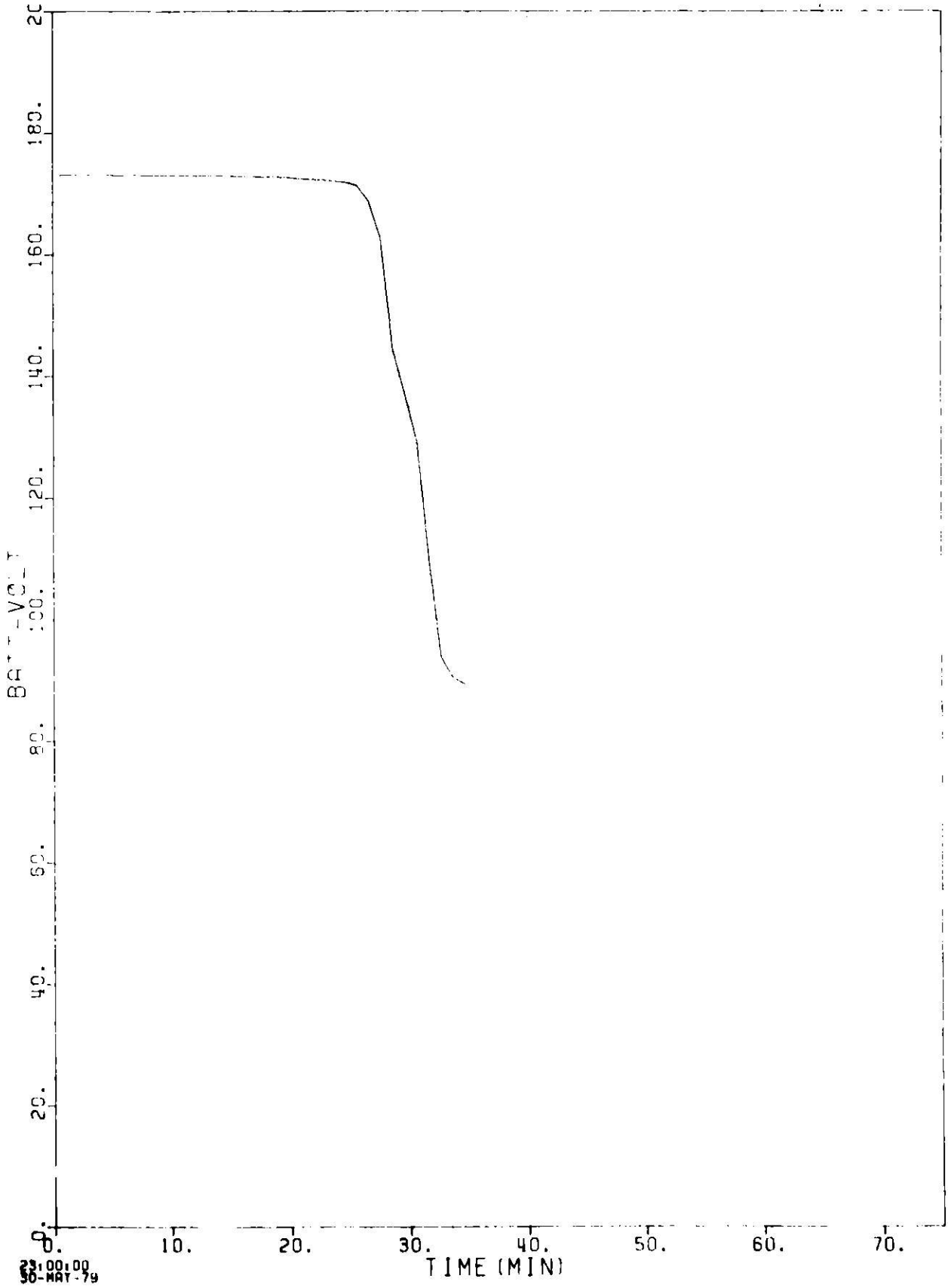

Fig. III-8. Change of Mark IA Battery Voltage with Time

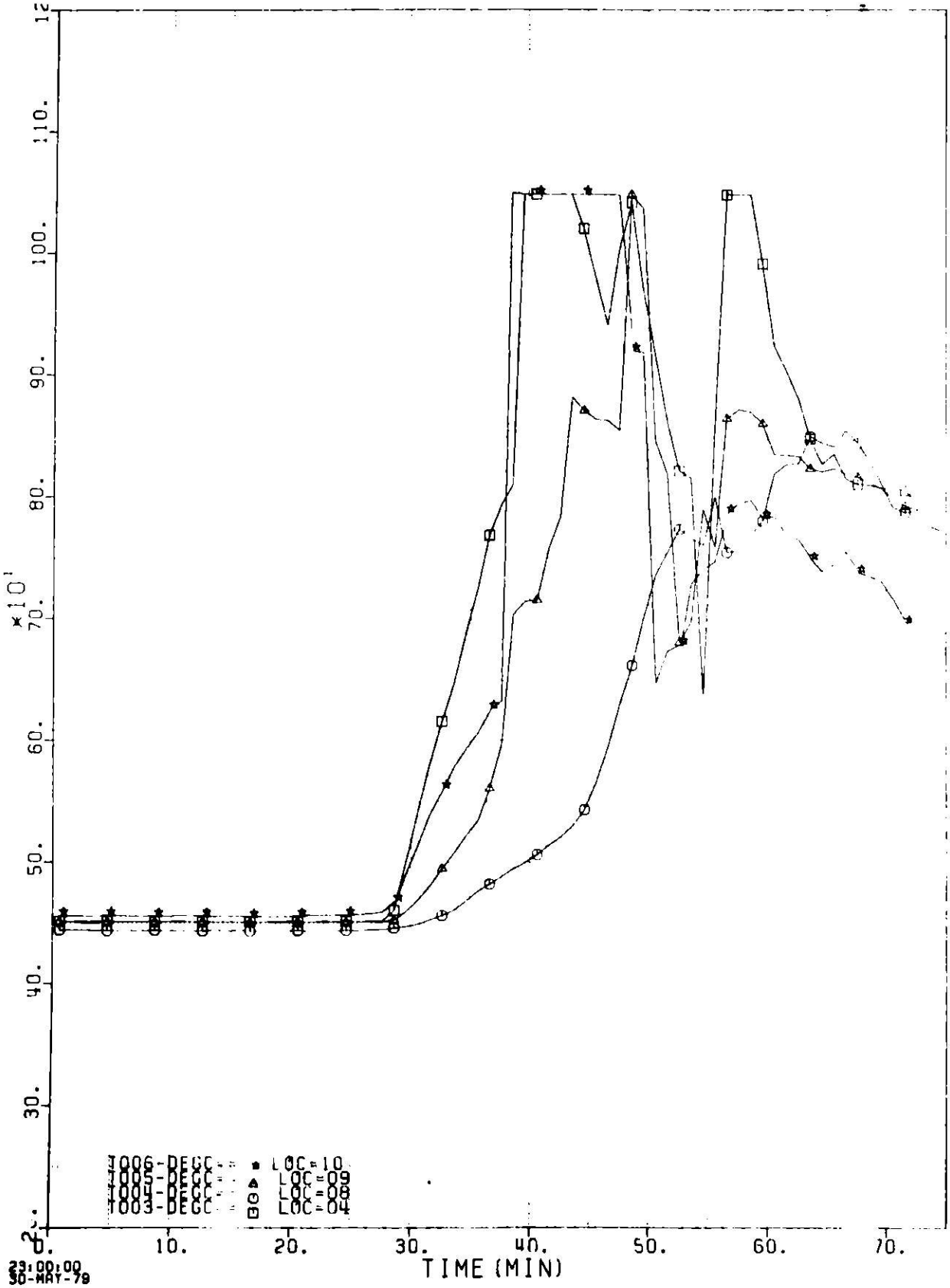

Fig. III-9. Temperatures of Several Thermocouples Near Region where Initial Voltage Decline was Observed

Fig. III-10. Modules in Van after Event

to hold the insulation material in place and to seal the edges of the insulation pads. A view of the cavity in the van after removal of Module D-001 is shown in Fig. III-11. Charring of the tape is noted, but there is no other effect evident from the failure. Module D-001, after removal from the van, is shown in Fig. III-12. There was no discoloration of the Module D-001 case, nor any other visible change in its appearance other than a bowing, which indicated a loss of vacuum in the annulus. (The top and bottom of the outer case were designed to be bowed as fabricated and to be flat when the annulus was evacuated.) Resistance measurements showed that both terminals of the module were in electrical contact with the case. Module D-002 appeared to have been totally unaffected by the failure.

In summary, the module failure resulted in no external breach of the D-001 module case, no detectable release of noxious gases, and no thermal or electrical effects on the adjacent module (D-002). There was a progressive degradation of cell voltage from the rear of the battery module to the front, a thermal rise which lagged behind the voltage decline, a maximum internal temperature >1040°C, and a measured external case temperature of 113°C.

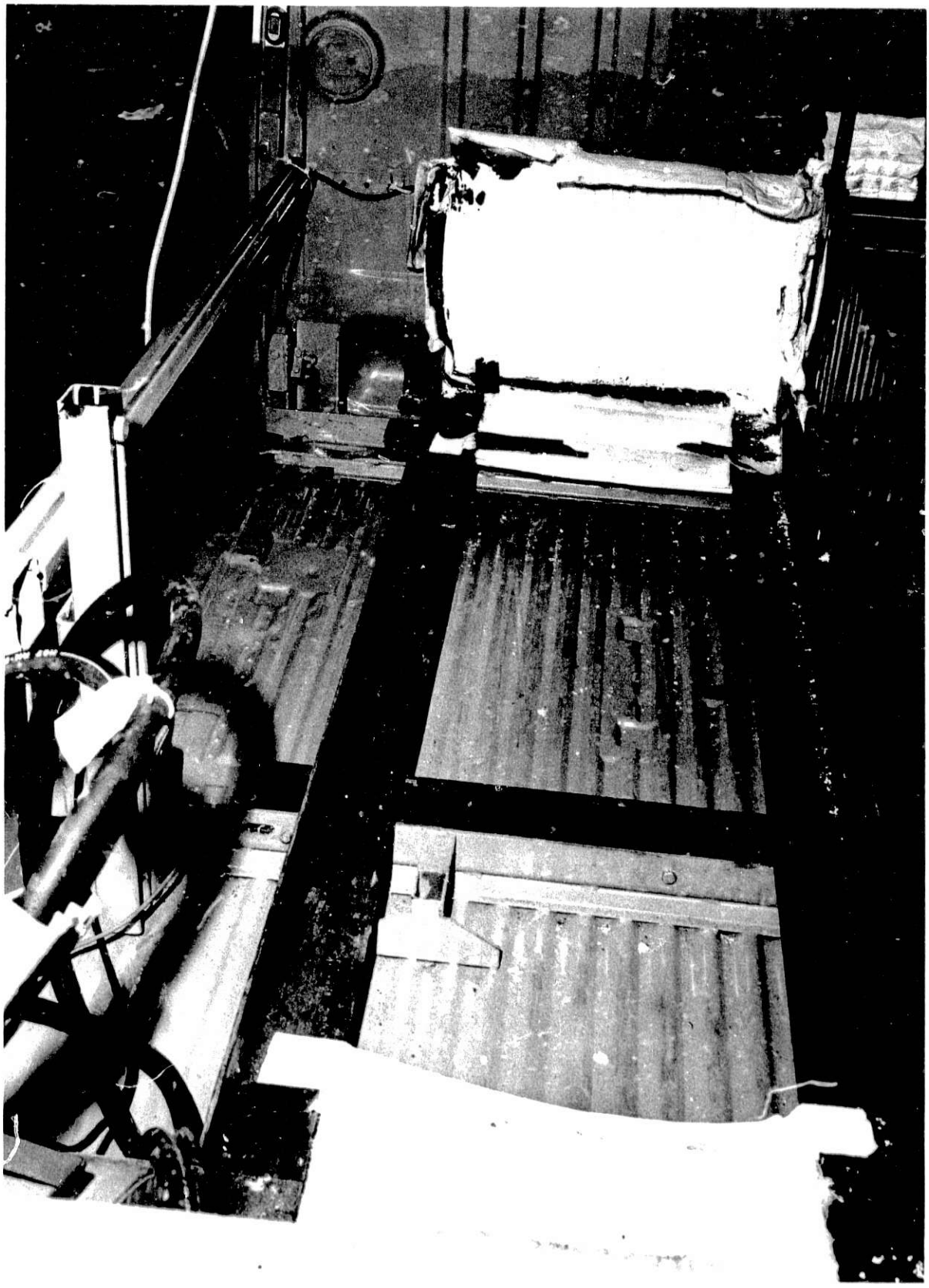

Fig. III-11. Van Floor after Removal of Module D-001

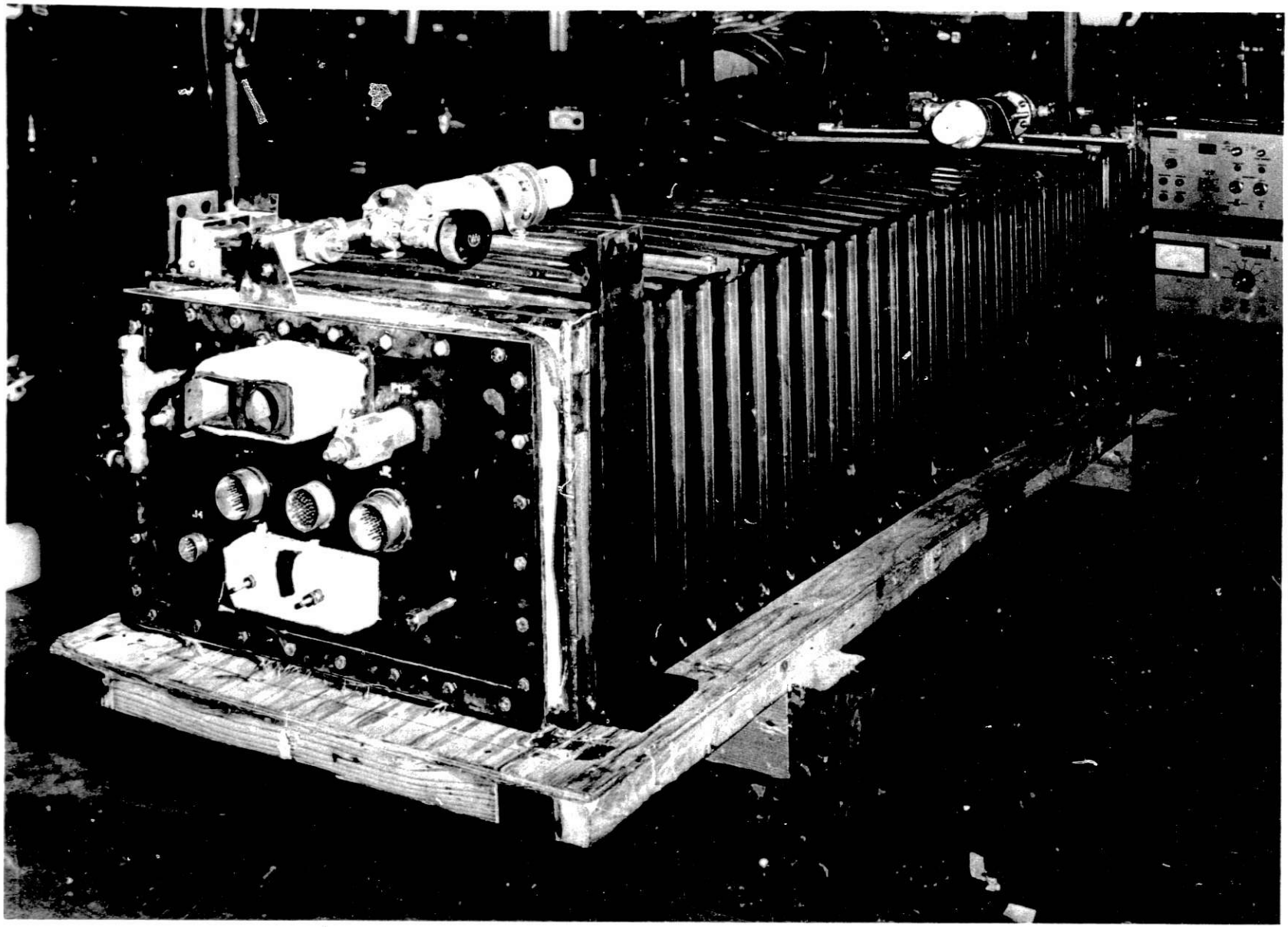

Fig. III-12. Module D-001 after Removal from Van

IV. FAILURE ANALYSIS

Immediately after the failure of Module D-001, the following team was formed to conduct a failure analysis:

V. M. Kolba, Chairman (ANL)
J. E. Battles (ANL)
J. D. Geller (ANL)
K. Gentry (Eagle-Picher Industries)

This team was assigned the task of determining the cause of failure and making recommendations for corrective actions.

A. Procedure

The Failure Analysis Team reviewed the options for disassembling the modules, and decided upon an approach for conducting a thorough examination of the modules and cells. It was decided to obtain a complete photographic record of the examinations; some of these photographs are included in this report. For the post-failure examination, the failed module (D-001) was retained at ANL; the other one (D-002) was shipped to Eagle-Picher for disassembly and examination in their dry room.

The procedures followed prior to disassembly of Module D-001 were as follows. The module was removed from the van; a sample of the gas atmosphere in the module was taken; and the module was purged with argon. The exterior of the module was inspected visually and photographed. Electrical resistance measurements were then made on the individual cells and the electrical resistance heaters. Resistance checks were also made to determine whether there was electrical contact between (1) the cells and the containment vessel, (2) the cells and thermocouples where they were adjacent, (3) the heaters and the containment vessel, (4) the thermocouple leads and the containment vessel, (5) the heaters and the cell equalization leads, (6) the voltage sensing and cell equalization leads, and (7) the battery terminals and the containment vessel or (8) the battery terminals themselves.

Three options were proposed for the disassembly of Module D-001. The first option was to pull the cell tray out of the front of the module, as it was designed to be removed; however, attempts to do this, even with a pulling force of up to 680 kg (1500 lb), failed. The next option was to remove the liner (added to the inside of the containment vessel to correct a difficult-to-repair leak) and the cell tray as a single unit. The seal weld attaching the liner to the containment vessel was ground off, and appropriate pull tabs were welded on the liner (Fig. IV-1). This option also failed, even at pulling loads in excess of 900 kg (2000 lb). The final option was to sacrifice the module case by cutting it apart. A selective procedure was developed and was reviewed at each successive step. This procedure allowed examination of the foil, inner case, liner, cells in the tray, etc., as the disassembly progressed.

For the third option, the outer corrugated case was cut away to expose the aluminum multifoil insulation, which showed melting of the aluminum foil after the first 15 outer layers. The aluminum foil was then removed to

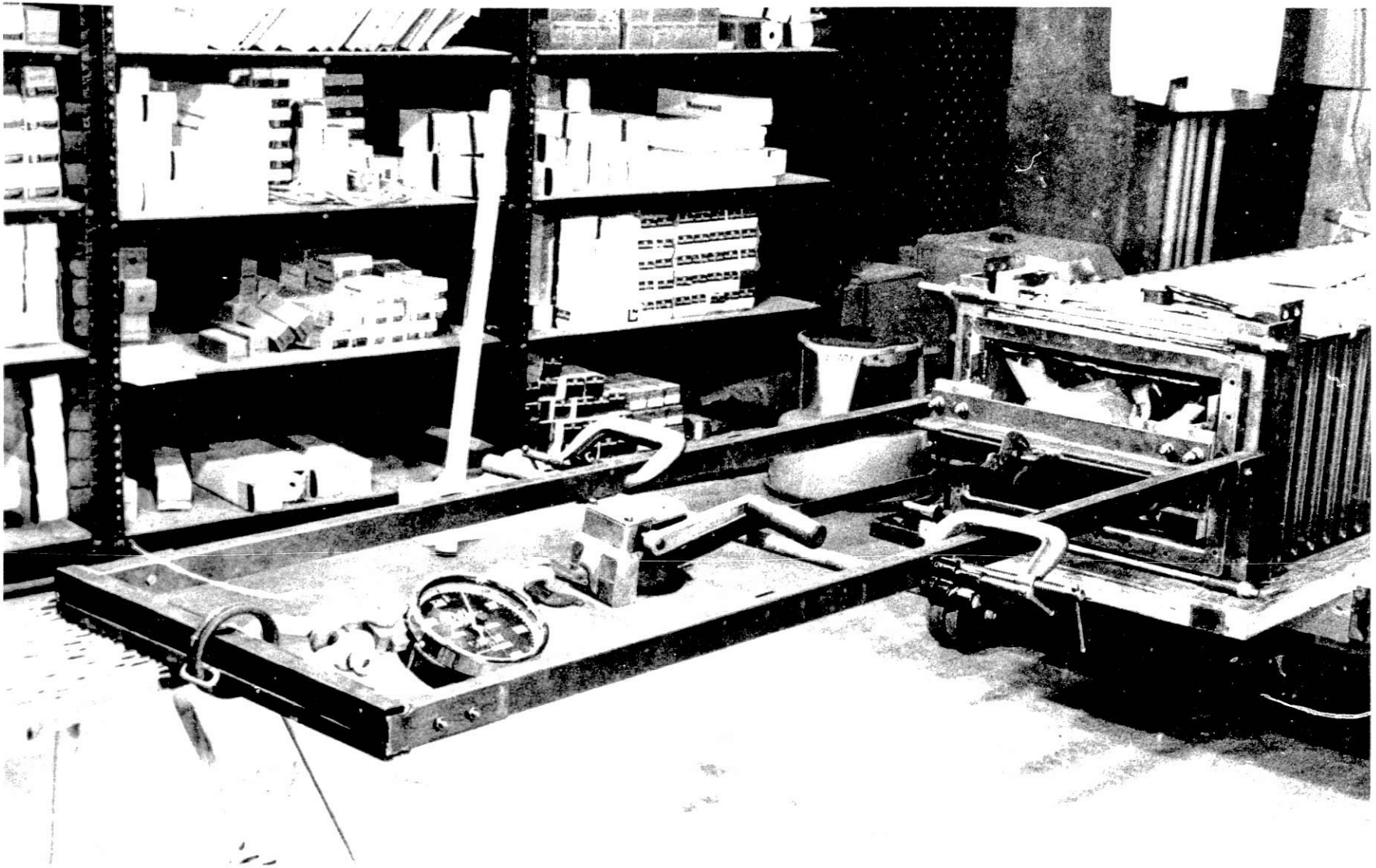

Fig. IV-1. Fixture for Tray Removal

expose the inner stainless steel foil; local reaction areas of the stainless steel and aluminum foil are shown in Fig. IV-2. The large reaction area on the right is in the region of Cell 40. The inner corrugated case was cut off next, and finally the Inconel liner was cut off. After removal of the liner, the insulation sheet which had been placed on top of the cells was exposed; this is shown in Fig. IV-3.

After the module had been taken apart, the exposed cell assembly was examined visually and photographed. Electrical resistance measurements were then made to verify the results obtained prior to disassembly of the module and to obtain additional data. The hardware and insulation in the upper part of the cell tray were removed and examined, and the cell tops and associated components were inspected visually. Critical dimensions of the cells, cell tray, and hardware were measured. The cells were then removed from the tray and examined for shape change, holes, evidence of iron-aluminum reaction, corrosion, weight loss, condition of feedthroughs, and other effects. Selected cells and areas of the cell tray and cross-over straps were subjected to detailed microscopic examination. Chemical analyses were performed to identify corrosion products and various other materials found on the cells and tray. Results of the above examination are presented in detail in the following sections of this report.

B. Examination of Module D-002

After disassembly of Module D-001, it appeared desirable to also examine D-002 in order to aid in the search for clues to understand the initiation mechanisms for failure. In addition, two cells had developed short circuits, as previously noted, and these cells would ultimately have to be replaced. Therefore, the module was disassembled in a dryroom at Eagle-Picher under direction of the Failure Analysis Team. The previously discussed disassembly and post-disassembly procedures were utilized as applicable.

Resistance measurements of this module showed no grounding of the cells to the case or of cells to the thermocouples, and no grounding or short-circuiting of the heaters to the cell tray or case. Although the tray (including cells) was removed from the containment vessel by the designed procedure (option 1), its removal was difficult because of lateral expansion of the tray, which was confirmed later by dimensional measurements. The Vitrabond mica-sheet insulation covering the top of the cells was slightly displaced at the rear portion of the module, exposing parts of the positive terminals on Cells 16 and 46; this may have occurred during removal of the tray from the containment vessel. There was also a slight displacement of the Vitrabond mica insulation sheets at the rear, in the cell tray. However, no physical defects were observed in the Vitrabond mica sheets of the cell tray. The cells were displaced somewhat relative to the cross-over straps of the cell tray, and most cells were convex along the vertical edges, this effect being the greatest at the outside edges adjacent to the cell tray. Also, the level of the tops of the cells was uneven. The short circuits in Cells 33 and 45 were traced to the feedthroughs, which had metallic bridges across the insulators as a result of electrolytic corrosion (see Fig. IV-4). Cell 34 had leaked electrolyte (see Fig. IV-5), and metallographic examination showed localized intergranular corrosion on the external surface only. Pinhole leaks were observed in the seal welds at the tops of Cells 17, 18, 21, 23,

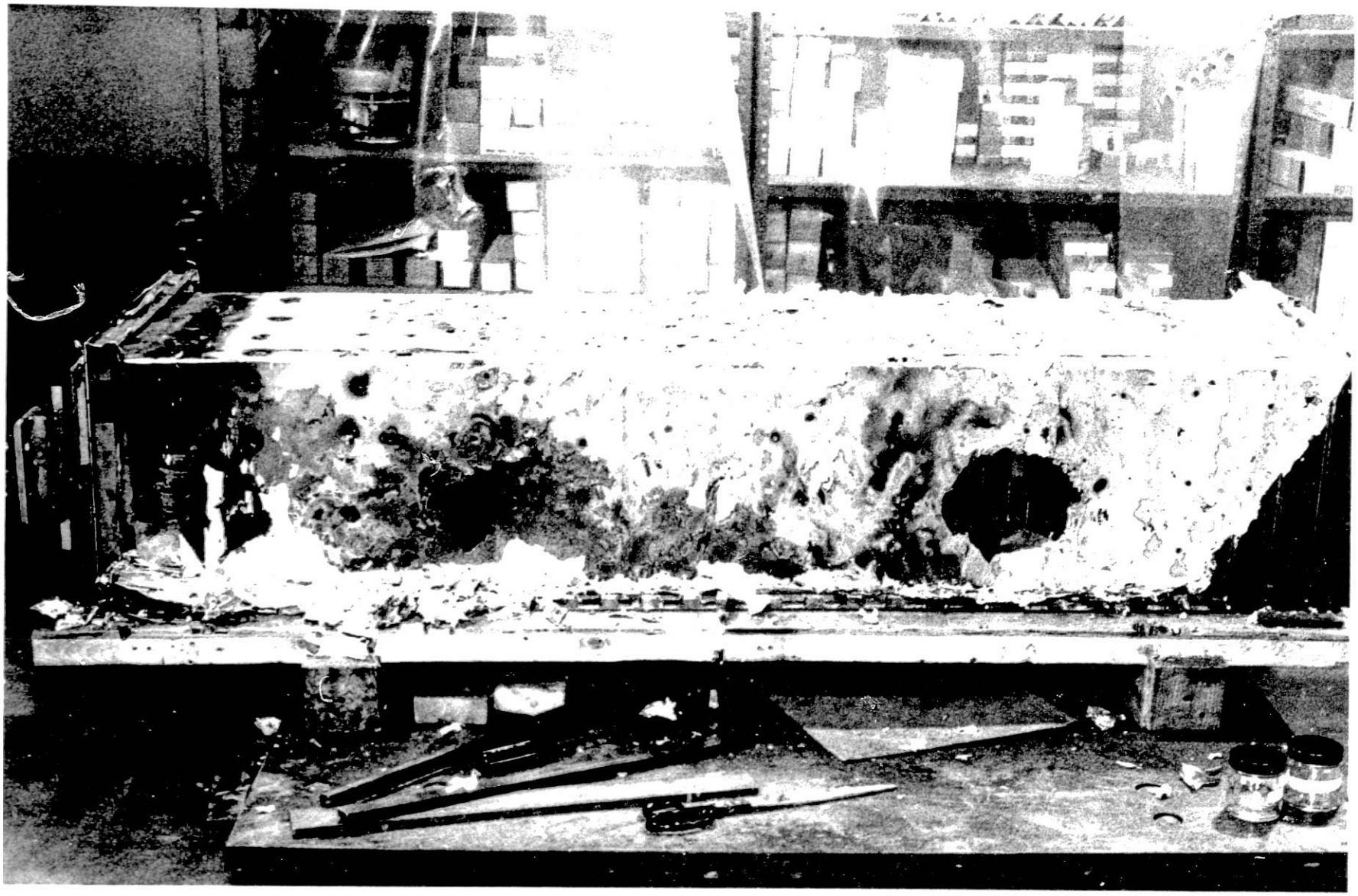

Fig. IV-2. Reaction Areas of Aluminum and Stainless Steel Foil in D-001

Fig. IV-3. Upper Insulation Sheet of D-001

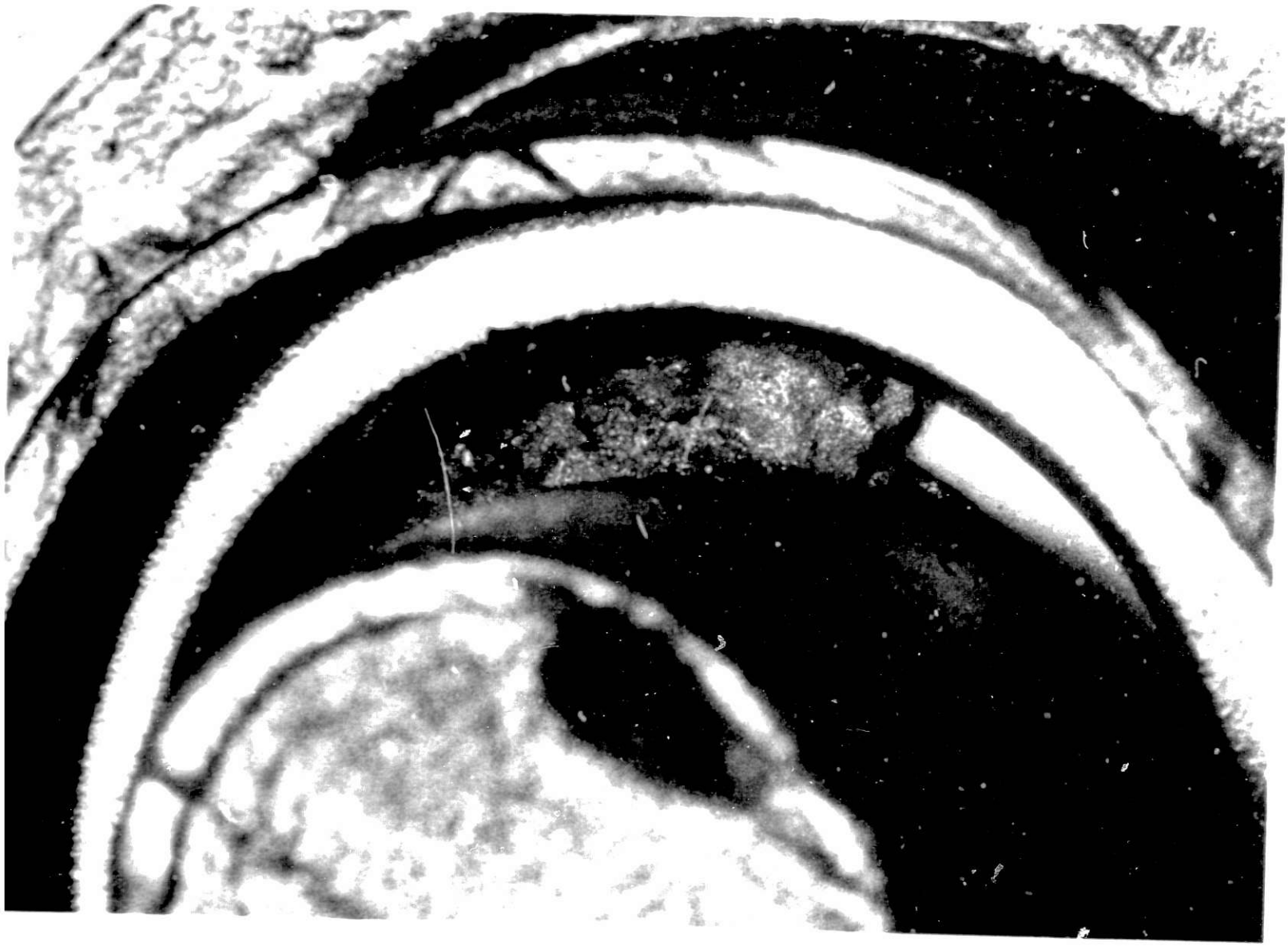

Fig. IV-4. Short Circuit in Feedthrough due to Metallic Bridge

Fig. IV-7. Blast fragment damage from Cell 34 in D-032

32, 43, 48, 52, and 58; this same problem had been observed in earlier tests[1] of individually cycled cells. Braze flux was found on most of the intercell connectors. Several small foreign objects (short steel wires from a wire brush and copper chips) were found in the cell tray.

C. Possible Failure Initiation and Propagation Mechanism

Prior to and during disassembly of the modules, many potential mechanisms for failure initiation and propagation were discussed; these are presented in Table IV-1. Each of these potential mechanisms was reviewed in the light of the data available and observations from the disassembly of Modules D-001 and D-002. The data available included the individual cell voltages, battery voltage, temperatures at eight locations in each module taken at one-minute intervals and the balance of the hourly temperatures, the pressure in the containment vessel annulus (ion pump) and argon purge-gas flow taken at hourly intervals, and the ion-pump current readings recorded continously for each module on a two-pen recorder. Samples of data from these sources were given in Section III of the report.

The investigation proceeded from the outside of the module to the inside. At the same time, all of the external equipment was checked. Results of these investigations are incorporated in the discussions to follow.

1. External Initiation Mechanisms

As shown in Table IV-1, four possible mechanisms for failure initiation outside Module D-001 were considered.

There was a possibility that the positive and negative terminals, external to the battery, had short-circuited. There were no observable indications of inappropriate connections, foreign objects, or arcing at these terminals. A review of the cell voltage data indicated that an external short circuit at these terminals was not the failure cause; such a short circuit would have decreased the entire battery voltage rather than the voltages of certain cells. It was concluded that this was not an initiation or failure mechanism.

The malfunction of the thermal management system was another possible mechanism for initiation of the failure. The off-board AC power to the heaters was limited by Variac transformers and fused at 25 A and 110 V; the fuses did not fail. A review of the temperature data showed (1) that, at the time of the initial voltage decline of Module D-001, all temperatures were normal, and (2) that the thermal rise in the module lagged behind the cell voltage decline. The fail-safe system had operated (evidenced by a flashing light on the console) and had shut the heaters off prior to manual shutoff of the power at the Variac console. Once DC power (12 V) was supplied, the module cooling blower functioned as planned, indicating proper sequencing of the thermal management system. No short circuits or discontinuities were found in the external leads.

Table IV-1. Potential Failure Initiation and Propagation Mechanisms

Failure Initiation -- External
Positive and negative terminals short circuited
Thermal control failure
Short circuits in electrical components
Short circuits in electrical leads
Failure Initiation -- Internal
Contact between cell(s) and cross-over straps
Contact between cell(s) and cell tray
Cell-to-tray electrical contact due to electrolytic corrosion
Contact between cell series jumper and cell
Dielectric breakdown of Vitrabond mica and Raybestos sheet insulation
Contact between electrical leads and cells
Foreign materials
Arcing between cells and cell tray across an argon gap
Localized overheating by heaters
Chemical reactions within the cells
Dielectric breakdown of insulation saturated with electrolyte
Incorrect thermocouple readings
Nonuniform heat-up of the cells
Failure Propagation
Electrolyte leakage from cells
Melting and flow of braze alloy and/or copper
Chemical reactions within cells
Cell expansion
Metallic bridges caused by electrochemical corrosion
Corrosion or short circuits caused by braze flux
Thermal effects
Dielectric breakdown of insulation saturated with electrolyte
Arcing

Short circuits in the electrical components used to monitor the battery performance were also a possible initiator of the event. Resistance measurements of the electrical components (e.g., distribution box, CAMAC data acquisition unit and other instrumention) showed no short circuits or unplanned grounds. Thus, short circuits in the electrical components were not an initiator.

Based on the above observations, it was concluded that the mechanism for failure was not external to the module.

2. Internal Initiation Mechanisms

Thirteen possible mechanisms for failure initiation inside Module D-001 were considered.

Observations indicated that some movement of the cells with respect to the tray had occurred. This movement was caused by cell expansion brought about by rapid discharge and/or high internal temperatures. Figure IV-6 is a photograph of the module and shows the shift in position of the cells relative to the intercell connectors and to the cross-over straps (employed to restrain the sides of the cell tray at the top). Figure IV-7 indicates schematically the observed movements. Little or no swelling of Cell 59 occurred; this may be because Cell 60 did not discharge until approximately 2.5 hr after the event. The cross-over straps had contacted the fill tubes at Cells 10, 20 and 29 (Figs. IV-8 and IV-9) and had contacted the feedthrough housing of Cells 41 and 51 (Fig. IV-10). Evidence of arcing was observed between the strap and fill tube of Cell 29 and between the strap and feedthrough housing of Cell 41. Straps by Cells 10 and 41 were broken, having the appearance of a brittle fracture.

Another possible initiation mechanism is mechanical contact of the cells with the tray. During examinations of Modules D-001 and D-002, gaps were observed at the butt joints of the mica insulation pieces within the cell tray. These butt joints of the insulation were located at the edge along the sides and bottom (at Cells 15-16 and 45-46). After removal of the cells, the bottom mica sheet at the rear of the module was found to be ruptured along the center line between the two rows of cells. On removal of the mica from the tray, there was evidence that arcing had occurred between the cells and the tray. An overall view of the tray is shown in Fig. IV-11. Evidence of reactions that had occurred at Cells 10 and 11, Cells 15 and 16, and Cell 24 is shown in Figs. IV-12, IV-13, and IV-14, respectively. There was also a metallic residue, determined to be Li-Al, on the tray bottom between Cells 1-2 and 59-60 (see Fig. IV-15). Deposits of Li-Al were also found on the tray angles near Cells 10-11 and 32-33. Formation of molten Li-Al alloy requires temperatures in excess of 600°C, as indicated by the phase diagram of the Li-Al system (Appendix D).

Electrolyte was present on all the cells and on the liner at the module header; therefore, short-circuiting of cells to the tray as a result of electrolytic corrosion is a possible initiation mechanism. The cell tray was corroded along the edge (Fig. IV-16) and down the middle (Figs. IV-17 and IV-18). Metallographic examination of the tray showed intergranular attack in the reacted areas. Cell cans were corroded at the bottom edges (Fig. IV-19), corresponding to the center line and edge of the tray. The copper conductors on top of some cells were corroded.

Short circuits formed by electrolytic corrosion of electrical feedthroughs had been observed in previous cell tests[2] as well as in the two cells that had developed short circuits in Module D-002. Tests at ANL and Eagle-Picher have shown that very severe corrosion of iron will occur at low voltages across a space filled with electrolyte. In addition, low voltages (<2.5 V) have been shown to support relatively large currents (about 6 A) through an electrolyte depth of 0.076 cm at a butt joint (cross section, 0.05 x 7 cm) formed by two Vitrabond mica insulation sheets between two iron plates.

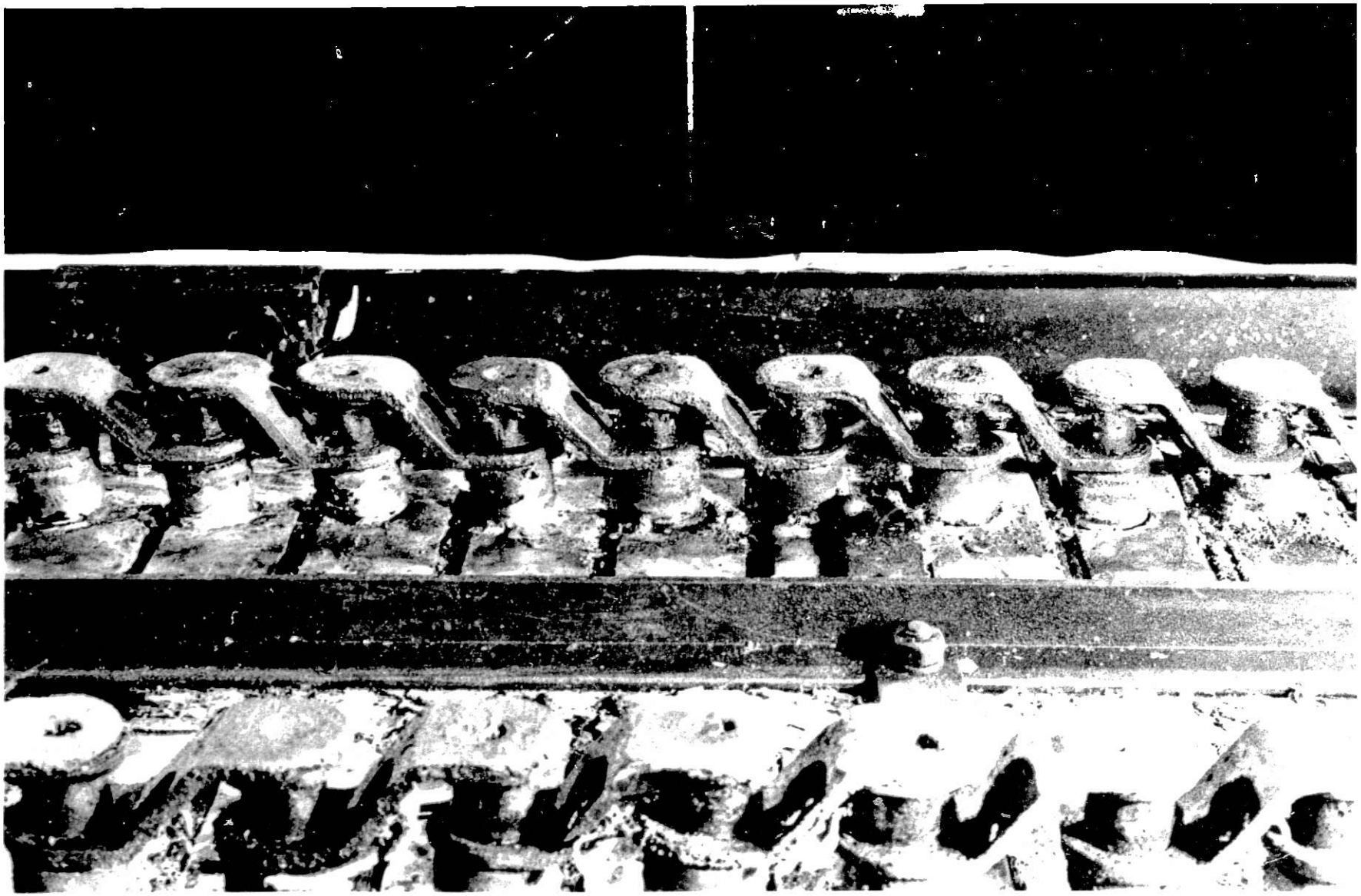

Fig. IV-6. View of Effects of Cell Movement with Respect to Cross-over Straps

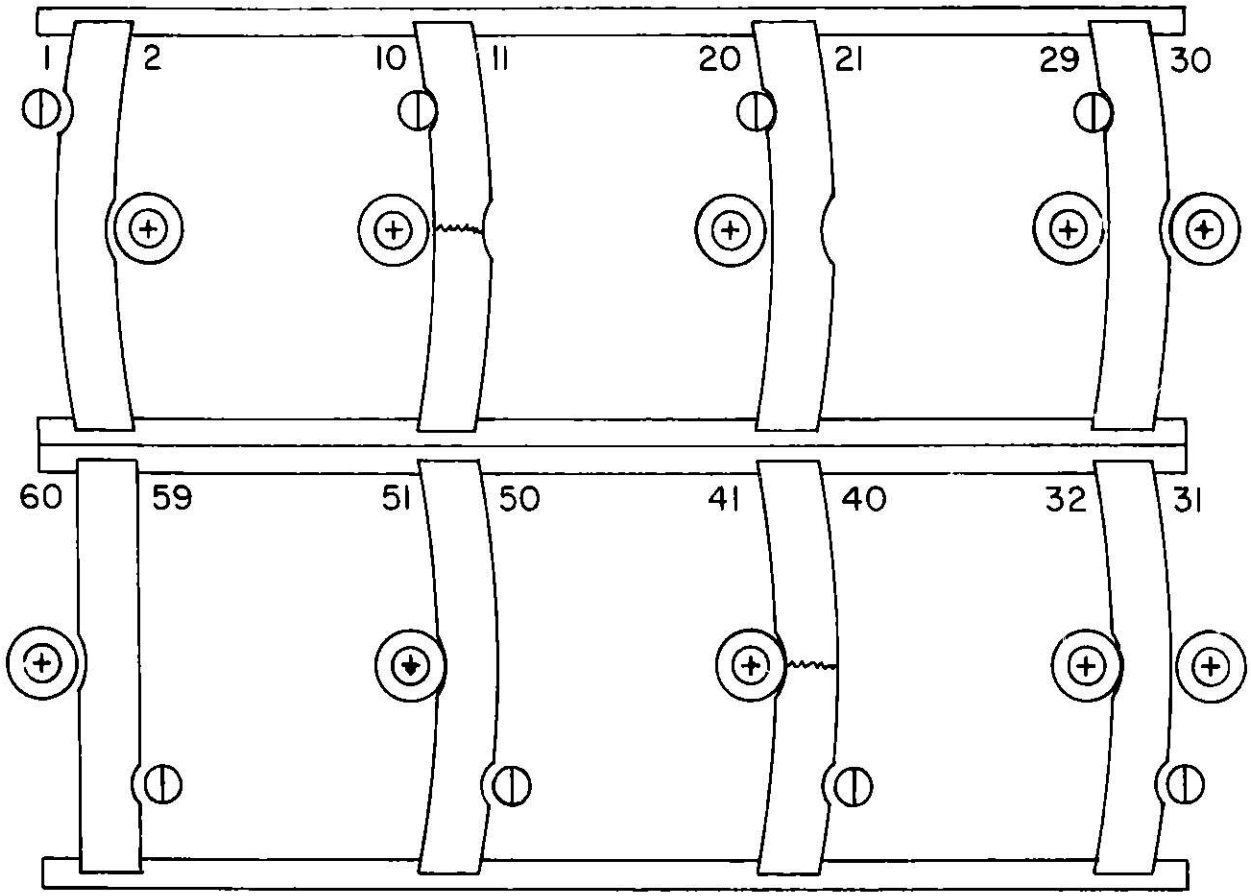

Fig. IV-7. Schematic Representation of Displacement of Cross-over Straps

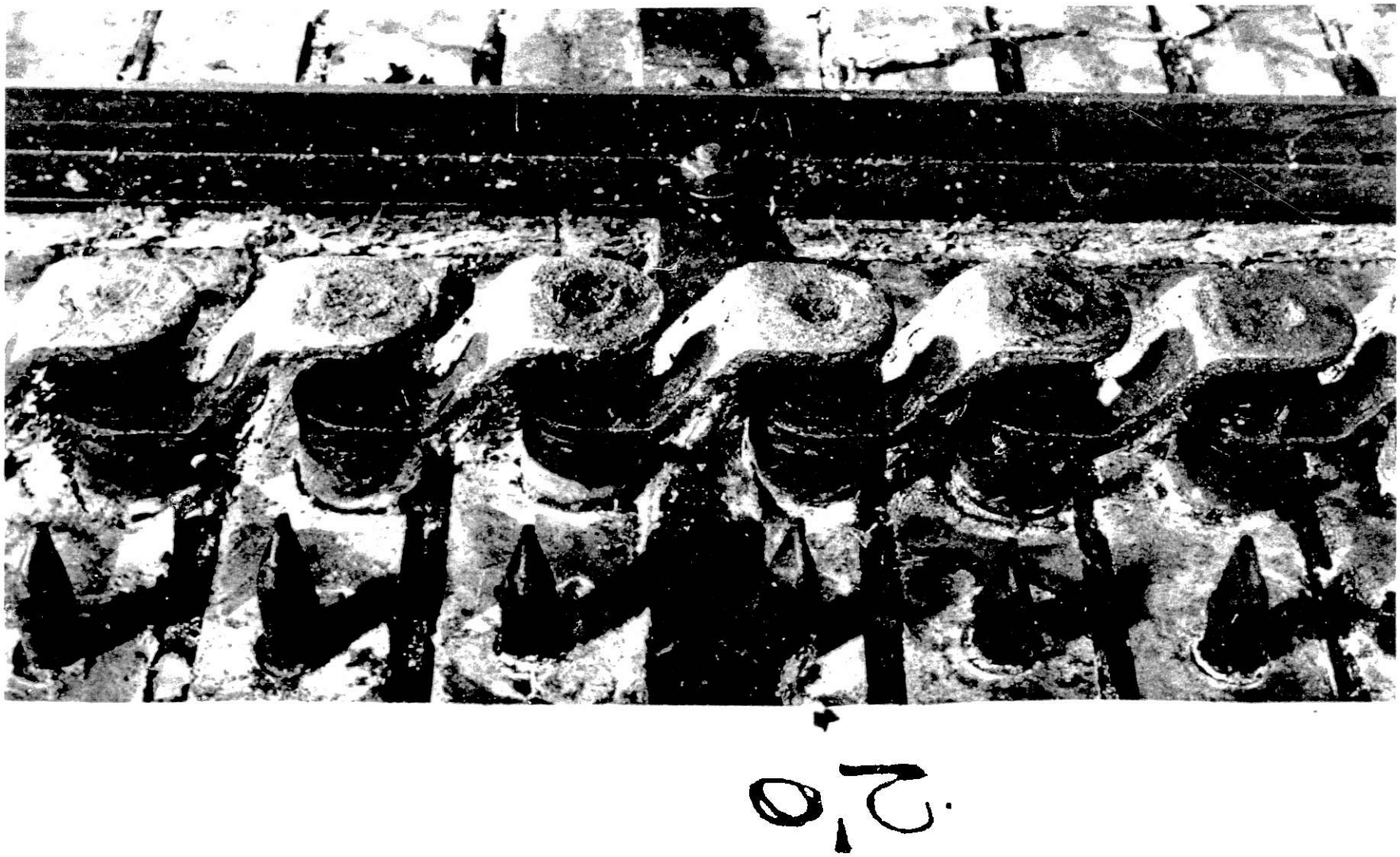

Fig. IV-8. Contact of Cross-over Straps with Fill Tube of Cell 20

Fig. IV-9. Closeup of Contact Area on Fill Tube

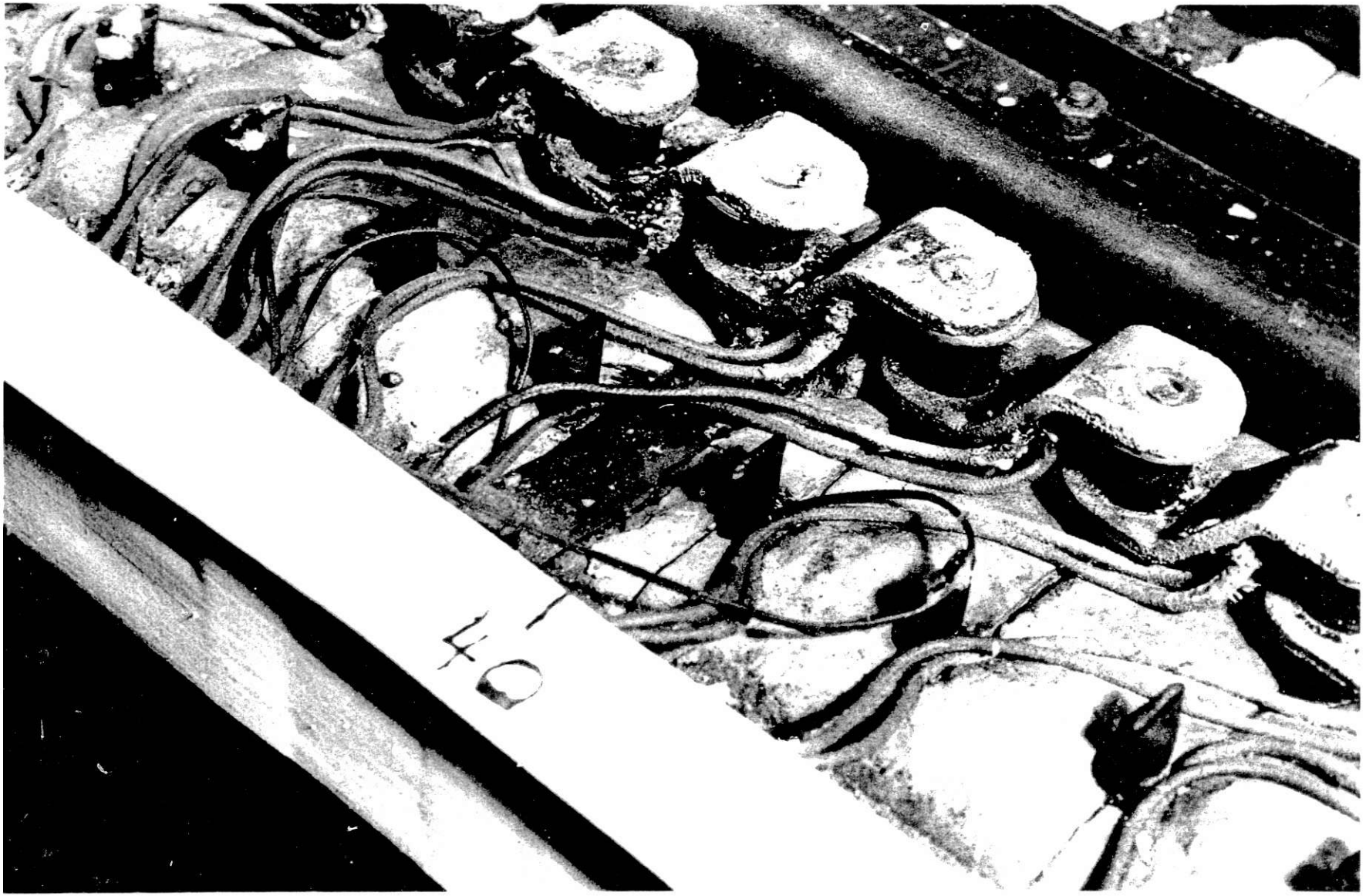

Fig. IV-10. Contact of Cross-over Strap and Feedthrough Housing of Cell 41

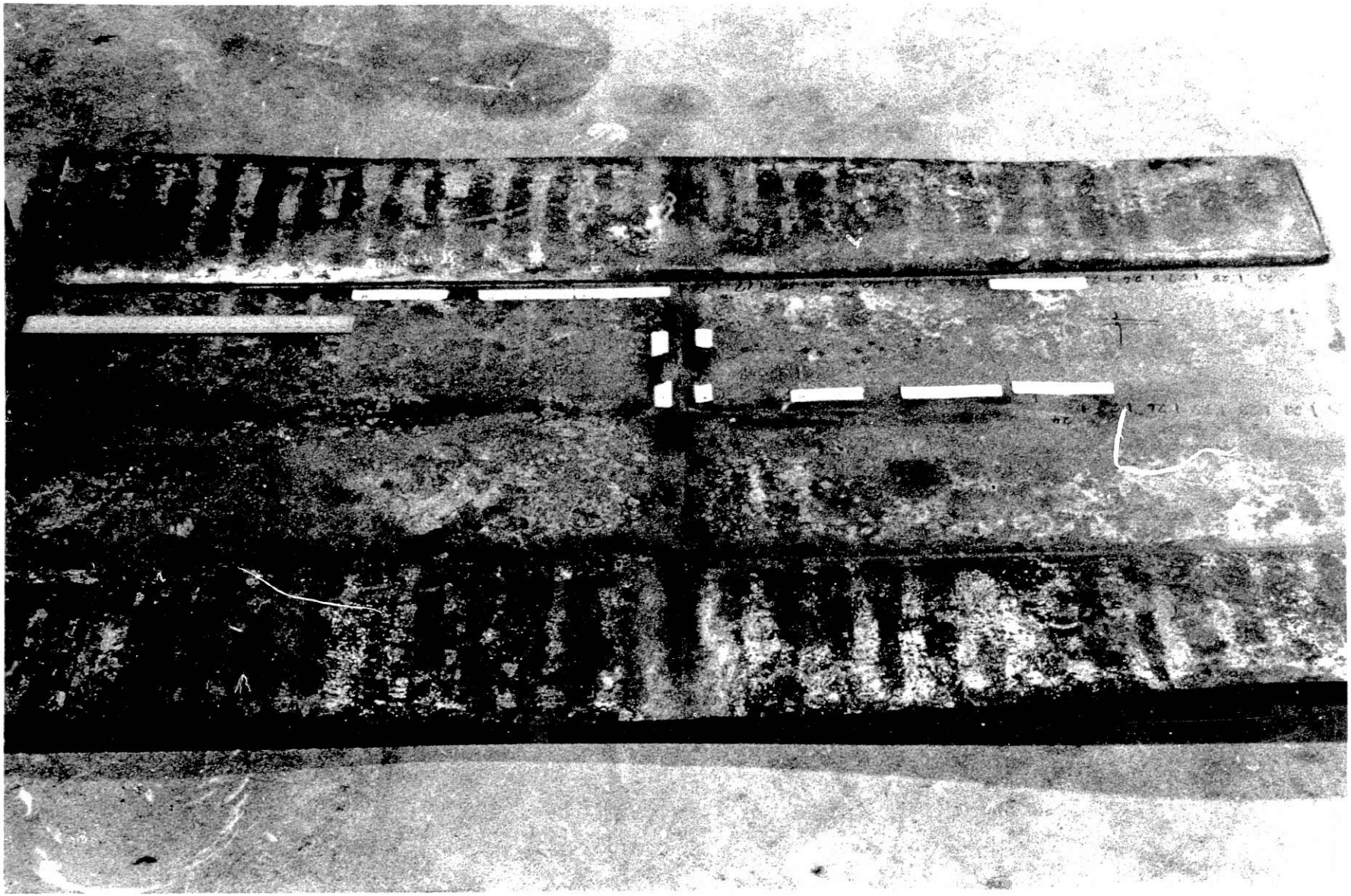

Fig. IV-11. View of Tray Bottom Showing Reaction Areas

Fig. IV-12. Reaction at Edge of Tray Bottom in Regions of Cell 8 to 10

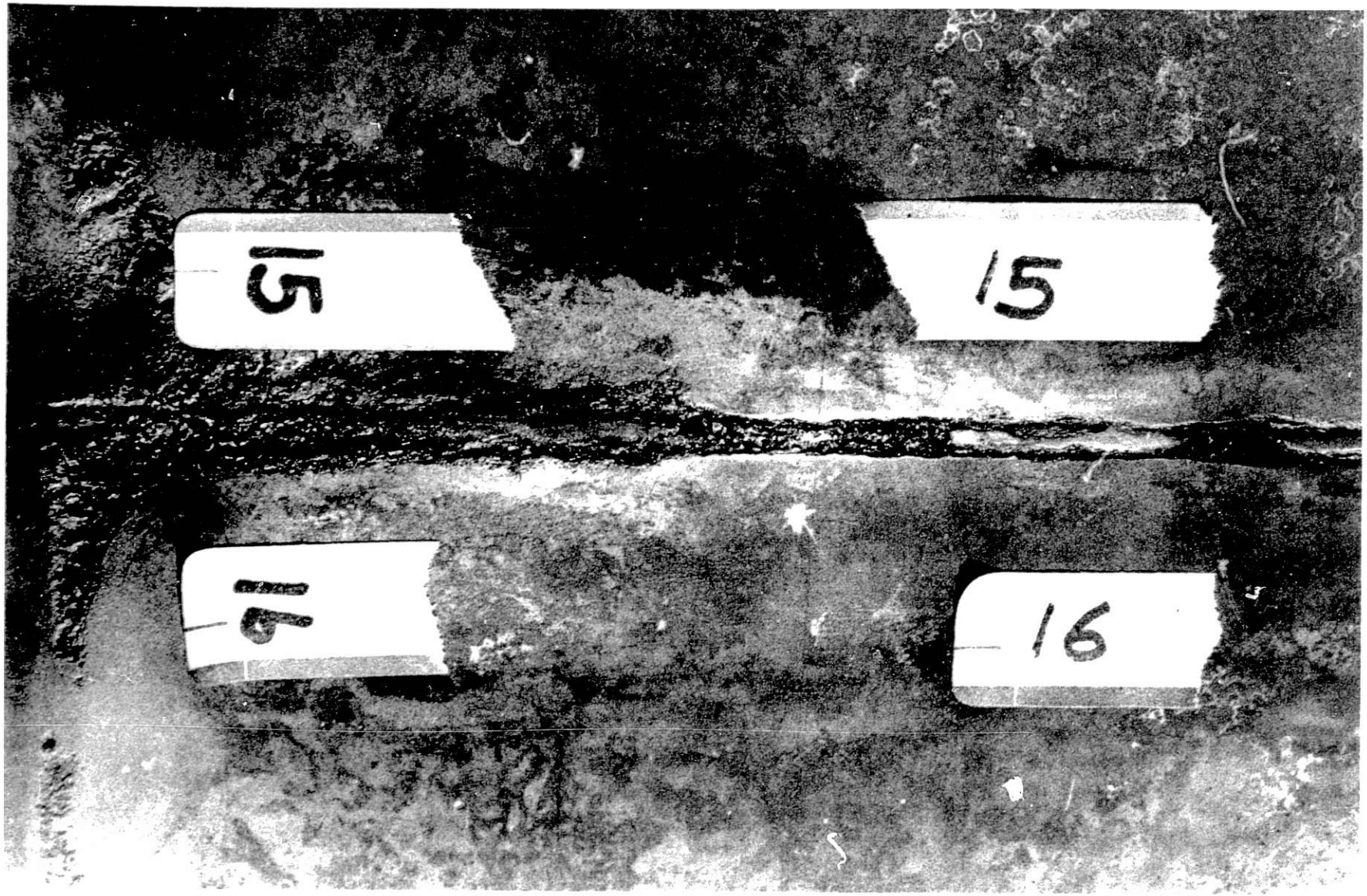

Fig. IV-13. Reaction of Tray Bottom Between Cells 15 and 16

Fig. IV-14. Reaction at Edge of Cell Tray Bottom in Regions of Cells 23 to 25

Fig. IV-15. Metal Deposit on Tray Bottom at the Junction of Cells 1, 2, 59 and 60

Fig. IV-16. Reaction at Edge of Tray Bottom in Region of Cells 13 to 15

Fig. IV-17. Weld Joint along Center Line at Tray Bottom

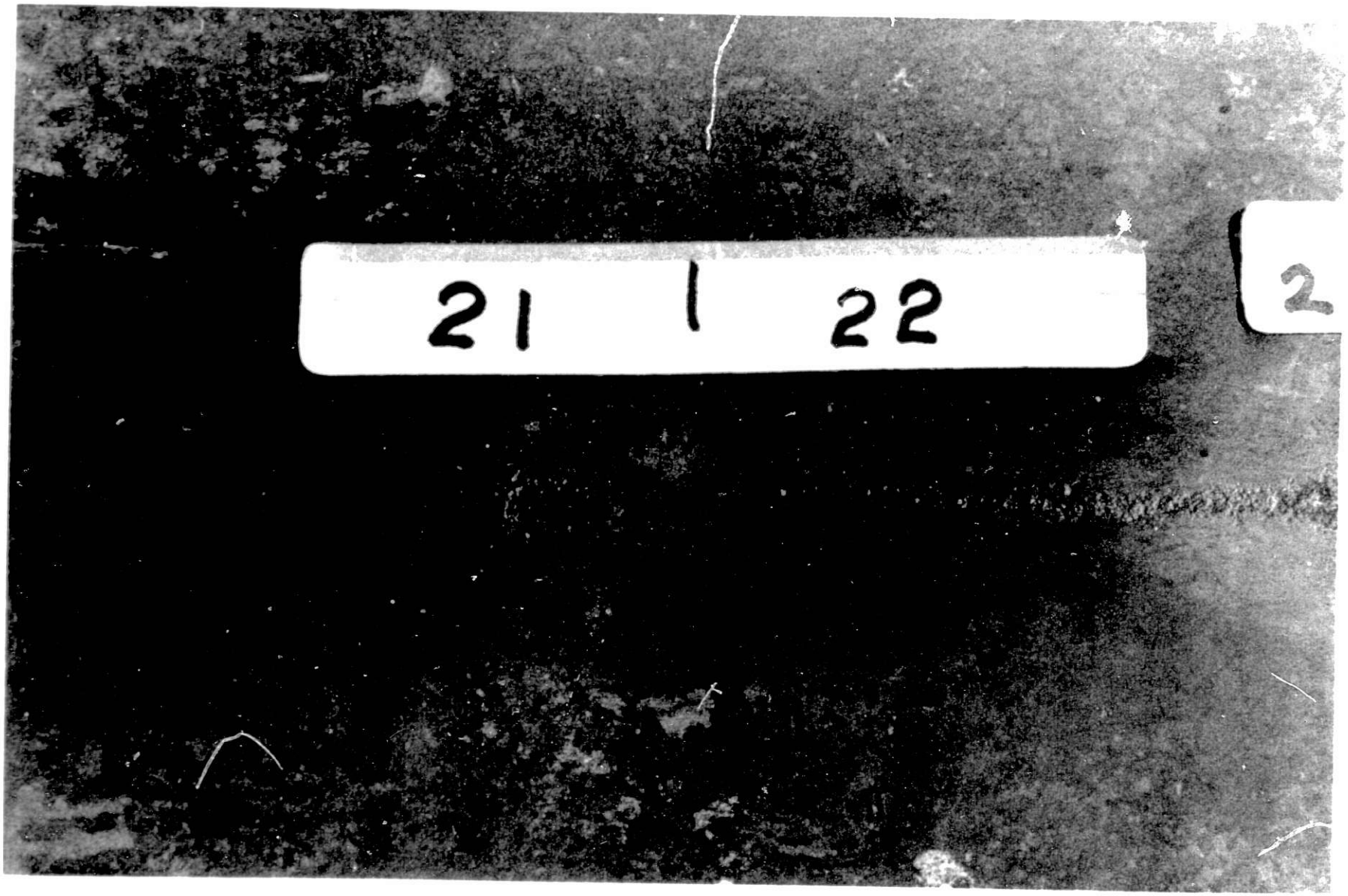
21 | 22
2

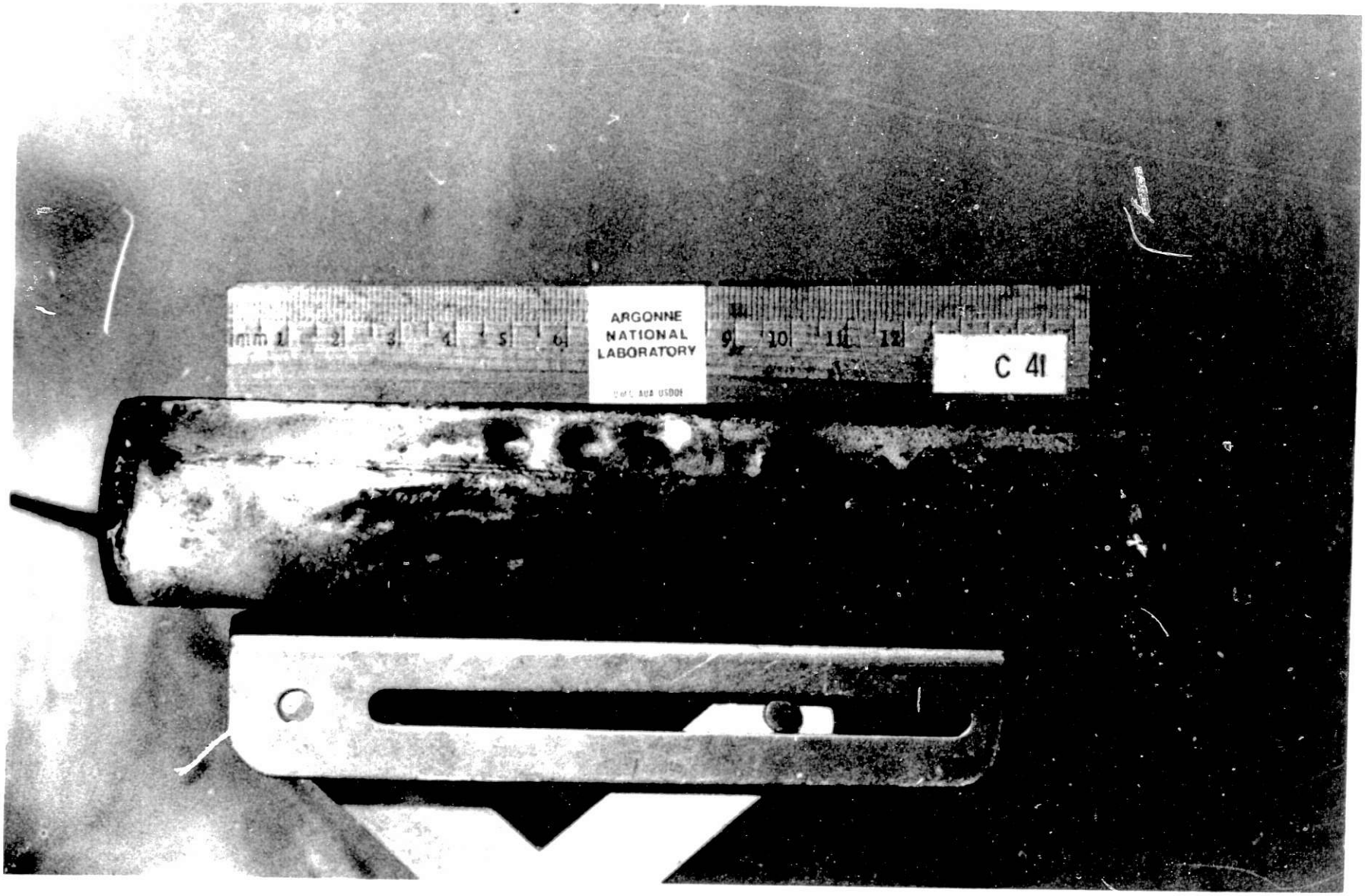

Fig. IV-19. Typical Reaction at Bottom Edge of Cell (Adjacent to Tray Center Line)

Mechanical contact was possible between the series jumper and the cell tray at the rear of the module. Visual observation showed that there was no contact between the series jumper and the cell tray (Figs. IV-20 and IV-21) and that the Raybestos insulation remained intact between the jumper and the center "T" bar.

Another possible failure mode was the dielectric breakdown of the Vitrabond mica and Raybestos insulation. Dissociation of mica [$KAl_2(OH)_2$-$AlSi_3O_{10}$] and asbestos [$Mg_3Si_2O_5(OH)_4$] is known to occur; however, past use of these materials in cell tests had shown no dielectric breakdown. There was no evidence of dielectric breakdown of the Vitrabond mica or Raybestos insulation in either module. Previous thermogravimetric analyses of these battery insulating materials had shown a continuing dissociation of Raybestos after 24 hr at 460°C, yielding CO_2, H_2O and CH_4 with a weight loss of about 4%. Vitrabond mica showed very little H_2 or H_2O at 450°C after 19 hr in a gas stream, either by gas chromatography or mass spectrometric analysis. Because of this, attempts had been made to minimize the use of Raybestos in the Mark IA battery, and to use Vitrabond mica wherever possible. Other insulating materials--Samox, Min K, and glass tape--were all stable after 24 hr at operating temperature.

Contact of electrical leads with other leads or cells is a possible failure initiation mechanism. The electrical leads used in the battery were Samox-insulated, nickel-clad copper for the 16-gauge equalizer wires and the 20-gauge voltage sensing wires. The thermocouples were glass-cloth insulated Chromel-Alumel (28 gauge). There was no evidence of short circuits between leads or between leads and the cells; furthermore, no evidence existed of leads having been melted. A thermocouple lead was in mechanical contact with the fill tube on Cell 41 (Fig. IV-10), but there was no electrical contact. The small wire size of the thermocouple would not support large currents. Estimates of the current capacity at 460°C indicate that the equalizer wires would melt at >25 A, the voltage sense wires at >15 A, and the thermocouple wires at >5 A. It was concluded that electrical lead contact was not an initiation mechanism.

Residual foreign materials in the module could have caused short circuits. Visual inspection of the battery as it was disassembled uncovered no large foreign objects. However, because of the deteriorated condition of module D-001, small foreign objects of the type found in D-002 would probably not be detectable. Such objects, if present, might have initiated the failure, although this failure mechanism seems unlikely. Figures IV-22 and IV-23 show the deteriorated condition of the two sides of the battery, which was evident after the sides of the tray were bent down.

Arcing between the cells and the tray or between adjacent cells across an argon gap might have occurred. Evidence of arcing was observed in several areas of the cell tray. Two holes completely penetrated the bottom of the tray in the region of Cells 15-16; metallographic examination of these areas indicated melting of the area around the hole. Conditions required for arcing have not been established for the battery environment; those conditions may involve the effects of temperature, voltage, electrode distance, electrode area, and gas composition (e.g., impurities such as electrolyte, metal vapors, etc.). Examination of Module D-002, which was heated under an argon purge gas at atmospheric pressure to 460°C, showed no evidence of arcing.

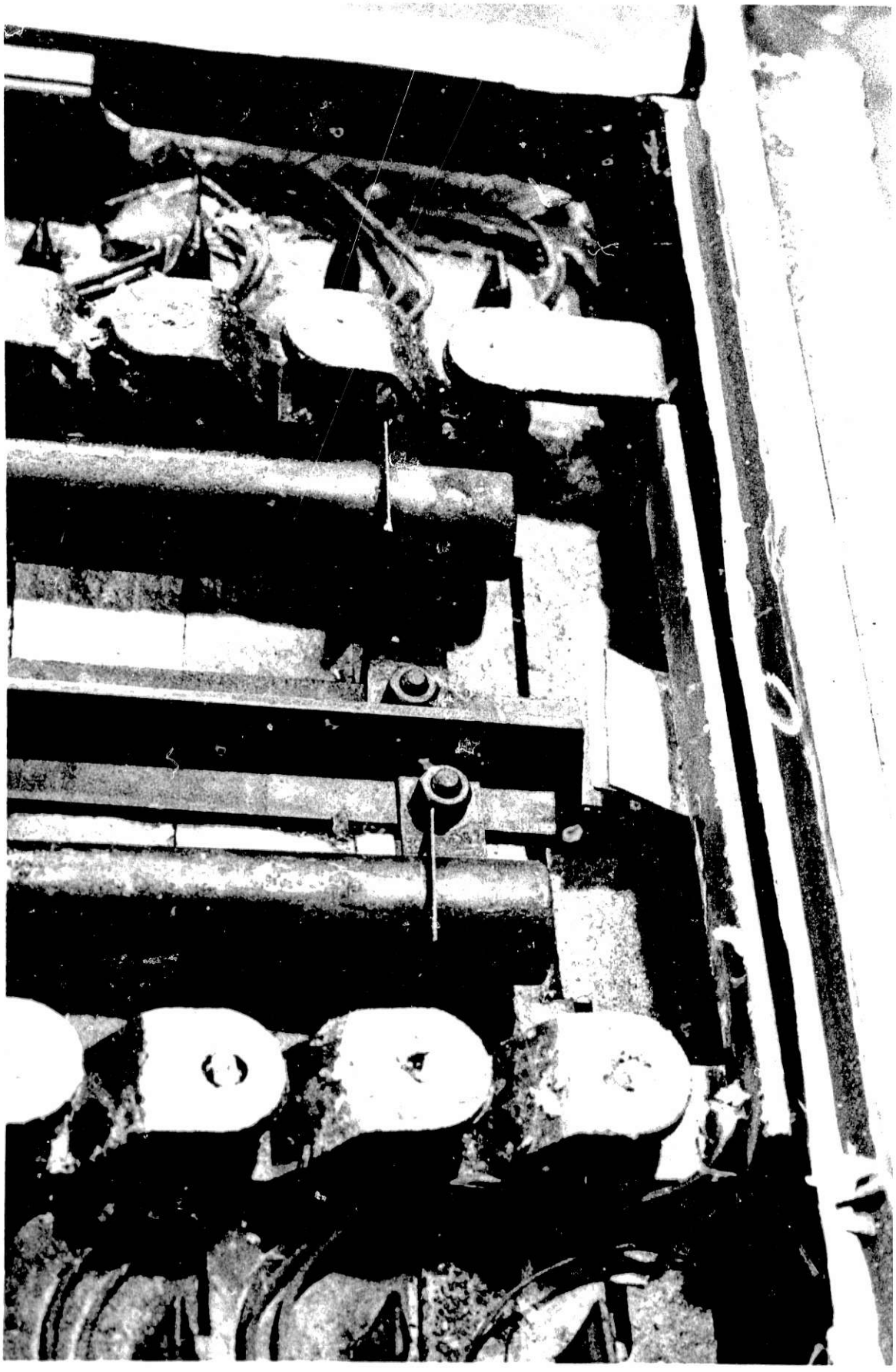

Fig. IV-20. View of Region of Series Jumper

Fig. IV-21. View of Series Jumper from Tray Rear

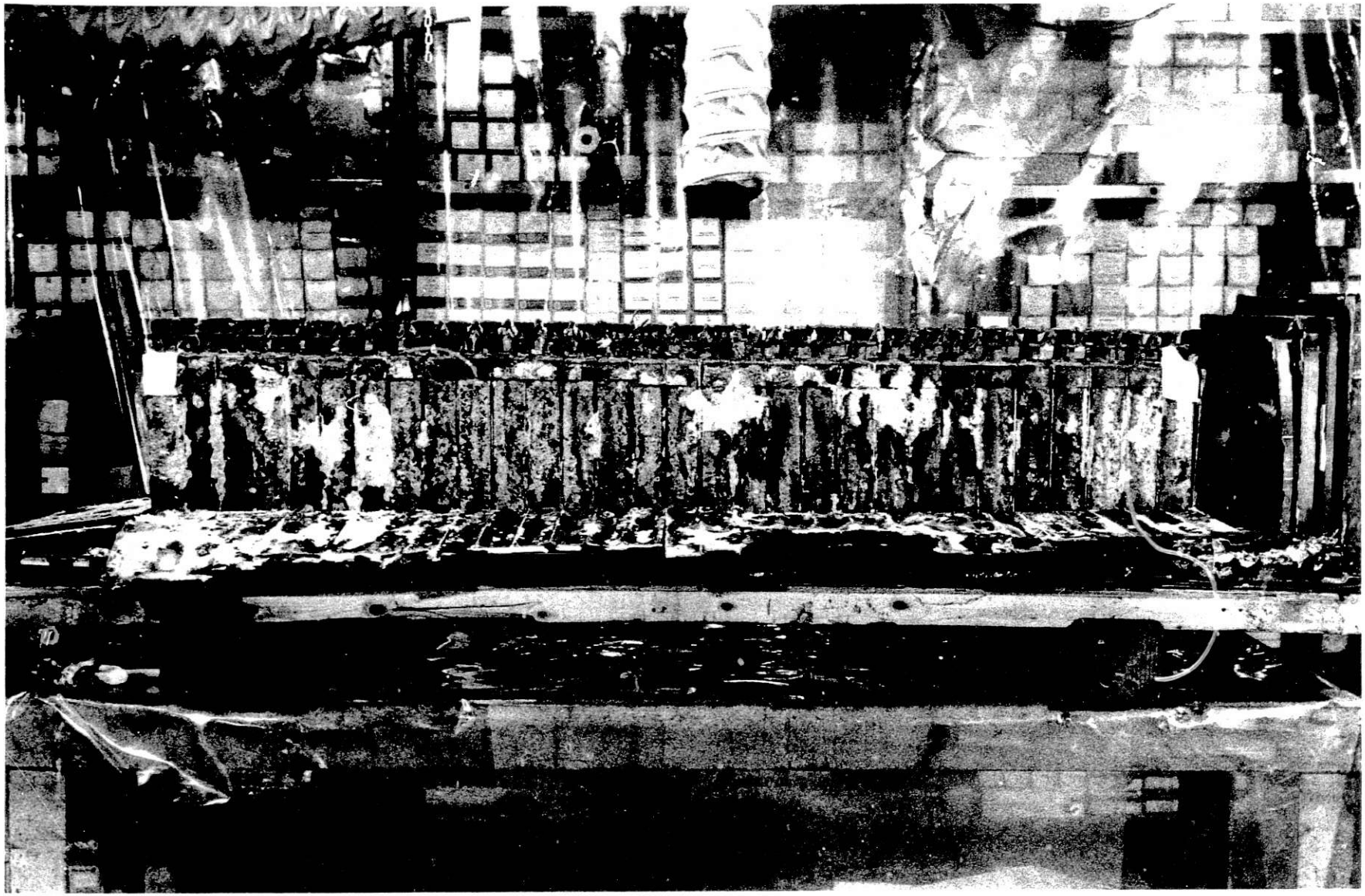

Fig. IV-22. Cell Stack (Cells 1 to 30) after Removal of Cell Tray Side

Fig. IV-23. Cell Stack (Cells 31 to 60) after Removal of Cell Tray Side

Overheating in a local area caused by a faulty heater was investigated as a potential initiation mechanism. Because of observations that cell-to-tray contact had occurred in the region of Cell 28, localized external heating was suspected. Examination of the rod-type heater in this region gave no visual evidence of local hot spots (Fig. IV-24), and resistance measurements of the heater itself showed no evidence of short circuits between the heating elements and c'adding of the heater rod. There is, at present, insufficient information concerning the possibility of internal arcing through argon gas within the heater element tube to reach a definite conclusion, but this is considered unlikely to be an initiator of the failure.

The possibility of chemical reactions within cells initiating the failure was investigated. In earlier post-test examinations[3] of certain development cells that had short-circuited, the positive (honeycomb design) current collector had sometimes cut through the separator to contact the negative electrode, thereby forming a short circuit. In these cases, there was very localized melting of the lithium-aluminum alloy, but no evidence of melting propagation through the electrode. Metallographic examinations of the cells from Module D-001 showed no evidence of ruptured separators, of direct contact between the lithium-aluminum and the iron sulfide electrodes, or of separators having been breached by molten lithium-aluminum. The latter event could only occur at temperatures above 600°C. No evidence of cross-contamination of electrodes was found; only the normal discharge products were observed in the electrodes. Very minute quantities of Al_2S_3 and/or Li_2S were found in the separator. The aluminum in the negative electrodes had reacted with the low-carbon steel current collectors and cell containers. Figure IV-25 shows this reaction on several cells in the stack, and Fig. IV-26 is a close-up view of a reacted area on Cell 35. The iron-aluminum reaction rate was found to be slow at 450°C, but rapid at temperatures above 700°C ($\Delta H \cong 8$ kcal/mol). Since the cells in the module had failed electrically before the temperature increase, the iron-aluminum reactions are not considered to be a possible cause of failure initiation. (The phase diagram for the Fe-Al system can be found in Ref. 4.) Calculations indicated that reaction of all the available aluminum in the cells with the iron would have raised the module temperature about 35°C.

In case of electrolyte leakage, dielectric breakdown of insulation saturated with electrolyte is a possible initiation mechanism. As noted earlier, electrolyte was found everywhere in the module. The insulator sheets on top of the cells are shown in Fig. IV-27, and a close-up of the only area with a crack is shown in Fig. IV-28. Silver and copper had been transported from the positive cell terminal to the containment vessel liner through the mica insulation. (The braze alloy used in the battery was Sil-Bond 50--a silver, zinc, cadmium, copper alloy.) This transfer also occurred across the Raybestos insulation between the cell tops and the tray angle at the edges. Numerous areas of the insulation were blackened and degraded (see Figs. IV-29 and IV-30) and showed low resistance. Electrolyte saturated with lithium is known to react with silicate, zirconate and aluminate materials. Tests at 450°C have shown that Vitrabond insulation saturated with electrolyte for about 22 hr conducts very little current (microamperes) at voltages up to 10 V. However, at 520°C, a peak current of about 4.5 A was obtained through this insulation at about 25 V after 140 hr of exposure to electrolyte.

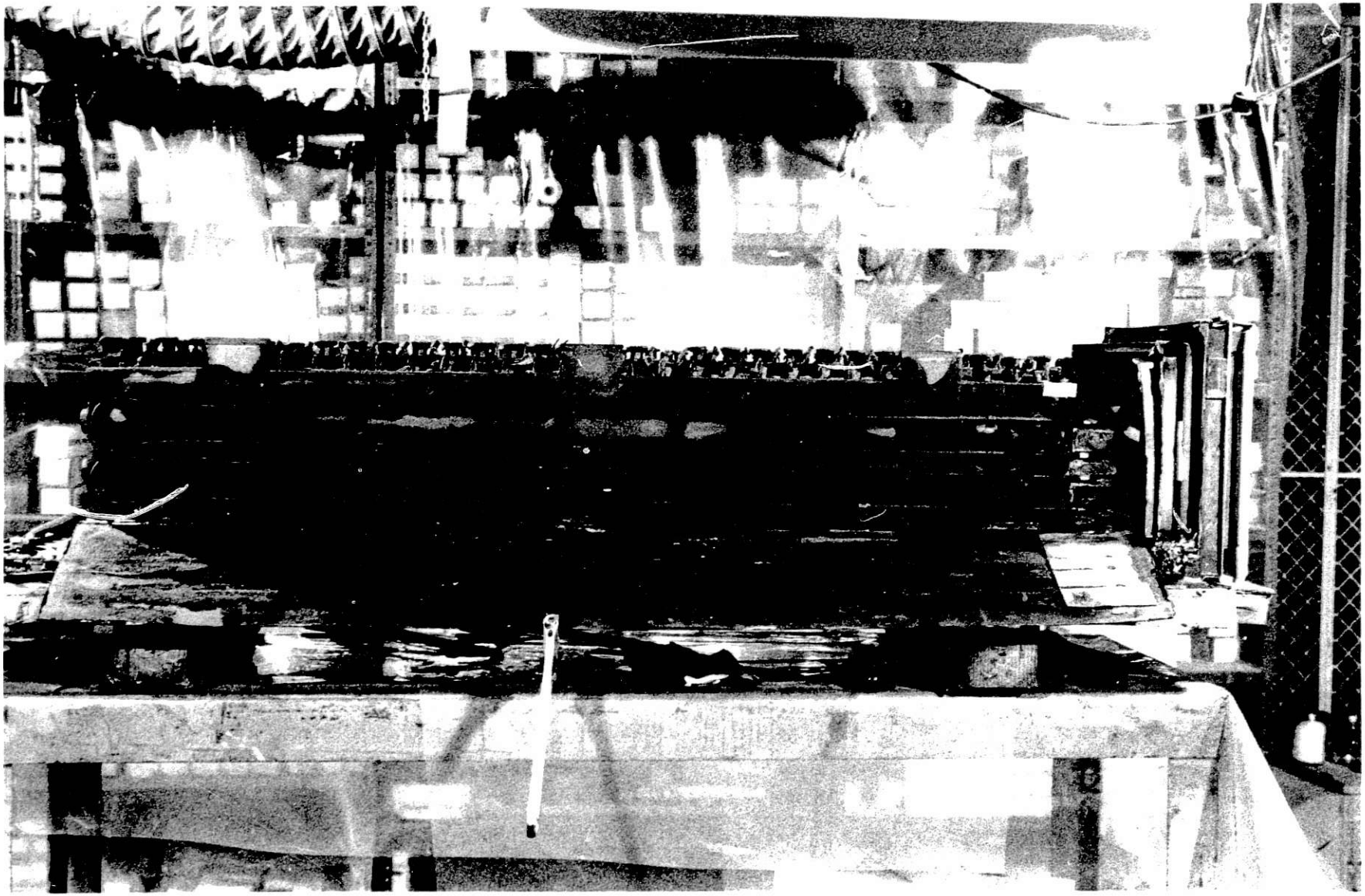

Fig. IV-24. Battery Heaters and Tray (Cells 1 to 30)

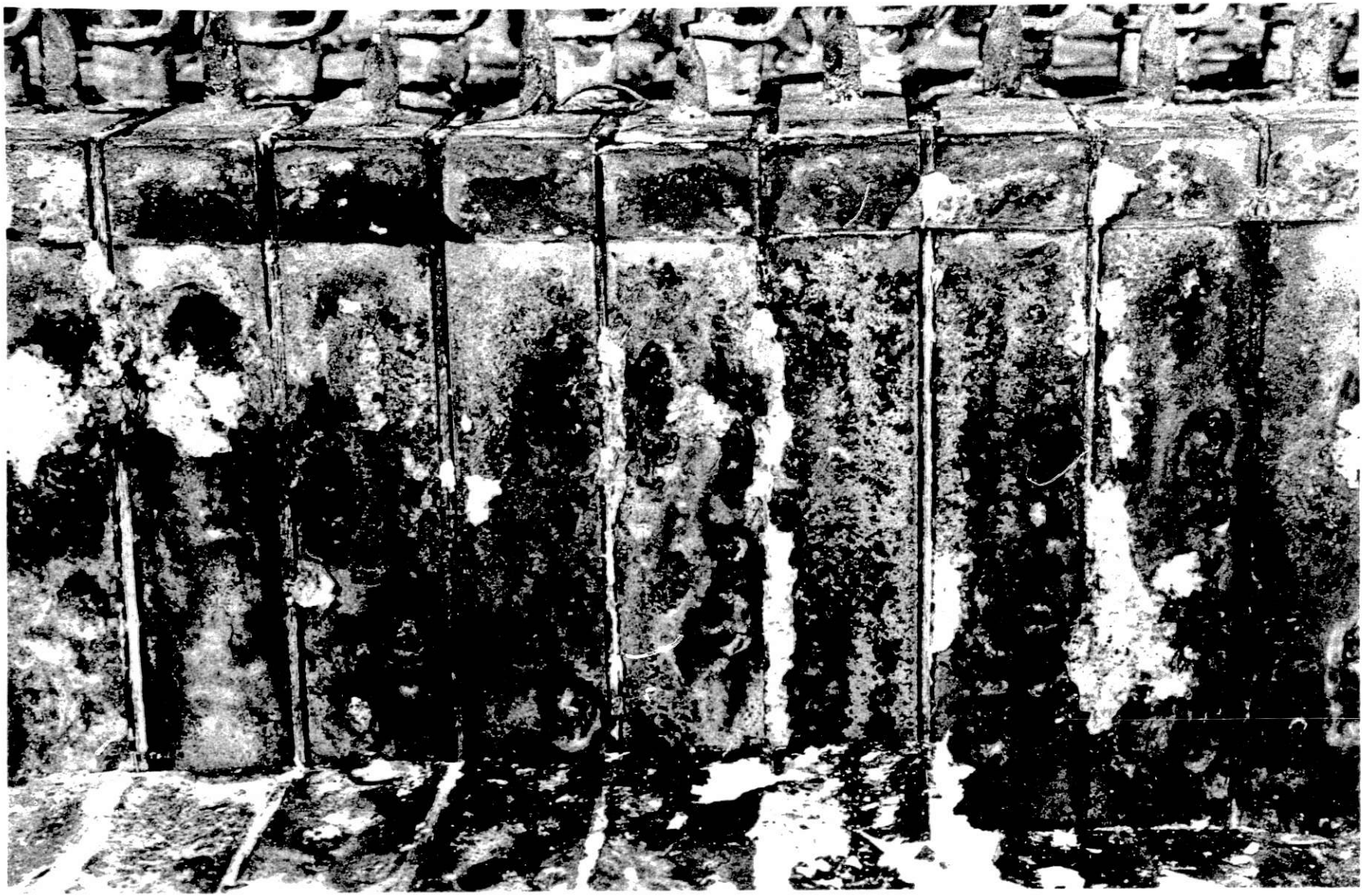

Fig. IV-25. Iron-Aluminum Reaction on Cells in Stack

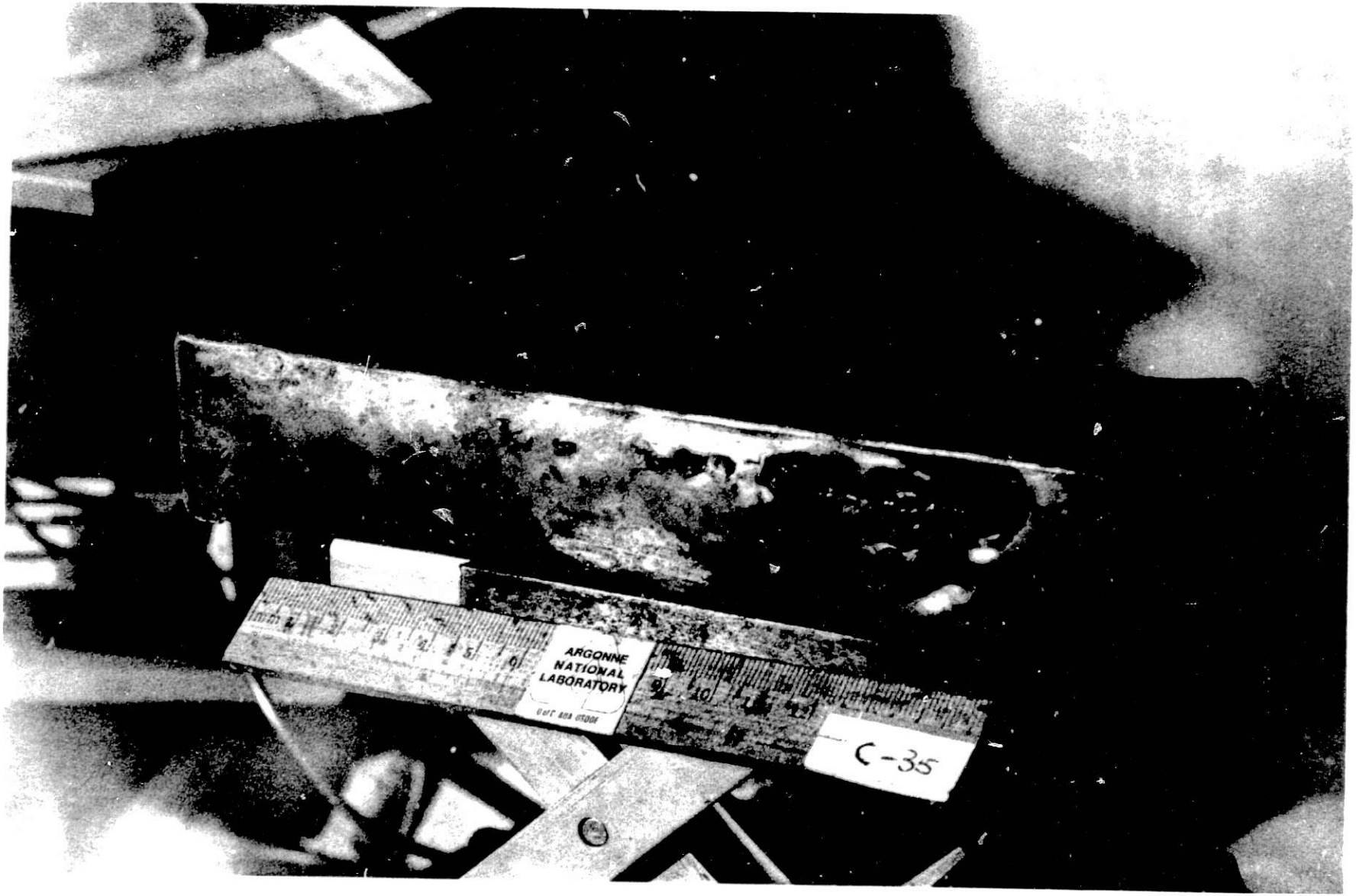

Fig. IV-26. Iron-Aluminum Reaction on Side of Cell 35

Fig. IV-27. View of Top Insulator Sheets

Fig. IV-28. Closeup View of Insulator Sheet Showing Crack

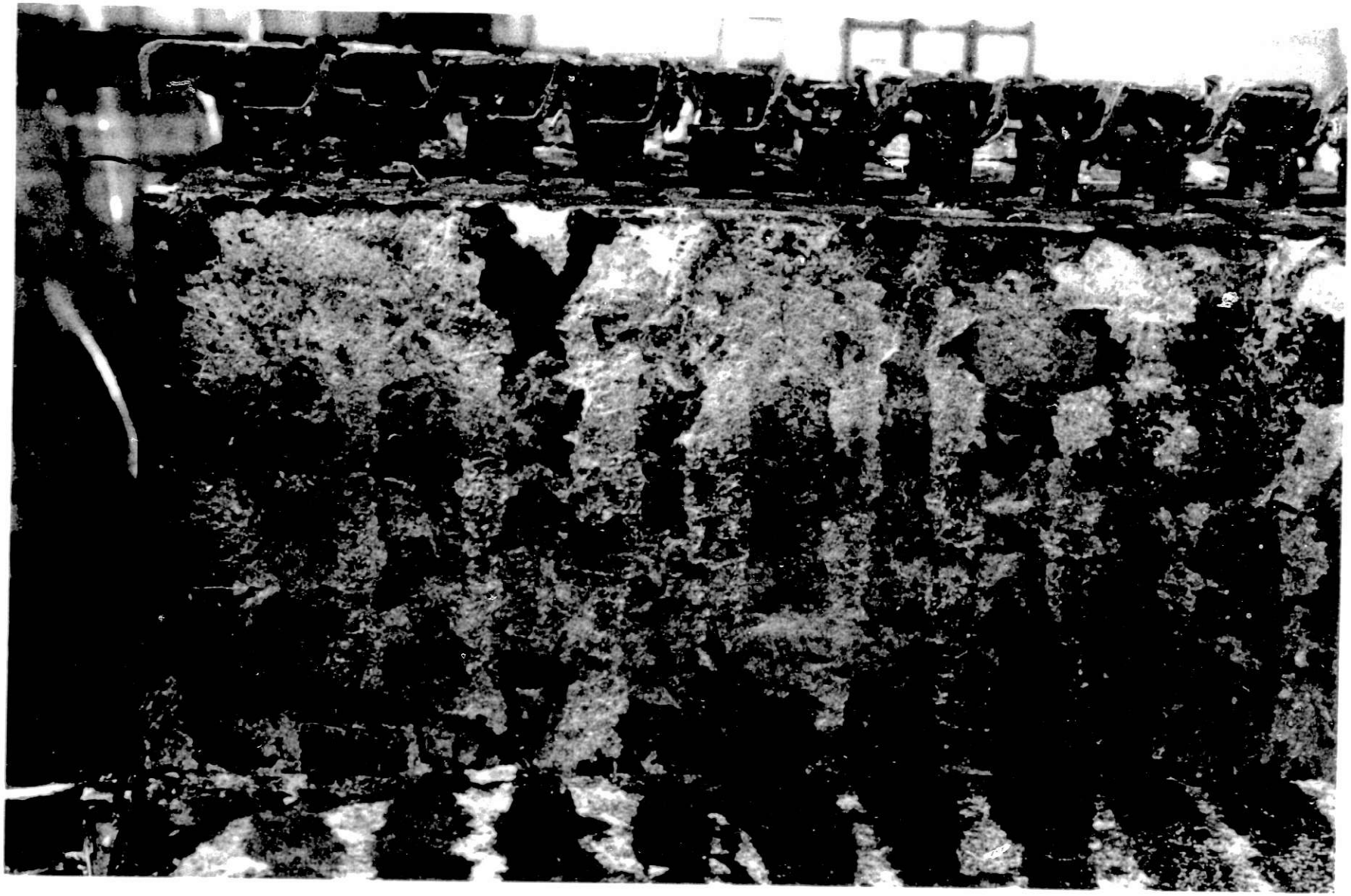

Fig. IV-29. Area of increased localization. Position of coils 2 and

The accuracy of the temperature measurements prior to failure was assessed. All thermocouples were calibrated prior to installation, and they were rechecked for proper resistance and grounding after having been installed in the modules. All thermocouples were operational at startup and registered melting of the electrolyte at the proper temperature (352°C). It was concluded that the thermocouples measured the temperature accurately, and that no overheating of the cells occurred prior to the failure.

Thermal gradients caused by nonuniform heat-up of the cells were also among the possible causes of failure initiation. Within the module, cells are heated from the edges at the sides of the tray. Thus, a thermal gradient within the cell during heat-up could have melted the electrolyte at the bottom first, thereby producing stresses within the cell. However, since the Mark IA cells had void space between the negative electrodes and cell can, this thermal gradient would have had little or no effect on the cell. Figure II-2 shows a vertical cross-section of a typical multiplate development cell in the Mark IA battery program. The gaps between the electrode edges and cell can are clearly visible in this photograph. In tests of individual restrained cells, it was found that Mark IA cells did not bulge even though a thermal gradient existed during start-up.

As a result of the above observations, it was concluded that the failure of Module D-001 was not initiated by any external factor. The most probable mechanisms for failure initiation within the module were (1) leakage of electrolyte followed by the formation of metallic bridges between cells or between the cells and cell tray through electrolytic corrosion, (2) electrical contact between the cells and the cell tray, and (3) arcing between the cells and the cell tray through butt joints in the electrical insulation.

3. Propagation Mechanisms

Several of the initiation mechanisms which have just been reviewed are also possible propagation mechanisms (see Table IV-1). One such mechanism is electrolytic corrosion. Electrolyte was observed on all of the cells; the insulation was saturated with electrolyte, which had flowed to the front of the module along the liner and the brackets attaching the front flange to the tray. The cell tray, Fig. IV-31, and many cell cans were corroded (see, for example, Cell 24 in Fig. IV-32). In addition, copper strips, which had been brazed on top of the cell cans, were corroded. As a result of this corrosion, metallic bridges were formed between cells and between the cells and the tray. For example, iron bridges were found at the tops of the cells between Cells 5 and 56, 10 and 51, as well as 48 and 49. There were also bridges of braze material between many cells as typified in Fig. IV-33.

Another possible propagation mechanism is the flow of braze alloy or copper from the cell due to melting. The melting temperature of the braze alloy (Sil-bond 50) is 625-650°C* and that of copper is about 1083°C; portions

*Differential thermal analysis (DTA) of samples of Sil-bond brazed copper showed no change in the remelt temperature of the braze alloy after repeated thermal cycling of a sample.

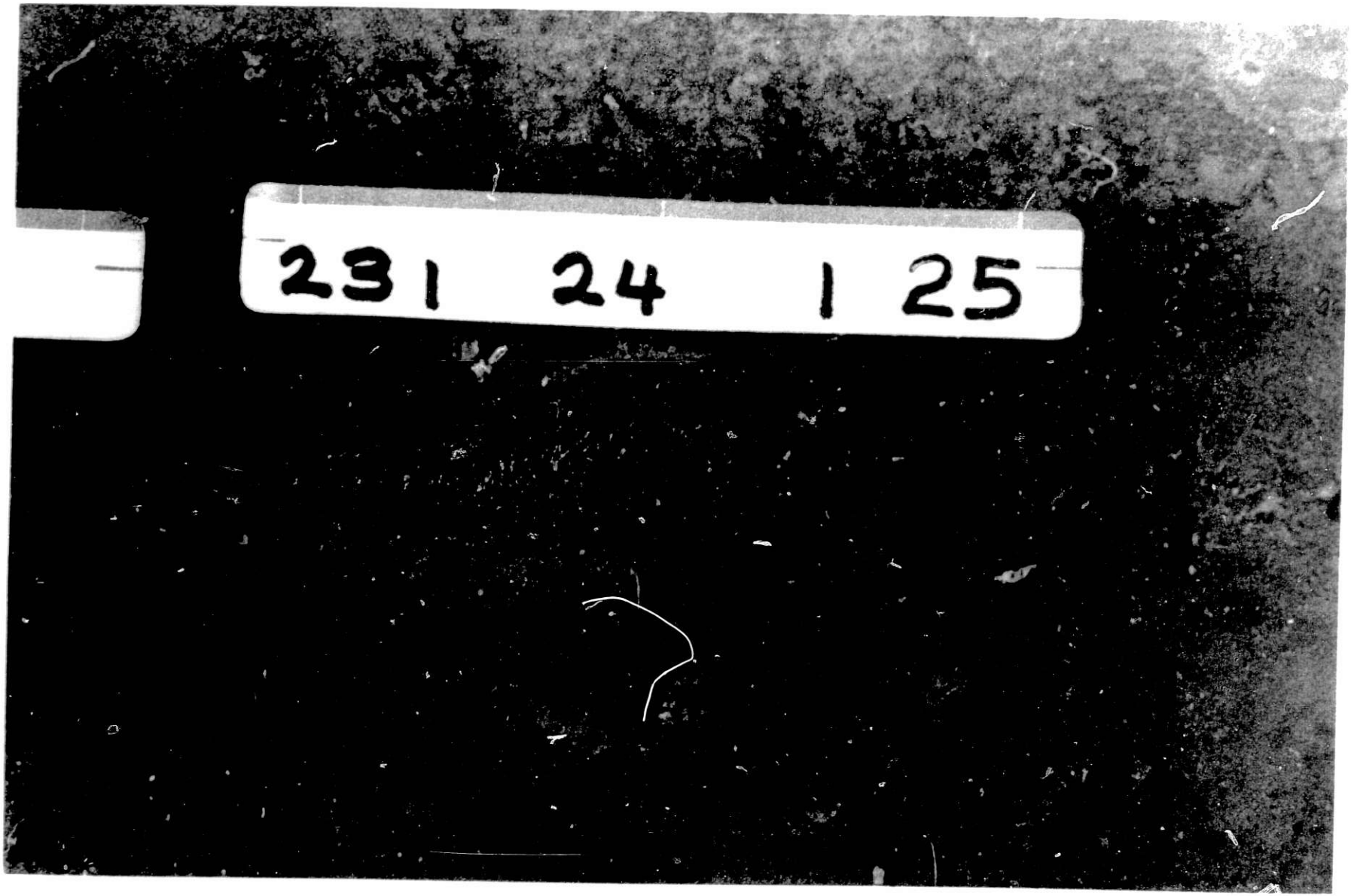

Fig. IV-31. Reaction of Cell Tray in Region of Cell 24

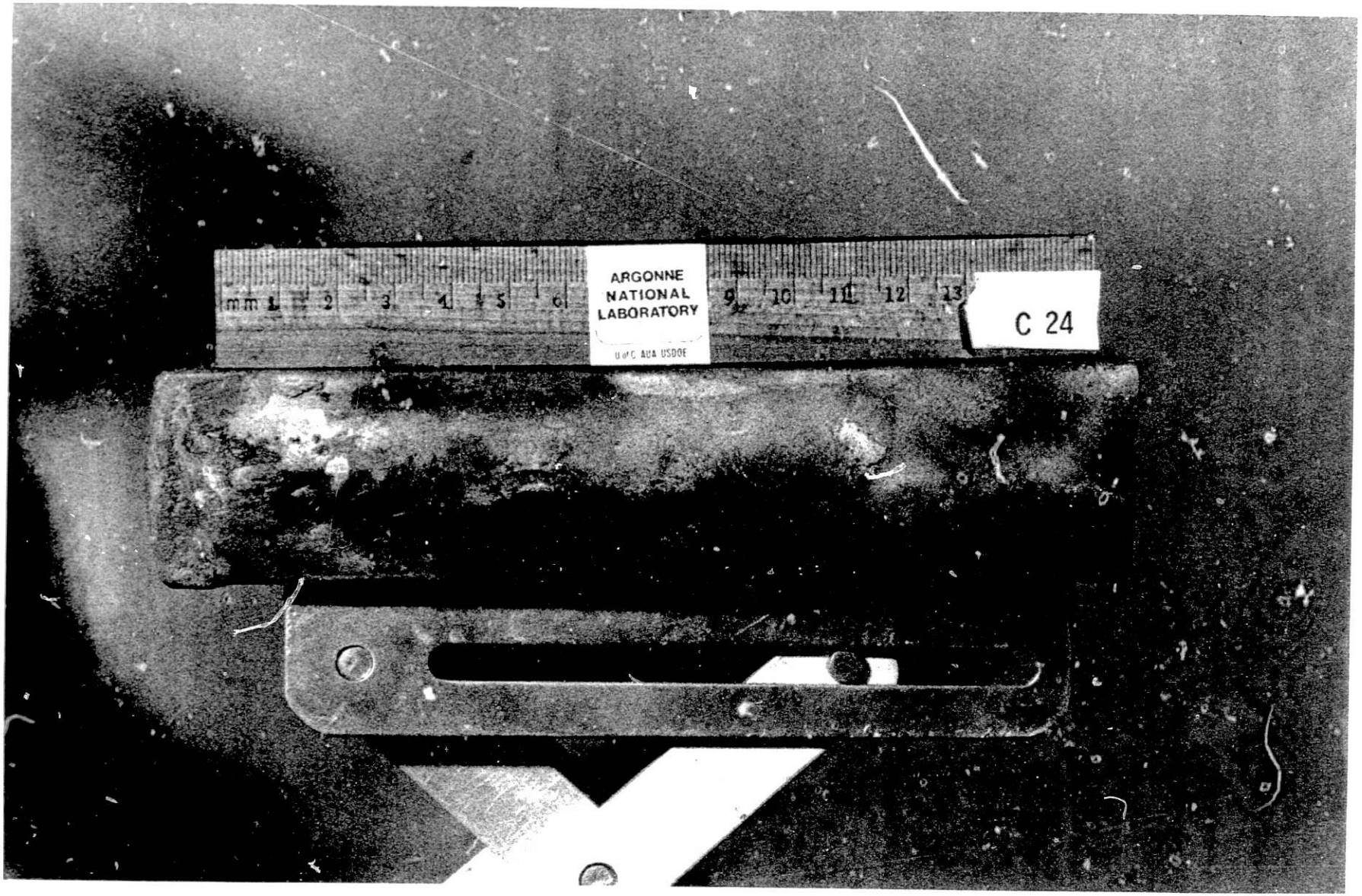

Fig. IV-32. Reaction at Lower Inside Edge of Cell 24

Fig. IV-33. Braze Bridge between Cells

of the module had exceeded these temperatures during the failure. Most cells showed braze alloy and/or copper bridges across the insulation between cells (Fig. IV-33); melting of braze and/or copper was observed to have occurred in some positive terminal rods (Fig. IV-34). The braze alloy from the intercell connection with the positive terminal rod had not entered the feedthroughs -- a condition that would have caused a short circuit. Subsequent tests indicated that temperatures exceeding 1000°C could be generated in the positive terminal rod during a short circuit.

Chemical reactions within cells were presented earlier as a potential initiation mechanism. The evidence presented earlier that such chemical reactions were not a failure initiation mechanism also applied to failure propagation.

As mentioned in the previous section, expansion of cells due to the high temperatures and rapid discharges caused displacement of cells within the tray; this could have been a mechanism for propagating the failure. The movement of cells with respect to the relatively stable intercell connectors is illustrated in Fig. IV-35. As a result of cell expansion, contact occurred between the cells and the cross-over straps (Fig. IV-36).

Braze flux was present on the intercell connectors in Module D-002. The flux, which contained KHF_2, $K_2B_4O_7 \cdot 8H_2O$, and H_3BO_3, was applied with a water medium. No effects of the braze flux were noted in Module D-002, and none were detectable in Module D-001 because of the presence of electrolyte.

The possibility of thermal effects as a propagation mechanism was reviewed. As noted above, the molten lithium-aluminum formed due to the high temperatures did not penetrate the BN separators, but did cause iron-aluminum reactions that ruptured many cell containers. As reported in Section III, the cell voltage-temperature data obtained during the module failure showed that the voltage decline of the cells preceded the temperature increase. Table IV-2 presents the time differentials between the initial voltage drop of ten cells and the time when the six thermocouples located at these cells registered 630°C. (The calculated response time of the thermocouples is less than one second to register a 5°C temperature rise for a 50°C ramp).

Dielectric breakdown of insulation saturated with electrolyte is another possible propagation mechanism. This is similar to the proposed initiation mechanism mentioned in the previous section. This was not a failure propagation mechanism since, even with reduced local resistances, large currents could not be supported by the insulation.

Arcing as a possible propagation mechanism was also reviewed. As discussed in the previous section, there was much evidence of arcing at Cells 10, 11, 15, 16, and 24 and the tray, as well as at the tops of the cells. The electrochemical formation of a metal bridge would conduct current; with increasing current, this bridge could melt and result in an arc.

In summary, the most probable mechanisms for failure propagation were identified as (1) electrolyte leakage from cells followed by electrolytic corrosion, (2) cell expansion, and (3) arcing.

Fig. IV-34. Molten Positive Terminals and Molten Bridges across Insulation between Cells

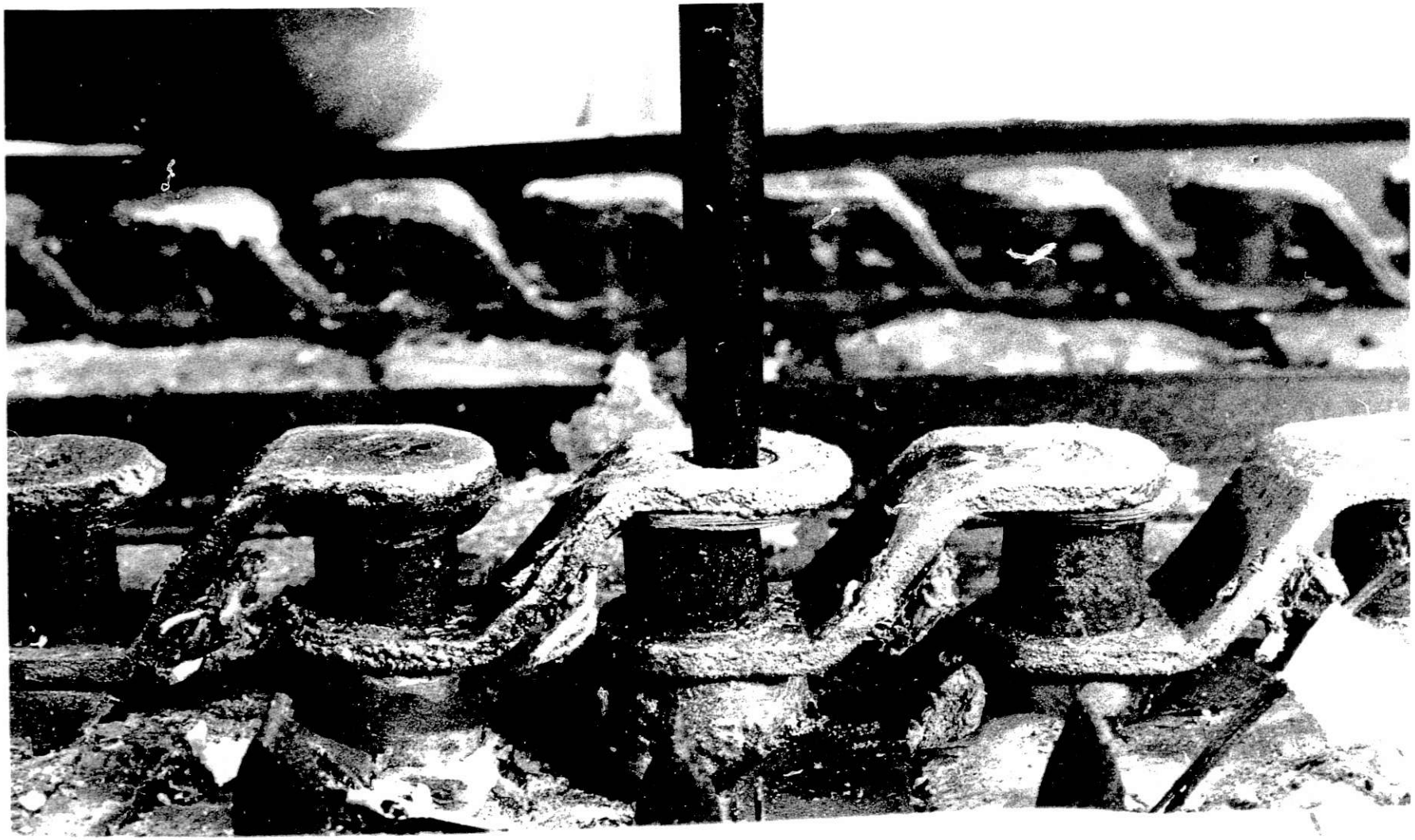

Fig. IV-35. Movement of Cell with Respect to Intercell Connector

Fig. IV-36. Relative Movement between Cell and Cross-over Straps (indication of arcing at strap and alloy bridges across insulation)

Table IV-2. Time Differentials between Initial Voltage Decline and Temperature Rise to 630°C

Thermocouple Location	Cell Location	Time of Day		Difference, min
		Voltage Decline	630°C Temperature	
2	50	2328	2348	20
	51	2328	2348	20
12	5	2330	2355	25
	6	2330	2355	25
4	41	2326	2333	7
11	15	2328	2342	14
	16	2327	2342	15
10	25	2316	2337	21
	26	2314	2337	23
9	30	2322	2328	16

V. MOST PROBABLE SEQUENCE OF EVENTS DURING FAILURE OF MODULE D-001

As discussed in the previous section, the Failure Analysis Team considered all of the possible mechanisms for the initiation and propagation of failure in Module D-001. Based on the results of this failure analysis, the most probable mechanisms involved in the failure initiation and propagation were identified. These mechanisms are used in this section to reconstruct the most probable sequence of events in the module failure.

This most probable sequence of events is based on individual cell voltage data and the results of the complete examination of the failed module. The individual cell voltages were recorded at one-minute intervals on the data acquisition system (DAS). These data provided an accurate record of the time of the initial voltage decline in each cell. The criterion used as an indicator of cell failure initiation was a decline of 30-40 mV from the previous steady-state voltage.

A. Failure Initiation

From the recorded cell voltage data, which showed the initial voltage decline at 2316, it is clear that the initial failure involved four cells (Cells 24, 25, 26 and 27). The simultaneous discharge of these four cells, and only these four cells, required contact of only Cells 24 and 28 with the cell tray. The cell tray was the only hardware common to both cells. The can of Cell 28 was at the same potential as the positive terminal of Cell 27, as well as being the negative terminal of Cell 28. Thus, the discharge path was from the negative of Cell 24 via Cells 25, 26 and 27 through the positive of Cell 27 and back to Cell 24 through the cell tray. The discharge path was completed only when the second point of contact was made; however, the two points of contact did not have to occur at the same time and most likely did not. The magnitude of the voltage drop indicates that the discharge current at this time was about 40 A.

Examination of the cell tray showed that considerable corrosion had occurred along the center line of the length and width of the cell tray (see Fig. IV-11). The longitudinal corrosion band (left to right) corresponds to the gap between the two rows of cells, while the lateral corrosion band corresponds to the butt joint in the mica insulation that lined the cell tray. Also, evidence of reaction was observed at the junction of the vertical sides of the tray with the bottom. The most severe reactions (and possibly arcing) occurred at cell positions 8 to 10, 15 and 16, and 24. Metallographic examination of samples from cell locations 24 (edge of tray, see Fig. IV-14) and 15/16* showed alloying of the low carbon steel from the cell cans with the Type 304 stainless steel cell tray,† intergranular corrosion, and localized grain growth. The alloying and grain growth are consistent with localized hot spots as might occur with arcing. It is possible that arcing occurred as a result of burnout of conductive bridges formed by corrosion due to the presence of electrolyte.

---

*The slash denotes the junction of the cell indicated.

†The alloyed material appeared as nodules of low carbon steel, which had been molten, on the surface of the stainless steel tray. Alloying had occurred at the interface.

A blackened area of the upper right corner of the cell-tray edge (Fig. IV-11) is of particular significance, since this location corresponds to the junction of Cells 27 and 28. This area is further illustrated in Fig. V-1, which shows a side view of the cell stack (Cells 1 through 30, reading right to left) with the edge of the cell tray pulled down and the mica insulation in place. The blackened area at the left indicates that the mica insulation had reacted at the location of Cells 27/28. A similar area is shown at the location of the junction of Cells 10 and 11. Figure V-2 is a side view of Cells 23 through 30 with the mica insulation removed. Evidence of cell can corrosion is clearly visible at the junction, and near the top of Cells 27 and 28. The metallic mass from the corroded area is visible at the bottom of the cells. Examination of this material showed the presence of aluminum and iron. Also, examination showed that the corrosion reaction had penetrated completely through the cell can. The corroded area of Cell 28 is shown in more detail in Fig. V-3. Similar corrosion reactions near the cell top were observed in only two other locations, namely, at Cells 32/33 and 10/11 (these will be discussed later).

Based on the above results, the most probable cause of contact with the tray by Cell 28 was electrolyte leakage at or near the top of Cells 27 and 28; the subsequent corrosion established a conductive path from the can of Cell 28 to the top edge of the cell tray. Other possible causes are localized hot spots resulting from arcing of heater elements or from short circuits caused by small foreign objects; however, evidence was not found to support either of these possible causes. (Small foreign objects would not have been visible after the failure.)

The most probable cause of contact at Cell 24 was (1) arcing due to direct contact of the cell with the tray through a gap in the insulation joint, or (2) electrolyte leakage and subsequent corrosion that established a conductive path and arcing. As noted earlier, evidence of arcing was observed at the edge of the cell tray opposite the bottom edge of Cell 24; however, bulging of the edges and bottoms of the cells make direct contact a less likely possibility than electrolytic corrosion. These reactions result in the release of additional electrolyte that flows toward the center and front of the cell tray; this becomes an important factor in the propagation of failure.

B. Failure Propagation

The first step in the propagation of failure was the short circuit of Cell 28 due to contact of the fill tube on Cell 29 with the cross-over strap (Fig. V-4), which was connected to the cell tray. This completed the circuit from the negative of Cell 24 through the positive of Cell 28. The initial decline in the voltage of Cell 28 occurred at 2318, two minutes after the start of voltage decline in Cells 24 through 27. The contact with the cross-over strap was attributed to thermal expansion differences in the cells and cell tray and to the expansion of Cells 24 through 27 as they discharged. This is the only case where cell expansion and contact with the cross-over strap was a primary factor in failure propagation. In all other cases, contact with the cross-over straps was merely a secondary contributor; this was verified by examining the voltage/time data for each cell relative to the cross-over strap locations.

Fig. V-1. Side View of Failed Module after Being Cut Open
(Mica insulation still in place)

Fig. V-2. Corroded Area near Top of Cells 27/28 (Mica insulation removed. Metallic mass from corroded area is visible at the bottom of Cells 27/28. Lesser corrosion appears at the top of Cell 24.)

Fig. V-3. Corroded Area in Cell 28 Can

Fig. V-4. Cross-over Strap in Region of Cell 29 Fill Tube (evidence of arcing or burnout apparent at contact point)

The next step in the failure propagation was the discharge of Cell 29, which occurred at 2322, as indicated by a slight decline in the cell voltage. The cause for the failure of this cell was not determined; possible causes are a short circuit in the feedthrough and electrolyte leakage from other cells with subsequent corrosion.

The failure propagation continued with the discharge of Cells 30 through 32. The initial voltage decline occurred at 2324. The most probable cause of this failure was electrolyte leakage at or near the top of Cells 32/33. The resulting corrosion in this area formed a conductive path between Cells 32 and 33 and the top edge of the cell tray. A view of this reacted area is shown in Fig. V-5 below the number 32. The feedthrough of Cell 32 was short-circuited; this is a probable source of heat that could have resulted in melting and flow of the braze material. The electrolyte could have provided another mode for the transport of braze material across the mica insulators between the cells. Evidence of reaction is clearly visible at the junction of Cells 32 and 33 and the cell-tray angle. Examination of Cell 32 showed that the upper corner adjacent to Cell 33 was badly corroded (see Fig. V-6) and appeared very similar to the condition observed at the junction of Cells 27 and 28. Contact at the junction of Cells 32/33 established a discharge path from Cell 24 through 32 via the cell tray. Also, secondary discharge paths were probably occurring because of the additional electrolyte leakage and the subsequent corrosion.

The next step was the discharge of Cells 33 and 34. The initial voltage decline occurred at 2325. The most probable cause of failure was electrolyte leakage and corrosion. Examination showed a large hole in Cell 33 at the lower inside edge and a similar hole in Cell 34 along the outside edge at the bottom. The holes in these cell cans were caused by corrosion due to the presence of electrolyte which probably had leaked from previously corroded cells. At this time, the tranport of braze alloy, by electrochemical reaction or melting, across the mica insulators between the cells must have provided additional discharge paths. Figure V-7 shows a top view of the module (looking toward the front) with the insulation removed. Evidence of corrosion and melting of braze alloy and copper strips can be seen in this photograph. In many areas, metallic bridges were formed between adjacent cells. This behavior was an effect rather than a cause of failure and merely provided additional discharge paths.

The propagation continued with discharge of Cells 35 through 38 and 23, as indicated by voltage decline which started at 2326. With these cells, the failure had extended to all cells in the rear of the module and was propagating toward the front in both rows of cells. Severe corrosion was observed along the lower edges of the cell cans at the junction of Cells 23, 24, 37, and 38. Also, severe corrosion was observed in the cell tray in this area, as shown in Fig. IV-31. The corrosion was probably accelerated by the large potential difference between cells across the stack.

The next step was the discharge of Cells 39 through 44 in one stack and Cells 22 through 18 in the other stack, with a voltage decline beginning at 2327. At this stage, failure was rapidly propagating in both cell stacks toward the front of the module, and several modes for propagation were simultaneously involved. As noted earlier, electrolyte leakage and subsequent corrosion resulted in the formation of large holes along the bottom edge of

Fig. V-5. Evidence of Reaction Similar to that Observed at Cell 27/28 (analysis of metallic material from this area showed mostly iron and aluminum)

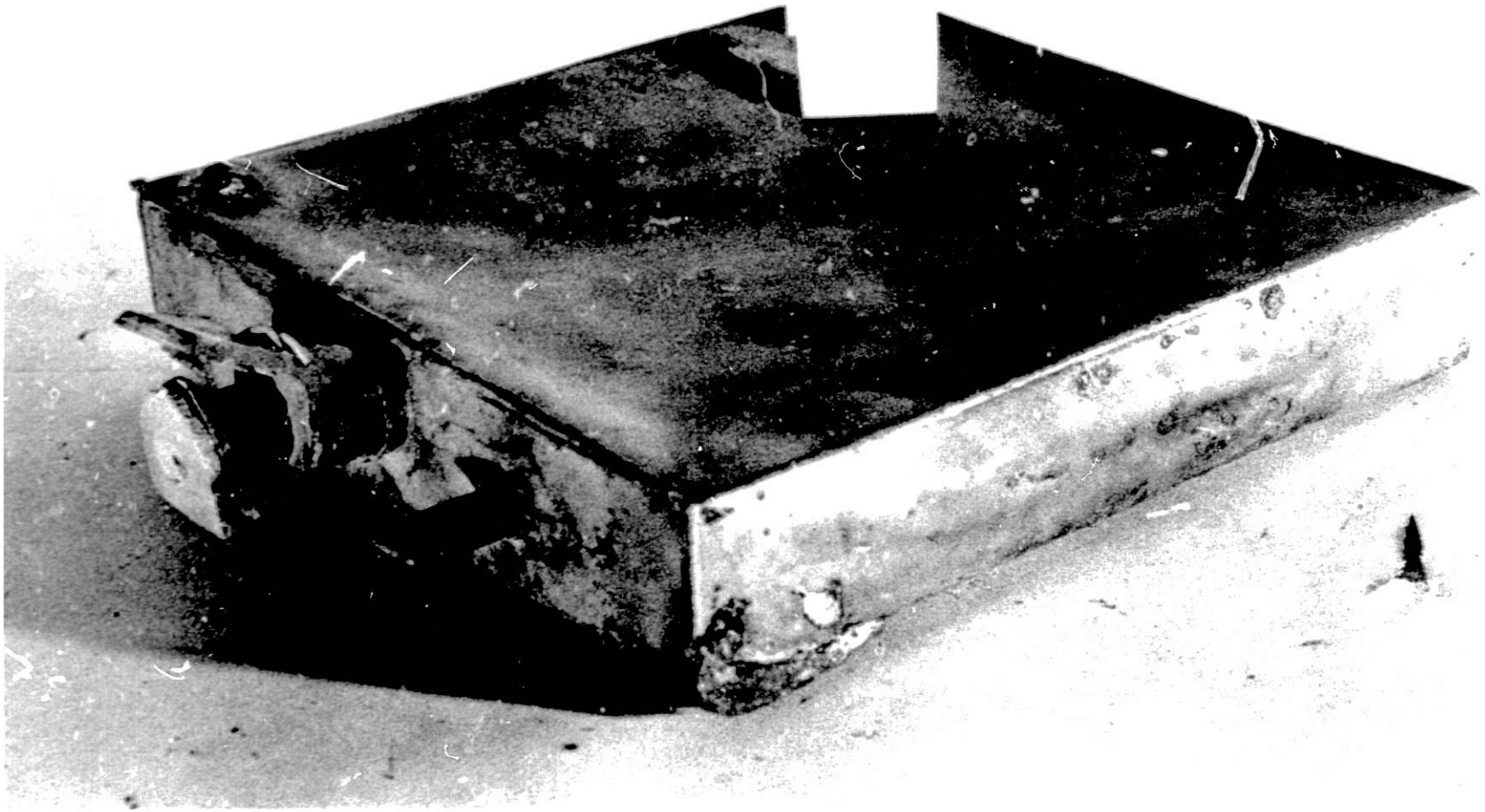

Fig. V-6. Corroded Upper Corner of Cell 32 (lower center in photograph)

Fig. V-7. Top View of Module (The cell top insulation has been removed and evidence of electrolytic corrosion and braze melting is visible. In many areas, metallic bridges were formed between cells across the top of the mica insulation.)

several cells (see Fig. V-8, for example), thereby causing additional leakage of electrolyte. The primary mechanism of propagation was electrolyte leakage and corrosion that formed conductive paths from cell to cell and from cell to cell tray (see Fig. IV-18). Arcing at Cell 41 between the feedthrough and cross-over strap (Fig. IV-36) and the contact at Cell 20 between the fill tube and the cross-over strap (Fig. IV-9) provided additional discharge paths for some of the cells.

Cells 45 and 46 in one stack and Cells 17 through 15 in the other then began to discharge. Evidence of severe corrosion and arcing was observed in a large area at the junction of Cells 45, 46, 16 and 17 with the center of the cell tray (Fig. IV-13). The arcing effect observed in this area (and in other areas) may have been the result of burnout of small metallic bridges formed by corrosion reactions due to the presence of electrolyte.

The failure propagation continued with the discharge of Cells 47 through 52 in one stack, and 14 through 9 in the other; a total of 12 cells. The voltage decline of these cells occurred at 2329. As noted earlier, evidence of corrosion and contact was observed at Cells 9 through 11 with the tray angle at the top of the cells (Fig. V-9). This area appeared very similar to that observed at the junctions of Cells 27 and 28 (Fig. V-2) and Cells 32 and 33 (Fig. V-5) Numerous conductive paths, which resulted from the presence of electrolyte and the subsequent corrosion reactions, were observed between cells and between the cells and cell tray. Contact was made at Cell 20 between the fill tube and the cross-over strap, and a metallic bridge (iron with some silver and copper) had formed between the tops of Cells 10 and 51.

Propagation of failure to all cells except Cell 60 was completed by contact of Cells 1, 2, and 59 with one another and with the cell tray via corrosion caused by electrolyte leakage. The voltage decline for these cells occurred at 2330 (2331 for Cells 58 and 59). Thus, the entire failure propagation required only about 15 minutes. Figure V-10 shows evidence of the molten pool of lithium-aluminum alloy that flowed from Cell 2 after the temperature had exceeded 600°C. The hole in Cell 2 (Fig. V-11) was probably initiated by corrosion (due to the presence of electrolyte) and occurred long before the cell temperature had reached 600°C.

C. Summary

Table V-1 provides a summary of the most probable sequence of events in the initiation and propagation of failure. As discussed above, the single most important factor in both failure initiation and propagation was electrolyte leakage with subsequent corrosion that formed conductive paths between cells and between the cells and cell tray. The arcing effects observed in the examination were possibly due to the burnout of small metallic bridges that had been caused by this type of corrosion. Cell expansion was a factor only in the first step of failure propagation, i.e., contact of the Cell 29 fill tube with the cross-over strap. Contact with other cross-over straps provided contributory discharge paths, but was not the primary cause of failure propagation.

Fig. V-8. Large Hole at Lower Inside Edge of Cell 41 (Examination showed that many cells had similar holes which would allow electrolyte to flow freely from the cells.)

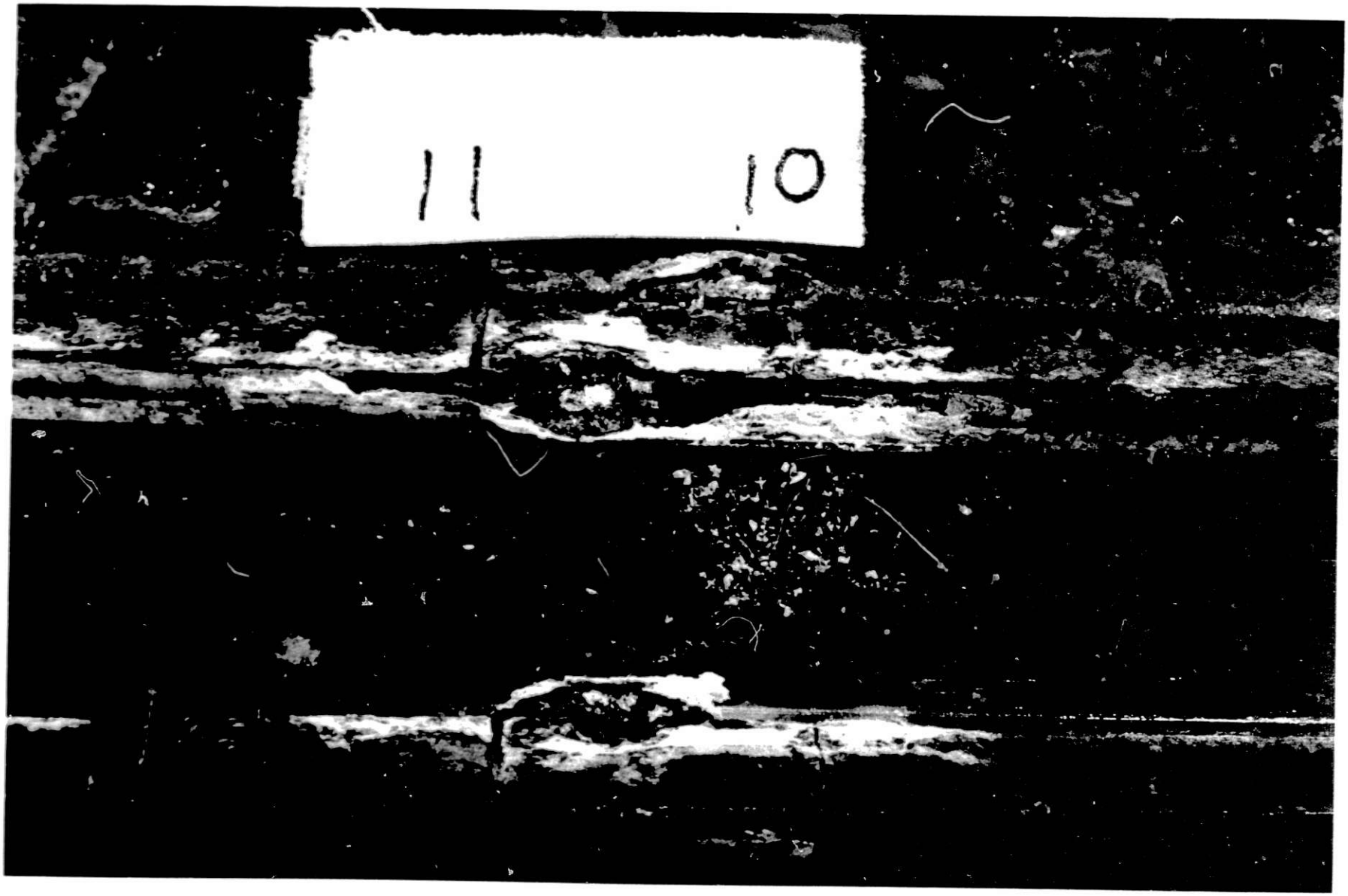

Fig. V-9. Badly Corroded Area at Top Edge of Cells 10/11 (Similar to that observed at Cells 27/28 and 32/33. Part of the corroded material is adhering to the tray angle.)

Fig. V-10. Lithium-Aluminum Alloy from Cell 2 (The Li-Al leakage occurred after the cell temperature had exceeded 600°C and after the corrosion caused by the presence of electrolyte.)

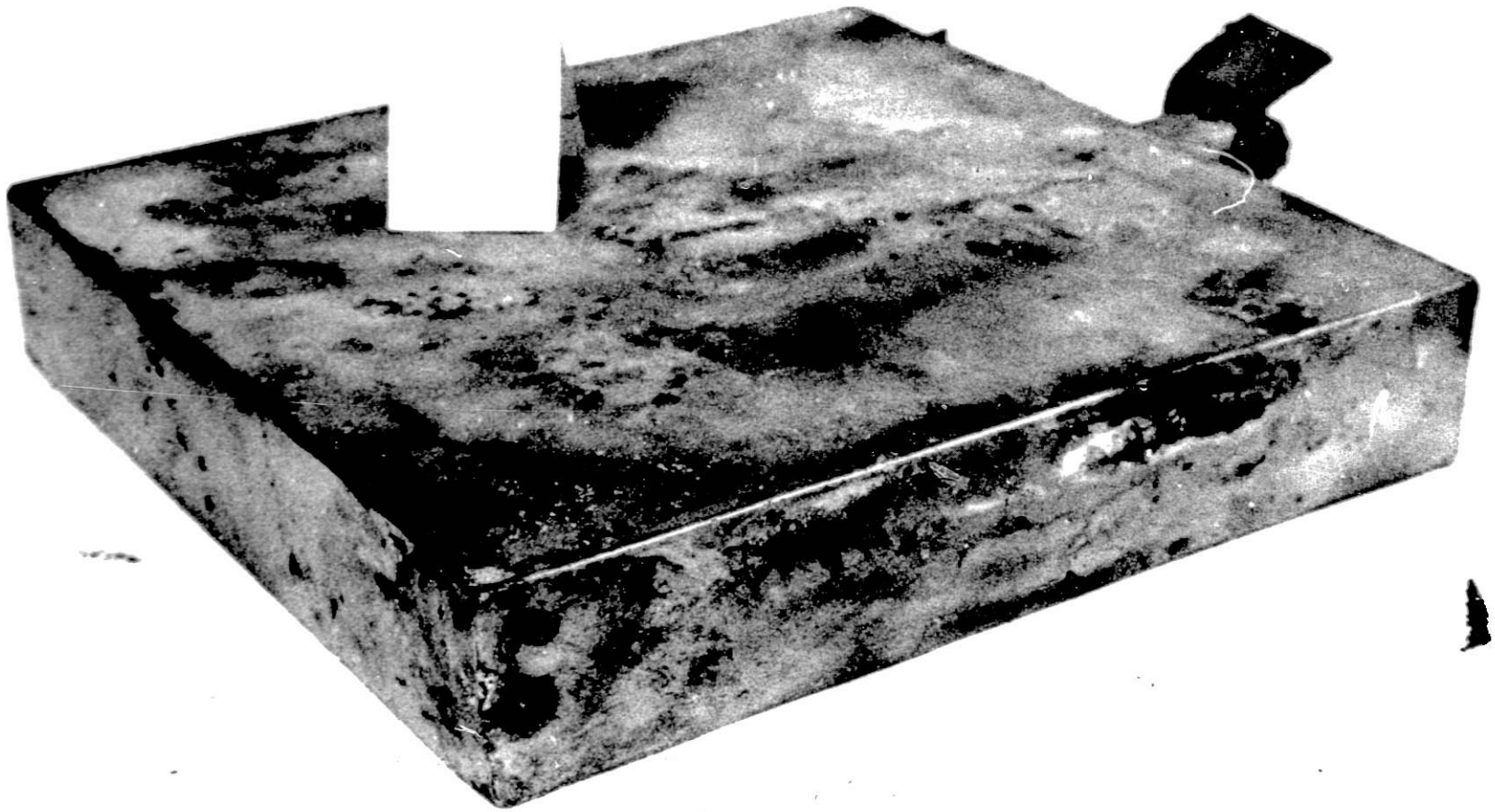

Fig. V-11. Photograph of Cell 2 (note the hole and corrosion effects at lower inside edge)

Table V-1. Summary of Most Probable Sequence of Events

Failure Initiation

1. Contact between Cells 24 and 28 and the cell tray provided a discharge path for Cells 24 through 27.

Failure Propagation

1. The fill tube on Cell 29 contacted a cross-over strap on the cell tray.

2. The cause of the discharge of Cell 29 was not identified.

3. Contact was established between the cell tray angle and Cells 32 and 33 at the top of the cell tray.

4. Cells 33 and 34 failed, probably due to corrosion,transport of braze alloy, or feedthrough failure.

5. Cells 23, 24, 37, and 38 contacted the cell tray as a result of corrosion.

6. Cells 18-22 and 39-44 contacted the cell tray at several locations as a result of corrosion.

7. At the junction of Cell 15/16 and 45/46 contact was made with the cell tray via arcing and corrosion.

8. At Cells 9-14 and 47-52, multiple contacts were established between the cells, the cell tray, the tray angle, and cross-over straps.

9. Propagation of the failure was completed (except for Cell 60) by contact between Cells 1, 2, and 59 and the cell tray as a result of electrolytic corrosion.

VI. DESIGN RECOMMENDATIONS

The final task of the Failure Analysis Team was to formulate a set of design recommendations, based on the results of the failure analysis. Table IV-1 lists design modifications for the cells and the battery that are believed to warrant consideration.

Table VI-1. Recommended Design Modifications

CELLS
1. Consider higher strength materials for cell cans.
2. Consider increased thickness of can material.
3. Avoid additions to cells (e.g., copper strips) that require brazing.
4. Modify design to eliminate or reduce cell expansion.
5. Consider isolation of the cell can from both electrodes.
6. Develop design modifications and/or fabrication techniques to prevent electrolyte leakage from cells.
BATTERIES
1. Temporarily relax volumetric and specific energy requirements.
2. Modify cell tray design to provide adequate cell restraint.
3. Modify intercell connectors and attachment method to eliminate stresses.
4. Develop a method and/or materials to eliminate or accommodate thermal expansion differences between cells and tray assembly.
5. Modify the cell arrangement to minimize voltage differences between adjacent cells.
6. Eliminate gaps in sheet insulators between cells and between the cells and cell tray.
7. Utilize more suitable high-temperature insulating materials.
8. Provide an external circuit breaker between modules.

VII. EXPERIMENTAL PROGRAM ON FAILURE MECHANISMS

During the course of the failure analysis, it became apparent that some experimental work was needed to obtain supplemental data on potential failure mechanisms and their effects. The information from these experiments together with that from the failure analysis will be used to develop a reliability analysis study for the lithium/iron sulfide battery and to provide guidelines for the design of Mark II cells and batteries. The reliability analysis study will consist of a system description, a failure modes and effects analysis (FMEA), a fault tree or equivalent, and a resolution of the identified potential problems.

For the experimental program, studies will be conducted on the following: (1) the effects of short circuits, overheating, and mechanical stresses on individual cells, (2) the behavior of Vitrabond mica electrical insulation in molten LiCl-KCl electrolyte under applied potentials, (3) the conditions under which electrical arcing between metallic components can occur within a battery, and (4) the conditions that cause short circuits in electrical feedthroughs in the presence of molten-salt electrolyte or mechanical stress. In addition, a few calculations or experiments are needed to answer several specific questions that arose during the failure analysis. Among these questions are the adiabatic temperature rise for complete discharge of a short-circuited cell; the maximum temperature rise that could result from iron-aluminum reactions in a cell; the thermal stability and decomposition products of Vitrabond mica insulation; the current required to burn out voltage sensing, equalization, and thermocouple wires; and the effect of remelting braze alloy in contact with copper on the melting point of the braze alloy.

These studies involve a variety of tests on Mark IA cells. The cells from Module D-001 are obviously unusable for this purpose. In addition, 42 of the cells from Module D-002 underwent sufficiently severe expansion that they are not considered reliable for testing purposes. As indicated below, 48 of the Mark IA cells appear to be suitable for these studies and other tests:

Spares for Mark IA battery	12
Acceptable cells from Module D-002	13
Slightly off-dimension cells	23
Total	48

VIII. CONCLUSION

As a result of the Mark IA experience, the original strategy for the development of the Mark II battery was changed. A strong emphasis is being placed on cell and battery hardware reliability, taking into account the design recommendations and other information gained from the Mark IA failure analysis. Instead of proceeding directly to the design and fabrication of a full-scale Mark II battery, the initial effort is directed toward the development of high-reliability cells and the fabrication and testing of groups of identical cells to establish their reliabiltiy. The next step of the development is to design, fabricate, and test 10-cell modules to evaluate battery hardware designs. The final stage of the Mark II program will then involve the design, fabrication, and testing of full-scale electric-vehicle batteries.

ACKNOWLEDGEMENTS

The successful completion of the failure analysis and the supportive efforts associated with it depended on the work of many individual contributors at Argonne and Eagle-Picher. The overall direction of the program was the responsibility of Dr. D. L. Barney and Dr. R. K. Steunenberg, whose guidance in this effort is gratefully acknowledged. The cooperation of S. Preto, D. Vissers, E. Hayes, and M. Farahat in reacting to and providing information regarding the event was invaluable. J. Thomas, G. Chapman, and S. Gabelnick and his group provided excellent computer output data to support the time frame of the event. Photographs taken by A. Meyers and W. Choy of the Graphic Arts Department at ANL provided an excellent historical record of the disassembly of the modules for subsequent review and guidance in the analysis. The following played key roles in the disassembly of the modules: J. Hamilton, G. Redding and W. Miller from CEN, D. Sandberg and T. Denst of ANL central shops, I. Pollack from the Engineering Division, and J. Miller and W. Costley of Eagle-Picher. Thanks are due to Z. Tomczuk and P. Cunningham and his group for the timely analysis of samples. Detailed cell and battery component examinations and metallography were the result of the dedicated efforts of N. Otto, F. Mrazek and J. Smaga. M. Slawecki provided information and guidance in the electrical and arcing problem areas. M. Farahat was instrumental in the area of thermal analysis of the system. The editorial assistance of J. Harmon in the preparation of this report is appreciated.

REFERENCES

1. P. A. Nelson et al., High-Performance Batteries for Stationary Energy Storage and Electric-Vehicle Propulsion: Progress Report for the Period April-June 1977, Argonne National Laboratory Report ANL-77-68, p. 23 (October 1977).

2. P. A. Nelson et al., High-Performance Batteries for Electric-Vehicle Propulsion and Stationary Energy Storage: Progress Report for the Period October 1978-March 1979, Argonne National Laboratory Report ANL-79-39, p. 47 (May 1979).

3. ANL-79-39, p. 48.

4. W. L. Link and L. A. Wiley, Metals Handbook, American Society for Metals (1948).

APPENDIX A

MATERIALS OF CONSTRUCTION

Item	Material
Cell	
Negative Reactant	Li-Al Alloy
Positive Reactant	FeS, Cu_2S
Electrolyte	LiCl-KCl Eutectic
Separator	BN Cloth
Particle Retainers	Y_2O_3 Felt & 304 SS Screen
Can (case), Positive Rod Clad	1010 Carbon Steel
Added Conductor	OFHC Copper
Braze	Sil-Bond 50
Battery Hardware	
Tray & "T" Bar	304 S.S.
Angles and Cross-Over Straps	304 S.S.
End Plates	Inconel 718
Cooling Tubes	300 Series S.S.
Insulation	
Cell-cell, Cell-tray, Cell-liner	Vitra-Bond Mica 27-08
Cell angle, Cell-"T" Bar	Raybestos FM 1776
Wires Equalizer, Voltage Sense)	SAMOX
Thermocouples	Fiber glass braid
Front Plug	Min-K
Wires	
Equalizer & Voltage Sense	Nickel clad copper
Thermocouples	Chromel-alumel
Intercell Connectors	Nickel clad OFHC copper
Wrap-Min K & Wire Bundle	Glass cloth
Braze Flux	Airco Flux #12
Insulated Case	Inconel 718
Foils Inner (1)	Stainless Steel
Balance	Aluminum
Liner	Inconel 718

APPENDIX B

MELTING POINTS OF SELECTED MATERIALS

Materials	Temperature, °C
Lithium-Aluminum Alloy	~600 (min.)
Silbond 50 Braze Alloy	635
Aluminum	660
Iron-Aluminum Alloy	655 (min.)
Copper	1083
304 Stainless Steel	1400-1450
Alumel	1400
Chromel	1430
Nickel	1455
Iron	1540

APPENDIX C

MARK IA TEST LOG

ednesday, May 30

630 D. R. Vissers and S. K. Preto reported for duty on the 1630-0030 shift.

1700 All readings normal, i.e., temperatures, cell voltages, vacuum annulus pressure, argon pressure and flow rate in cell chamber.

1800 All readings normal. M. McGinnty (Eagle-Picher) and M. Farahat reduced voltage on heaters from 30 to 26 V. McGinnty and Farahat departed.

1900 All readings normal.

2000 All readings normal.

2047 McGinnty arrived and increased voltage on heaters from 26 to 30 V. Thermocouples #6 and #12 reading 444.2 and 446.2°C, respectively. McGinnty departed.

2100 All readings normal.

2200 All readings normal.

2300 All readings normal.

2316 Slight drop observed in voltages of cells in middle of D-001; temperatures stable. Argon flow from chamber of D-001 high--off scale on rotameter. Reduced to desired value of 2.4 cfh. Indication of pressure rise in vacuum annulus of D-001 from 10^{-5} to about 1.1×10^{4} torr, suggesting that a leak may be developing.

2325 Attempted to call V. Kolba.

2327 Preto, monitoring cell voltages of visual display, noticed voltages starting to "sag" below 1.0 V (normal values 1.4-1.5 V) in D-001. Voltage loss largest in middle region of module (Cells 25-30). Called M. Farahat and talked for about 17 min.

2340 Per Farahat's instructions, cell heaters on D-001 were turned off and mass spectrometer on vacuum annulus was checked for mass No. 40 (argon). A large argon peak was observed, which indicated a leak from the cell chamber into the vacuum annulus. The ion pump went off automatically due to increasing pressure. Sorption pump was turned on. A "hot electrical" odor was noted, and thermocouple No. 3 was reading off scale on a digital meter (>999.9°C).

2344 Per Farahat's instructions, temperature controller was turned off on D-001. Work was started on connection of two 12-V lead-acid batteries to operate blower on cooling tube of D-001.

2345 Called E. Hayes and informed him of situation. Preto heard "popping" sound. Vissers called Fire Department to stand by.

2350 Blower on cooling tube started. Called V. Kolba. Firemen arrived and were advised to use CO_2 rather than water if need arose. Their personnel obtained 20 lb of dry ice in case it was needed.

Thursday, May 31

0100 M. Farahat arrived and took charge. An air fan was directed on the exterior of the modules.

0015 E. Hayes and N. Otto arrived.

0020 V. Kolba arrived. All cell voltages except No. 60 were zero. Diverted argon purge into cell chamber of D-001 from D-002 to take advantage of slight additional cooling effect.

0045 Vacuum annulus pressure 320 microns. Argon peak evident on mass spectrometer. Maximum temperature on manual thermocouples 718°C. Outside case temperature 113°C with cooling fans. Condensation observed in exit gas from cell chamber (yellowish liquid). Thermocouple placed in exhaust air from cooling tube-temp. 266°C.

0255 Sorption pump up to 1 atm. Mechancal vacuum pump attached to vacuum annulus and started.

0315 Voltage of Cell 60 dropping. Temperature of thermocouple No. 4 rising to about 695°C.

0520 Thermocouple on cooling tube exit showed cooling. Blower placed on 110 V ac power source.

0800 Module D-001 cooled below the melting point of the electrolyte (352°C).

1132 Heaters on D-002 turned off.

1235 The folling plan of action was adopted: Module D-002 to be cooled at a rate of 10°C per hour. Module D-001 to be cooled as rapidly as possible.

1310 Resistance measurements between D-001 case and terminals showed zero ohms.

Friday, June 1

1700 Module D-002 cooled below melting point of the electrolyte (352°C).

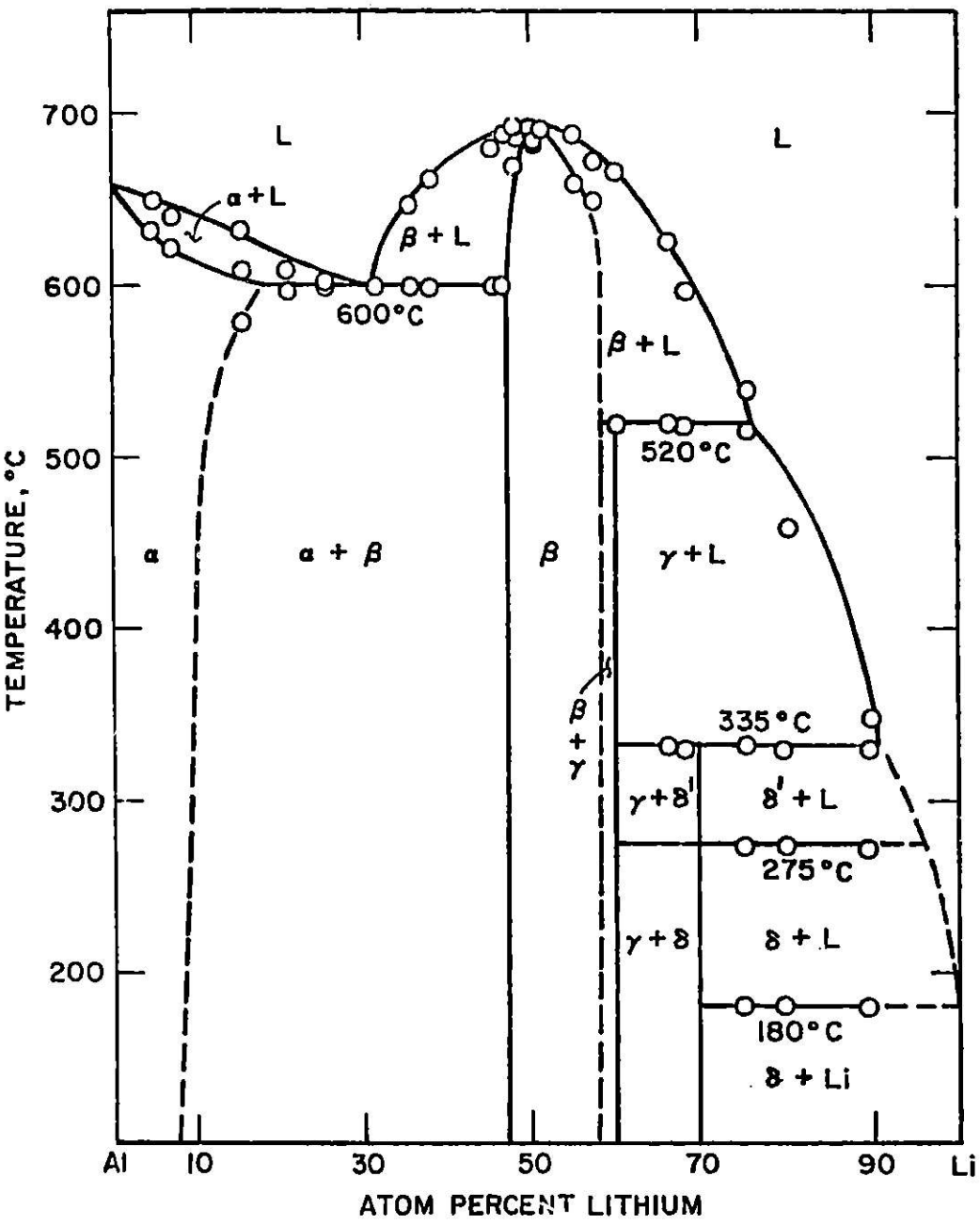

APPENDIX D. PHASE DIAGRAM OF BINARY ALLOY Li-Al SYSTEM (K. M. Myles, et al., Proceedings of the Symposium and Workshop on Advanced Battery Research and Design, Argonne National Laboratory, ANL-76-8, p. B-50, March 1976).